POLITECNICO DI TORINO

Master's Degree in Energy and Nuclear Engineering

Master's Degree Thesis

Hydrogen purification using Pd-based membranes

Supervisors
Prof. Massimo Santarelli
Prof. Hilde J. Venvik
Prof. Nicola Paltrinieri

Candidate
Sheikh Md Rashedul Alam Sayem

November 2025

Abstract

On the verge of a global climate crisis, renewable energy is the best bet for the academicians to reverse greenhouse effects and ensure sustainability. Hydrogen, having the highest energy density per weight is considered the most promising leader in this fight against adversity. However, hydrogen being a highly risky component, rises concern in the case of its transportation and storage. So, among many alternatives, ammonia is considered a suitable hydrogen carrier. However, upon ammonia cracking, the hydrogen mixture possesses contaminant and requires separation and purification. For a long time, researchers have considered Pd-based membranes a technically promising technology for hydrogen purification. Furthermore, SINTEF industry has advanced this membrane by addressing its permeability issue by designing thin Pd-Ag based membrane using sputtering technology.

The aim of this thesis is to experimentally evaluate hydrogen transport through two Pd-based membranes of differing thicknesses (5.5 µm and 10 µm), and to assess the governing mechanisms influencing flux, permeability, and permeance. Experiments were conducted under low pressure at various temperatures (300–400 °C) and feed gas compositions. Various analyses have been conducted based on Fick's First law as well as Sievert's Law. Permeability was extracted from the slope of the flux–driving force plots and found to be higher for the thicker 10 µm membrane, suggesting non-diffusive mechanisms at play. Arrhenius analysis of temperature-dependent permeance further supported the dominance of surface or interface-controlled transport rather than bulk diffusion.

After studying and analyzing two Pd-based membranes, it can be concluded that membrane thickness is not only determining factor of its performance, and that surface topography, membrane support substrate, and synthesis method play a critical role. Therefore, in order to design Pd-based membranes for optimum hydrogen purification applications, it is crucial to emphasize on both mechanical stability and thickness factors to achieve optimal selectivity and flux performance. Also, it is crucial to emphasize on fabrication parameters to obtain the optimum structure and composition.

Sommario

Sull'orlo di una crisi climatica globale, le energie rinnovabili rappresentano la soluzione migliore per gli accademici per invertire l'effetto serra e garantire la sostenibilità. L'idrogeno, con la più alta densità energetica in rapporto al peso, è considerato il leader più promettente in questa lotta contro le avversità. Tuttavia, essendo un componente altamente rischioso, l'idrogeno desta preoccupazione per il suo trasporto e stoccaggio. Pertanto, tra le numerose alternative, l'ammoniaca è considerata un idoneo vettore di idrogeno. Tuttavia, durante il cracking dell'ammoniaca, la miscela di idrogeno contiene contaminanti e richiede separazione e purificazione. Per lungo tempo, i ricercatori hanno considerato le membrane a base di Pd una tecnologia tecnicamente promettente per la purificazione dell'idrogeno. Inoltre, l'industria SINTEF ha sviluppato questa membrana affrontandone il problema della permeabilità progettando una membrana sottile a base di Pd-Ag utilizzando la tecnologia dello sputtering.

L'obiettivo di questa tesi è valutare sperimentalmente il trasporto di idrogeno attraverso due membrane a base di Pd di diverso spessore (5,5 μm e 10 μm) e valutare i meccanismi che influenzano flusso, permeabilità e permeanza. Gli esperimenti sono stati condotti a bassa pressione a diverse temperature (300-400 °C) e con diverse composizioni del gas di alimentazione. Sono state condotte diverse analisi basate sulla prima legge di Fick e sulla legge di Sievert. La permeabilità è stata estratta dalla pendenza dei grafici delle forze di flusso e si è rivelata maggiore per la membrana più spessa da 10 μm, suggerendo l'esistenza di meccanismi non diffusivi. L'analisi di Arrhenius della permeabilità dipendente dalla temperatura ha ulteriormente confermato la prevalenza del trasporto controllato dalla superficie o dall'interfaccia piuttosto che dalla diffusione in massa.

Dopo aver studiato e analizzato due membrane a base di Pd, si può concludere che lo spessore della membrana non è l'unico fattore determinante per le sue prestazioni, ma che anche la topografia superficiale, il substrato di supporto della membrana e il metodo di sintesi svolgono un ruolo fondamentale. Pertanto, per progettare membrane a base di Pd per applicazioni ottimali di purificazione dell'idrogeno, è fondamentale concentrarsi sia sulla stabilità meccanica che sui fattori di spessore per ottenere selettività e prestazioni di flusso ottimali. Inoltre, è fondamentale concentrarsi sui parametri di fabbricazione per ottenere la struttura e la composizione ottimali.

Contents

Abstract **2**

Sommario **3**

List of Figures **8**

List of tables **9**

List of Abbreviations **10**

List of Symbols **11**

1. Introduction **12**

1.1 Background and Motivation 12

1.1.1 Global climate change and the shift to renewable energy 12

1.1.2 Hydrogen as a clean energy vector 13

1.1.3 Hydrogen transportation challenges and safety concerns 14

1.1.4 Ammonia as a Hydrogen Carrier 15

1.1.5 Ammonia Cracking and Impurities 16

1.2 Hydrogen Purification 16

1.2.1 Importance of high-purity hydrogen in energy and industry 16

1.2.2 Methods of Hydrogen Separation 17

1.3 Objectives 18

2. Literature Review **19**

2.1 Various Techniques of Hydrogen Separation 19

2.1.1 Cryogenic Distillation 19

2.1.2 Pressure Swing Adsorption 19

2.1.3 Electrochemical Purification 20

2.1.4 Membrane Separation 21

2.2 Membrane Technologies for Hydrogen Purification 22

2.2.1 Polymer membranes 22

2.2.2 Zeolite Membranes 23

2.2.3 Carbon-based membranes 23
2.2.4 Ceramic membranes 24
2.2.5 Metallic membranes 24
2.3 Palladium-Based Membranes 25
2.3.1 Synthesis Methods of Palladium based Membranes 26
2.3.2 Properties and Performance Characteristics 28
2.3.3 Applications in Real World uses 29
2.3.4 Pd-Ag Membrane by SINTEF 31
2.4 Literature Gap 31
3. Theory 32
3.1 Pd-H_2 System 32
3.2 Fick's First Law 33
3.3 Sieverts' Law and Arrhenius Plot 34
3.3.1 Background and Significance 34
3.3.2 Integration of Flick's Law and Sievert's Law 36
4. Materials and Membranes 38
4.1 Magnetron Sputtering 38
4.1.1 Magnetron Sputtering on Si Wafer 39
4.1.2 Magnetron Sputtering on Glass plate 39
4.2 Membrane by SINTEF Industry 39
4.2.1 Topography of the membrane 40
4.2.2 Characteristics and Performance 40
4.3 Membrane by Hydrogen Mem-Tech 40
4.3.1 Topography of membrane 41
4.3.2 Characteristics and Performance 41
4.4 Comparison between Glass membrane and Si Wafer Membrane 42
4.5 Conclusion 43

5. Experimental **44**
5.1 Risk Analysis 44
5.2 Experimental Setup 44
5.2.1 Membrane Assembly 44
5.2.2 Lab View 46
5.3.3 Gas Flow 47
5.3 Heat Treatment 47
5.3.1 Heat treatment in air (HTA) 47
5.3.2 Heat treatment in H_2/N_2 atmosphere 48
5.4 Permeation Experiments 48
5.4.1 Permeation Experiments of 10 $\boldsymbol{\mu m}$ Membrane 48
5.4.2 Permeation Experiments of 5.5 $\boldsymbol{\mu m}$ Membrane 49
6. Results **51**
6.1 Comparison to Literature 51
6.2 Gas mixture effects 52
6.2.1 Total Flow Dependency 52
6.2.2 Depletion and Concentration Dependency 53
6.3 Temperature Dependence 54
6.4 Hydrogen Solubility and Diffusivity in Pd-Ag Membrane 55
6.3.1 5.5 µm Membrane 56
6.3.2 10 µm Membrane 57
6.5 Anomaly of 5.5 µm membrane 59
7. Discussion **62**
7.1 Performance Analysis 62
7.2 Determination of Rate Limiting Step 62
7.2.1 5.5 µm Membrane 62
7.2.2 10 µm Membrane 63

7.3 Discussion of Abnormal Phenomena of 5.5 μm Membrane 63
7.4 Limitation of Experimentation 63
8. Conclusion 64
References 65
Appendix 71
Appendix A 71
Appendix B 77
Appendix C 84
Appendix D 90
Appendix E 104
Appendix F 105

List of Figures

1. Figure 1.1: (a) Energy use by fuel in Aviation Sector (b) Marine Sector Energy Mix [11] ……13
2. Figure 1.2: (a) Low carbon energy demand by Sector (b) Demand of different types of hydrogen by 2035 and 2050 [11] ……14
3. Figure 1.3: Ammonia value chain as a hydrogen carrier [19] ……16
4. Figure 2.1: Schematic of PSA [27] ……20
5. Figure 2.2: Schematic of PEM Elctrolyzer Reaction [28] ……21
6. Figure 2.3: Schematic of Polymer Membrane [36] ……22
7. Figure 2.4: Zeolites used for CO2 Capture from syngas mixture ……23
8. Figure 2.5: Transport Process of Ceramic membranes [41] ……24
9. Figure 2.6: The heated precursor is deposited on the porous support [45] ……27
10. Figure 2.7: The target metal is sputtered using the argon ion [46] ……28
11. Figure 3.1: Solution-diffusion transport mechanism through Pd-based membrane adopted from [37,53] ……32
12. Figure 3.2: Sievert's constant as a function of the thickness of Pd77%Ag23% thin film membranes at various temperatures [70] ……37
13. Figure 5.1: Microchannel parts and configuration ……46
14. Figure 5.2: Gas flow of the microchannel membrane reactor system ……47
15. Figure 6.1: Total Flow Dependency of 10 μm Membrane (a) For 80:20 Flow Rate, (b)For 100:0 Flow Rate ……52
16. Figure 6.2: Total Flow Dependency of 5.5 μm Membrane ……53
17. Figure 6.3: Hydrogen Concentration effect on (a) 10 μm membrane, (b) 5.5 μm Membrane ……54
18. Figure 6.4: ln D Vs 1/T Plot for 5.5 μm Membrane ……55
19. Figure 6.5: ln D Vs 1/T Plot for 10 μm Membrane ……57
20. Figure 6.6: Hydrogen permeability as a function of inverse thickness at 300 °C, 350 °C, and 400 °C for (a) flow rate 80:20, (b) flow rate 100:0 ……58
21. Figure 6.7: Alteration of behaviour of 5.5 μm Membrane ……60
22. Figure 6.8: Curled-up 5.5μm membrane……61

List of tables

1.. Table 1.1: Comparison of the safety parameters of different fuels [14] ……..15
2. Table 1.2: Summary of chemical properties for hydrogen and ammonia [18] ……..15
3. Table 1.3: Hydrogen purity and its respective applications [20] ……17
4. Table 2.1: Interaction Properties of H2 for Pure Metals [34] ……25
5. Table 2.2: Available commercial metal membranes for hydrogen separation [44] ….26
6. Table 2.3: Pd-based Membrane Properties and Performance [47] ……..29
7. Table 3.1: Rate limiting steps in the hydrogen permeation through Pd-based membranes (Adopted from [53]) ……..34
8. Table 4.1: Performance comparison between Pd–Ag on Vycor glass (Gobina et al.) and Pd–23%Ag (Si wafer → steel) (SINTEF) (Adopted from [58,63]) ……..42
9. Table 5.1: Experiment Conditions in the case of 10 μm Membrane ……..49
10. Table 5.2: Experiment Conditions in the case of 5.5 μm Membrane ……..50
11. Table 6.1: Comparison of the results of this study with Vicinanza et. al [37] and Mejdell et. al [16] ……..51
12. Table 6.2: Values for 5.5 μm membrane of Sievert constant and diffusivity adopted from figure 3.2 …… 56
13. Table 6.3: Values for 10 μm membrane of Sievert constant and diffusivity adopted from figure 3.2 ……57

List of Abbreviations

LOHCs	Liquid Organic Hydrogen Carriers
GHGs	Greenhouse Gases
RES	Renewable Energy Source
SMR	Steam Methane Reforming
PSA	Pressure Swing Adsorption
PEM	Proton Exchange Membrane
CMS	Carbon Molecular Sieve
ADF	Abbreviated decimal fraction
KET	Key Enabling Technology
LHV	Lower Heating Value
HTA	Heat treatment in air
MFC	Mass Flow Controller
GC	Gas Chromatography
SEM	Scanning Electron Microscopy
XRD	X-Ray Diffraction
ELP	Electroless Plating
PVD	Physical Vapor Deposition
CVD	Chemical Vapor Deposition

List of Symbols

μm	Micrometre
H_2	Hydrogen
CO_2	Carbon dioxide
Pd	Palladium
Ag	Silver
Ta	Tantalum
V	Vanadium
NH_3	Ammonia
H_2	Hydrogen Molecule
H	Hydrogen Atom
N_2	Nitrogen
D	Diffusivity
D_o	Pre-exponential factor (diffusion)
J	Flux
P	Permeability
p	Partial Pressure
R	Gas Constant
T	Temperature
E	Activation Energy
N_b	Bulk metal Pd concentration
t	Membrane thickness
C	Solubility of hydrogen
Ks	Sievert Constant
Al2O3	Aluminium Oxide
$\propto$	Proportional
E_D	Activation energy for diffusion

1. Introduction

Energy is the fundamental driving force in order to sustain our lives. We primarily get energy from the Sun. Since humanity's inception, we have been using solar energy in different forms and shapes. However, human being is able to use only a fraction of the solar energy available. During the dawn of humanity's inception, we progressed one step further by harnessing the control of energy with the discovery of fire. The sun drives photosynthesis in trees, storing energy in the form of lignocellulosic biomass, and with the discovery of fire, humans learned to harness this stored solar energy through the combustion of firewood. Following many millennia of human development, we have been able to bring about Industrial Revolution through the invention of labour-reducing machines that were mainly powered by hydrocarbon-based fossil fuels.

1.1 Background and Motivation

With the advent of Industrialization, the predominant use of traditional hydrocarbon-based fuels has altered the energy balance of the planet earth, emitting substantial amounts of greenhouse gases and exacerbating climate change [1]. Therefore, average global temperature has increased, and intense, erratic weather patterns are getting evident gradually but effectively [2]. Climate events—such as droughts, floods, and heatwaves—are significantly having adverse effects on various aspects of lives including agricultural productivity collapse, sea level rise, species loss, newborn mortality rises as well as food price hike [3,4]. At this rate, by 2050 the global temperature is speculated to rise by 3-6°C, that will escalate the catastrophic events and global crisis exponentially [7].

1.1.1 Global climate change and the shift to renewable energy

The escalating difficulties due to climate change require a shift to Renewable Energy Sources (RES) to reduce carbon emissions and secure a sustainable future [5]. Renewable Energy is mainly extracted from natural sources without interrupting the natural harmony and biodiversity. Apart from mitigating climate change, RES has made significant contributions to crucial issues like Energy Security, by assuring uninterrupted supply of energy for residential and industrial uses [1]. RES like solar, wind, geothermal, biomass and hydro-power energies are reliable for generating power without any emission. Since we can use these energy sources perpetually without harming the environment, these are called sustainable energy sources [6].

1.1.2 Hydrogen as a clean energy vector

Hydrogen is a crucial industrial chemical, possessing the highest lower heating value (LHV) of about 142 MJ/kg. Furthermore, atomic hydrogen (H) is one of the most prevalent natural elements on Earth [37]. Hydrogen is considered as a promising clean energy solution to mitigate the Greenhouse Gases (GHGs) emissions. High energy density and compatibility with renewable energy systems make it a suitable candidate to decarbonize the sectors responsible for climate change [7,9]. Hard to abate sectors like cement, steel, aviation and maritime industries are suitable candidates for adoption of low carbon hydrogen. We can acquire hydrogen from different sources and through different methods. While, blue hydrogen is derived from natural gas with carbon capture and storage, green hydrogen is produced via water electrolysis with exclusively renewable energy. Long-term forecasts indicate that green hydrogen will prevail as renewable energy capacity increases, while worldwide demand for blue hydrogen is anticipated to grow in near term owing to the current natural gas infrastructure [8]. It is speculated that using low

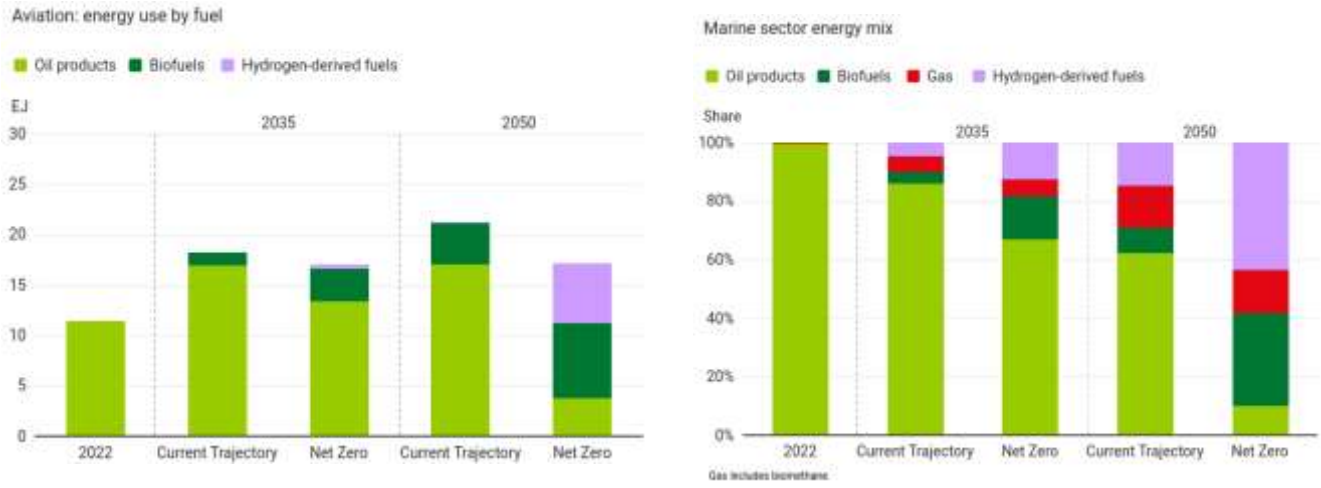

Figure 1.1: (a) Energy use by fuel in Aviation Sector (b) Marine Sector Energy Mix [11]

carbon hydrogen in cement production can reduce the emissions by 20-30%, while in the case of steel manufacturing the reduction rate is as high as 80-90%. In the case of highly carbon emitting sector like aviation, adoption of low carbon hydrogen can reduce the release of GHGs by 9% [10]. The statistics make it clear why the demand of green and blue hydrogen will be increasing both in short term and in long term. As expected, some of the industries with highest demand of low carbon hydrogen will be transportation sectors and industries. In the case of transportation sectors, apart from

aviation and maritime, medium and heavy-duty vehicles will have a significant share in this speculated demand. According to BP energy outlook, the demand and supply for blue hydrogen will be as dominant as that of green hydrogen in both near term and long term. So, the need for research in blue hydrogen is getting inevitable in the current time.

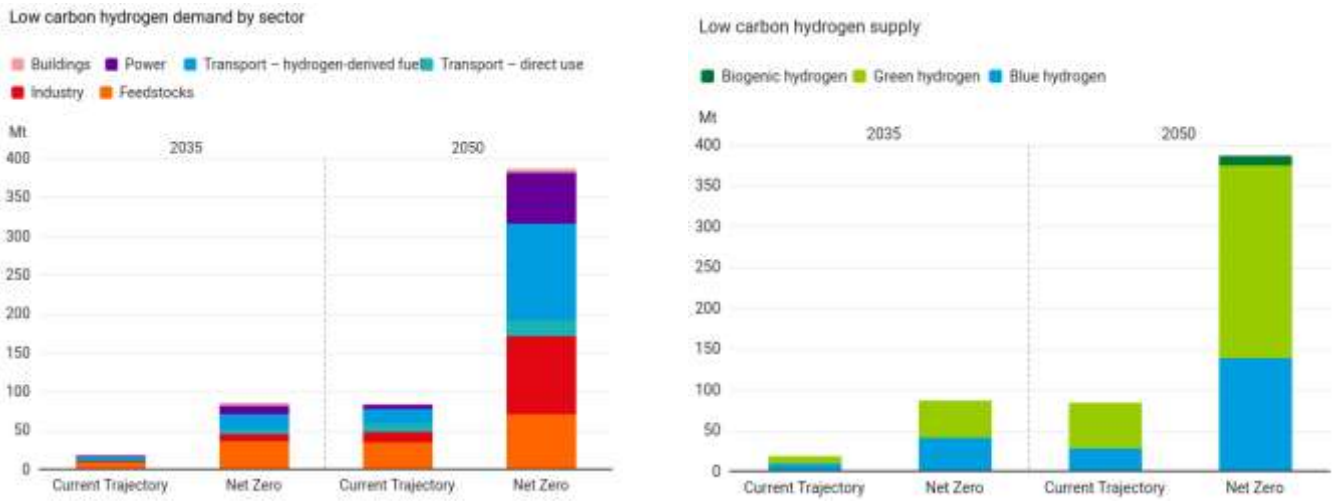

Figure 1.2: (a) Low carbon energy demand by Sector (b) Demand of different types of hydrogen by 2035 and 2050 [11]

1.1.3 Hydrogen transportation challenges and safety concerns

In comparison to conventional fuel like natural gas, hydrogen possesses numerous hazardous attributes, including low minimum ignition energy, extensive flammable range in air, broad explosion range, susceptibility to leakage, and embrittlement effects. One of the earliest and most prominent accidents regarding hydrogen transportation was the Hindenburg Disaster in 1937. A German passenger airship fuelled with 200,000 m^3 hydrogen caught fire due to ignition of hydrogen leakage by a spark. The catastrophe led to 36 deathsm[12]. In 2001, a transportation truck loaded with compressed hydrogen cylinder collided with another vehicle. As a result, the cylinder ruptured and ignited, producing intense flames and causing several injuries and property loss [13]. So, from the unpredictable characteristics of hydrogen and the mishaps that have taken place over course of history persuade us to look for innovative techniques for hydrogen transportation. In the next section, we will discuss why ammonia could be an apt candidate as a hydrogen carrier.

Parameters	Hydrogen	Natural Gas	Gasoline
Density (kg/m3)	0.082	0.67	4.4
Minimum ignition energy (mJ)	0.02	0.3	0.3
Flammable range (in air) (vol%)	4-75	5-15	1-7
Diffusion coefficient in air (cm2/s)	0.61	0.16	0.05
Laminar flame speed (m/s)	2.1	0.4	0.3
Ignition point (K)	843	923	700

Table 1.1: Comparison of the safety parameters of different fuels [14]

1.1.4 Ammonia as a Hydrogen Carrier

Ammonia contains 17.6% hydrogen by weight, considerably greater than numerous liquid organic hydrogen carriers (LOHCs). Ammonia is already a well-established commodity worldwide being produced approximately 180 million tonnes per year. Volumetric hydrogen density of liquid ammonia is much higher (121 kg-H_2/m^3) than that of liquid hydrogen (70.8 kg-H_2/m^3) [15]. Furthermore, ammonia is liquefied under significantly much more feasible conditions, particularly 8 bars at 20° C [16]. Apart from that ammonia is a well-established commodity being produced approximately 235 million tonnes per year [17]. Even though traditional ammonia is mainly produced from the hydrogen that comes from Haber-Bosch. However, there is a growing trend of green and blue hydrogen production [16]. Therefore, ammonia is widely considered as a suitable candidate as a hydrogen carrier.

Property	Hydrogen	Ammonia
Boiling point [°C]	-252.7	-33.34
Melting point [°C]	-259	-77.73
Gas density [kg/m^3]	0.089	0.769
Liquid density [kg/L]	0.071	0.6819
LHV [MJ/kg]	119.9	18.6
LHV as liquid [MJ/L]	8.5	12.7
HHV [MJ/kg]	141.9	22.5
HHV as liquid [MJ/L]	10.1	15.3
Auto ignition [°C]	585	651
Flammability/air [-]	4–75%	15–28%

Table 1.2: Summary of chemical properties for hydrogen and ammonia [18]

1.1.5 Ammonia Cracking and Impurities

With the development of high temperature fuel cells, ammonia can directly be used as a fuel. If ammonia is not utilized as a direct fuel, it can be reverted to hydrogen. The output acquired from ammonia cracking is not pure hydrogen, usually a mixture of hydrogen, nitrogen and ammonia that necessitates efficient and cost-effective separation and purification of hydrogen before its final application [19].

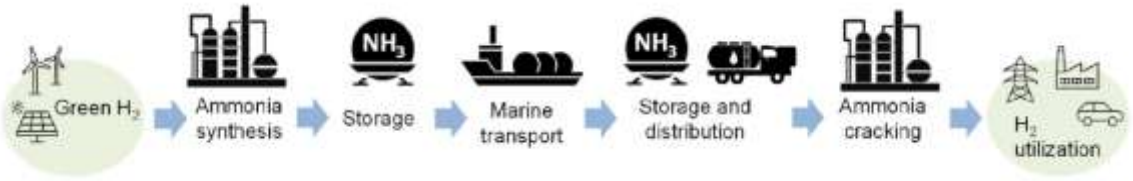

Figure 1.3: Ammonia value chain as a hydrogen carrier [19].

1.2 Hydrogen Purification

Hydrogen purification is a very crucial step in hydrogen value chain. With the growing demand for low carbon hydrogen, hydrogen purification is now a crucial part of most of the industries. In the following section, we will discuss about different sectors that require high purity hydrogen.

1.2.1 Importance of high-purity hydrogen in energy and industry

Abbreviated decimal fraction (ADF) is a commonly used by manufacturers to denote the purity of a gas. In simple terms, a gas with 99.99% purity can be marked with 4.0 purity in this system. Similarly, the expression 6.0 represents a gas with the purity of 99.9999% purity. Furthermore, the term 4.6 implies that the purity of the gas is 99.996%. We will use this system of expression throughout the thesis. [20] Traditionally, semiconductor industry has been known to require ultra-pure hydrogen with a purity of 6.0. Besides, general industries like steel and cement require 3.0 purity. With the rise of green hydrogen industries, the demand for pure hydrogen has only gone up. For instance, PEM fuel cell requires hydrogen fuel of 4.0 purity. [21]

Fuel	Type	Grade	Applications	Purity (mole fraction)
Gaseous	I	A	Internal combustion engines for transportation; residential or commercial appliances. (All applications, except fuel cells)	98.0
	I	B	Industrial fuel, for use e.g. in power generation or as a heat energy source	99.90 / 3.0
	I	C	Aircraft and space-vehicle ground support systems	99.995/ 4.5
	I	D	Fuel cells for vehicles	99.97/3.7
	I	E	Fuel cells for stationary applications - Category 1	50.0
			Fuel cells for stationary applications - Category 2	50.0
			Fuel cells for stationary applications - Category 3	99.9/ 3.0
Liquid	II	A	Aircraft and space-vehicle on board propulsion systems and electrical energy requirements; land vehicles except fuel cells	99.995/4.5
	II	B	Fuel cells for transportation	99.97/ 3.7
Slush	III		Aircraft and space-vehicle on board propulsion systems	99.995/4.5

Table 1.3: Hydrogen purity and its respective applications [20].

1.2.2 Methods of Hydrogen Separation

Hydrogen separation is an important processes in the process industry. Various ways including distillation, adsorption, membrane, catalyst as well as electrochemical devices have been used to acquire pure hydrogen. This topic will be discussed comprehensively in the literature review section of this article.

1.3 Objectives

From the previous sections, we have been introduced to the motivation of the study. Now, we will know the objectives of the study. For this study, we chose a particular mode of hydrogen separation, namely Pd-based membrane. This membrane is an alloy of Pd and Ag. In the literature review section, we will further study the criteria to select this mode of hydrogen separation. In short, the objective of the research was to study membrane performance under different conditions. Now, an elaborate description of the objectives will be presented. Our primary goal was to measure flux, permeability, and permeance under varied operating conditions including temperature, pressure, feed gas composition to assess hydrogen transport via Pd-based membranes. Furthermore, we wanted to evaluate the impact of membrane thickness (4 μm versus 10 μm) on hydrogen separation performance. Later we examined the transport pathways of hydrogen via Pd-based membranes utilizing Fick's First Law and Sievert's Law. Finally, we presented insights for the design and improvement of membranes that could promote the viability of Pd-based membranes in hydrogen purification for clean energy systems.

2. Literature Review

2.1 Various Techniques of Hydrogen Separation

2.1.1 Cryogenic Distillation

Cryogenic distillation is one of the oldest methods of hydrogen separation. It was mainly used to separate hydrogen from a mixture of CO2, CO, and other impurities produced by Steam Methane Reforming (SMR). Cryogenic distillation entails the separation of gas mixtures through partial condensation at elevated pressure and reduced temperature. When the gas mixture is cooled to cryogenic temperatures (typically below -150 °C), the denser constituents condense and separate. Hydrogen remains in the gaseous state due to its extremely low boiling point of −252.9 °C. This makes cryogenic distillation a great way to get a lot of hydrogen back from big industrial plants like petroleum refineries and ammonia synthesis units [25]. One of the significant advantages of cryogenic distillation is its ability to process large magnitude of inputs. This procedure is not cost-effective since it needs expensive tools and machines. It also doesn't deliver well in the case of producing high purity hydrogen, with a maximum efficiency of about 99% [24]. Even though, it is economically feasible to make H_2 with SMR technology and gasification, but the purification phase makes up around half of the expense.

2.1.2 Pressure Swing Adsorption

Pressure Swing Adsorption (PSA) employs multiple beds of solid adsorbents capable of independently capturing contaminants. Unlike Cryogenic Distillation, PSA provides a hydrogen purity of 4.0, which is suitable for many industries. Pressure Swing Adsorption (PSA) presents multiple challenges: hydrogen recovery generally remains under 90%, leading to reduced efficiency; the process requires numerous beds and valves, complicating operational procedures; and its efficacy is heavily dependent on the feed gas composition, with carbon monoxide and heavy hydrocarbons negatively impacting the adsorbent's durability. Moreover, akin to cryogenic distillation, the establishment and operational expenses for PSA are significantly elevated. Therefore,

it is not economically feasible. [22,23] However, lower hydrogen recovery makes it unsuitable for hydrogen separation.

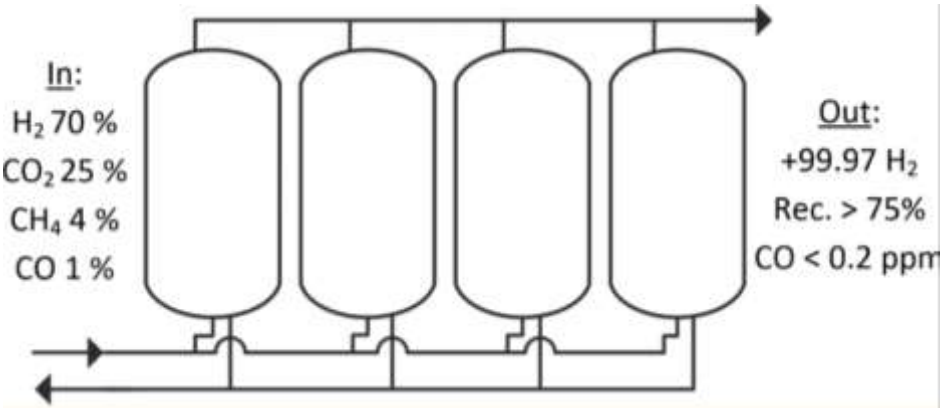

Figure 2.1: Schematic of PSA [27].

2.1.3 Electrochemical Purification

With the growing importance of decarbonization, the relavence of electrochemical processes is getting more and more prevalent. Proton Exchange Membrane (PEM) Electrolyzer is considered as one of the most promising technologies to decarbonize the chemical separation and production processes. In the case of electrochemical hydrogen separation, the feed mixture flows through anode, where among all the components, only hydrogen is oxidized. The resultant electron travels through external circuit and ends up in the cathode whereas hydrogen ion (proton) travels through the nafion membrane to meet the electrons and forming molecular hydrogen [30]. According to Norwegian hydrogen giant company Nel Hydrogen, PEM Electrolyzer can produce hydrogen with the purity of 5.0 that is suitable for most of the industry requirements [31]. However, as PEM Electrolyzer operates at low temprature, certain impurities including Carbon dioxide tends to decrease this purity because it permeates hydrated membrane of PEM Electrolyzer ending up in the mixture of Hydrogen. Another major issue of PEM is that the ion conductivity highly depends on the

hydration of the Membrane. Therefore, requirement of too much water makes this process not so sustainable [29].

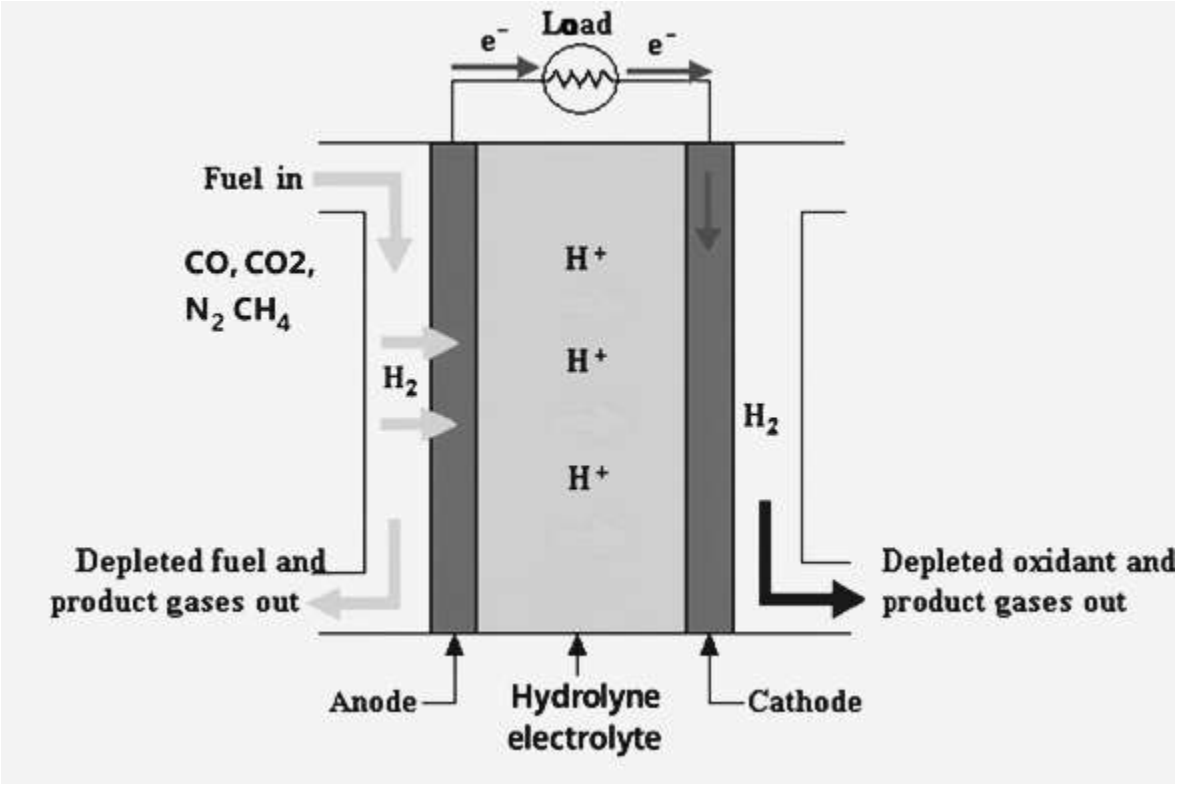

Figure 2.2: Schematic of PEM Elctrolyzer Reaction [28].

2.1.4 Membrane Separation

Upon going through other hydrogen separation methods almost all of them are not economically feasible. However, membrane-based separation has showed promising results in the case of hydrogen separation. Hydrogen comes primarily from fossil sources and requires purification from mixtures comprising CO_2, CO, CH_4, steam, and other substances. Traditional purification methods, such as PSA and cryogenic distillation, are effective but are energy-intensive and costly at elevated purities. With ultra-pure hydrogen purity, cost-effectiveness and durability, membrane technologies are considered promising for hydrogen purification. In the next section, we will discuss about different membrane technologies.

2.2 Membrane Technologies for Hydrogen Purification

The primary criteria for the choice of a membrane are its technical performance, such as permeability and selectivity, and practical feasibility for real-world application including durability and cost-effectiveness [32]. Various membrane technologies suitable for hydrogen separation and pros, and cons of them will be discussed in the next section.

2.2.1 Polymer membranes

Organic polymers possess an extensive and significant history that dates back to the 1840s, marked by the discovery of nitrocellulose and the vulcanization of polyisoprene. Polymeric materials have significantly influenced large-scale enterprises and the global economy owing to their extensive availability and diversity in contemporary society. Dupont's 1970s hollow fibre membrane designed for hydrogen separation was one of the first membranes of this kind [34]. Polymer membranes contain holes and channels of various sizes and topologies [32]. Polymeric membranes represent the most sophisticated membrane technology and are widely utilized across several sectors due to their cost-effectiveness; yet they are very prone to fouling and chemical deterioration [33]. Owing to its poor thermal resistance, polymeric membranes cannot withstand temperature above 100°C that makes it invalidated for high temperature gas separation applications. Polymeric membranes have been employed in industrial scale hydrogen separation from ammonia mixture. However, due to its poor selectivity, the products must go through multiple recycling before acquiring a high purity output. As a result, this makes polymeric membrane technology an unaffordable alternative for hydrogen separation. [37]

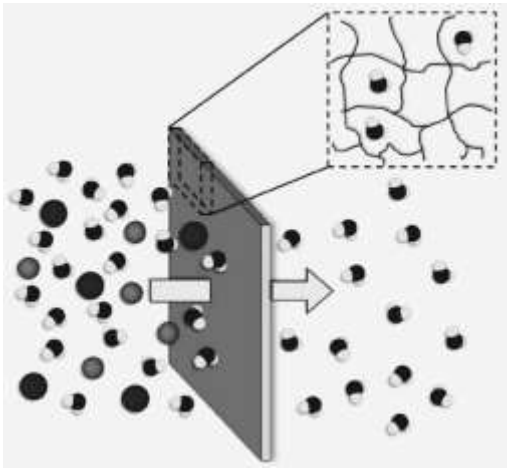

Figure 2.3: Schematic of Polymer Membrane [36].

2.2.2 Zeolite Membranes

Owing to its thermal stability and chemical inertness, zeolite membranes are considered superior to polymer membrane. Zeolite membranes uniquely integrate pore size and shape selectivity with essential mechanical, thermal, and chemical resilience required for sustained long-term separation operations. Even though zeolite membranes do not selectively adsorb hydrogen, some zeolites show acidic zeolites show affinity to carbon dioxide whereas some basic zeolites adsorb ammonia [34].

Figure 2.4: Zeolites used for CO2 Capture from syngas mixture [34].

2.2.3 Carbon-based membranes

Carbon membranes can be synthesized via the carbonization or pyrolysis of appropriate precursor materials containing carbon, including thermosetting resin, graphite, coal, pitch, and botanical sources, in an inert atmosphere or vacuum [34]. Carbon molecular sieve (CMS) membranes have become appealing gas membranes owing to their adjustable pore structure and, as a result, superior gas separation capabilities [39]. Carbon-based membranes are one to three orders of magnitude more expensive per unit area than polymeric membranes. The substantial investment cost is warranted only when their performance surpasses that of polymeric membranes. Polyimide is presently the predominant precursor for carbon membranes, significantly influencing the elevated manufacturing cost. Consequently, efforts have been undertaken to utilize more economical precursor materials, such as polyacrylonitrile. Nonetheless, the efficacy of these membranes continues to be subpar [38]. On the other hand, carbon molecular sieve (CMS) membrane shows promising result in gas

transport. However, it has major drawbacks including vapor induced pore blocking and brittleness [32].

2.2.4 Ceramic membranes

Dense perovskite and fluorite (BCZY–GDC) based ceramic membrane is another great option for hydrogen separation. With characteristics like high intrinsic selectivity, tolerance towards contaminants including CO_2, H_2S as well as mechanical robustness at high temperature up to 1000 °C, make it a viable candidate for gas separation processes. Also, flexibility of surface engineering to enhance performance makes it a versatile option. Moreover, owing to its material availability and affordability, it is a cost-effective membrane. However, this membrane requires catalyst to promote hydrogen adsorption and typically requires a high temperature above 900 °C to achieve a high enough hydrogen flux to make the process feasible [40].

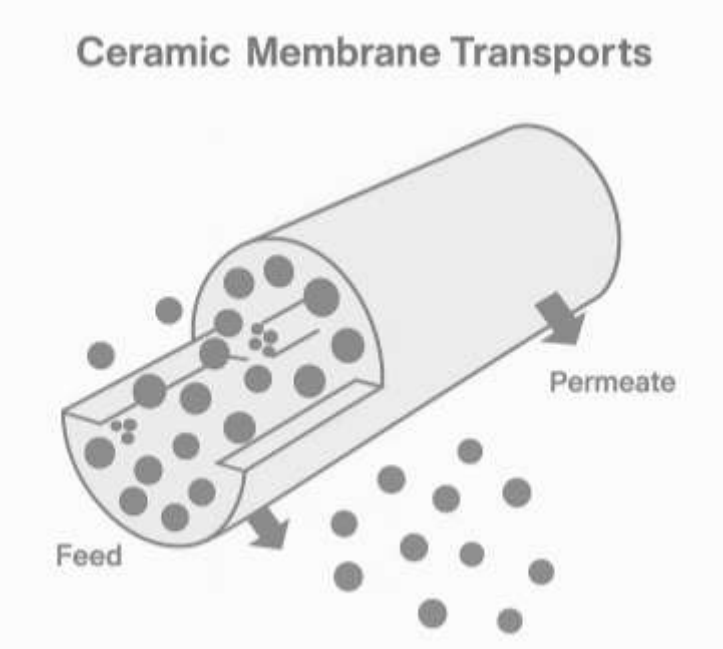

Figure 2.5: Transport Process of Ceramic membranes [41].

2.2.5 Metallic membranes

In Metallic membranes typically consist of dense sheets or films through which hydrogen permeates as its constituent protons and electrons. The primary mechanism of action in these dense metallic membranes necessitates the transfer of free electrons and the existence of particular catalytic surfaces to dissociate H2 on the raw feed flow

side and to recombine protons and electrons on the permeate side [34]. Metallic membranes may serve as optimal options for hydrogen purification owing to their capacity to provide extremely pure hydrogen at enough flux across a broad spectrum of operational conditions; hence, they are frequently utilized in the semiconductor industry, where clean hydrogen is essential [42].

Metal	hydride composition	H solubility (H/M @ 27 °C)	hydride ΔH formation (kJ/mol)	H_2 permeability @ 500 °C (mol/ms Pa^{1/2})
Ni	Ni_2H	$\sim 7.6 \times 10^{-5}$	−6	7.8×10^{-11}
Cu		$\sim 8 \times 10^{-7}$		4.9×10^{-12}
Pd	PdH	0.03	+20	1.9×10^{-8}
Pt	PtH	$\sim 1 \times 10^{-5}$	+26	2.0×10^{-12}
V	VH_2	0.05	−54	1.9×10^{-7}
Fe	FeH	3×10^{-8}	+14	1.8×10^{-10}
Nb	NbH_2	0.05	−60	1.6×10^{-6}
Ta	Ta_2H	0.20	−78	1.3×10^{-7}
Ti	γ-TiH_2	R ~ 0.0014; β ~ 1.0	−126	
Zr	ZrH_2	<0.01	−165	
Hf	HfH_2	R ~ 0.01; β ~ 1.0	−133	

Table 2.1: Interaction Properties of H2 for Pure Metals [34].

As shown in the table, niobium, vanadium, tantalum, and palladium are the metals with highest hydrogen permeability. Nonetheless, niobium, vanadium, and tantalum generate stable oxides within the operational temperature range that serve as a barrier to hydrogen diffusion. Palladium oxides can form at approximately 600°C; nevertheless, they are reduced in a hydrogen atmosphere, resulting in unchanged hydrogen permeability. As a matter of fact, palladium has historically been regarded as the most technically promising for extensive hydrogen purification. [37,42]

2.3 Palladium-Based Membranes

In the context of ultra-pure hydrogen production and separation, dense metallic membranes are favored, with dense palladium (Pd) based membranes being the most promising option. Palladium membranes can effectively isolate hydrogen from gaseous mixtures with exceptional selectivity and excellent permeability [43]. The use of such membranes with suitable catalysts in membrane reactors facilitates hydrogen

synthesis with CO2 capture, applicable in both small-scale bioenergy and combined heat and power (CHP) plants, as well as in large-scale power facilities. Pd-based membranes are considered a Key Enabling Technology (KET) to promote the shift towards a knowledge-driven, carbon neutral, and sustainable economy.

Supplier	Material	Dimension Parameters	Applications	Performance
Hysep-Energy Research Centre of The Netherlands	Pd–Au / YSZ / SS	0.04 / 0.1 / 0.5 m^2	Example: Coal-to-fuel project in New Zealand	3.5–6 Nm^3/h with 99.5–99.995% hydrogen at 21 bar pressure difference, from 33% reforming H_2
United Technologies Research Center	Pd–Cu trimetallic alloy	—	Coal gasification syngas	0.23 $mol \cdot m^{-2} \cdot s^{-1}$ with 99.9999% hydrogen
Tokyo Gas	Pd–Y(Gd)–Ag / SS	—	Reforming	40 Nm^3/h with 99.99% hydrogen
CRI	Pd and Pd-alloy	OD: 2 inch; L: 48 inch	—	40–70 $Nm^3/h \cdot m^2 \cdot h^1 \cdot bar^{0.5}$ with >99% hydrogen
REB	Pd and Pd-alloy	OD: 1/8 inch	Fluidized-bed membrane reactor	0.2 $mol \cdot m^{-2} \cdot s^{-1}$ on Pd–Cu alloy membrane at 673 K, 3.03 bar of syngas conditions

Table 2.2: Available commercial metal membranes for hydrogen separation [44].

2.3.1 Synthesis Methods of Palladium based Membranes

2.3.1.1 Chemical vapor Deposition (CVD)

Pd-based H_2 membranes synthesized via CVD are achieved by applying a thin, dense film of Pd (or Pd-alloy) onto a porous support, which is pre-treated and frequently refined with a ceramic interlayer. Prior to the actual process, the precursor is heated typically at 300-500 °C. Later, the precursor undergoes decomposition on the heated surface and at pore openings, while gaseous by-products are removed. The thickness and continuity of the film are adjusted by temperature, precursor partial pressure, and duration. Later the layer density is enhanced, and the microstructure is stabilized by a

post-annealing in inert. When completed correctly, CVD produces high-purity, extremely H_2-selective Pd films [33].

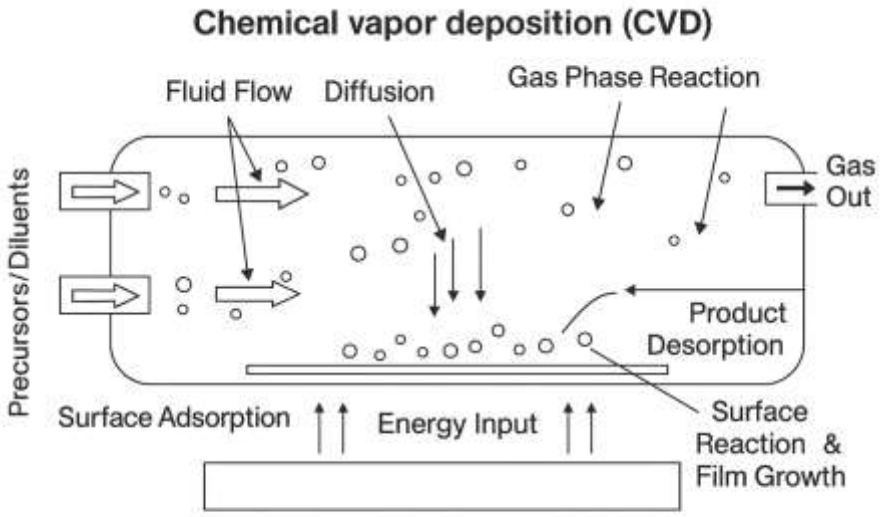

Figure 2.6: The heated precursor is deposited on the porous support [45].

2.3.1.2 Sputtering

Sputtering method includes bombarding a metal target (e.g., Pd or Pd-alloys) with energetic particles, such as Ar^+—ejecting atoms that condense on a nearby porous support to construct a dense, semi-permeable layer. A plasma is prepared within a vacuum chamber that has a little argon gas in it. Argon ions from this plasma hit a metal target, like palladium or a Pd-alloy, and knock out single metal atoms. These atoms that have been released go across the chamber and land on a support that is close by, like a porous tube or sheet. If the support stays warm and the discharge stays steady, the atoms will stick together to make a thin, dense, and continuous coating. This metal skin lets hydrogen through but keeps bigger gases out of hydrogen-separation membranes. The method is clean and exact since only metal atoms are deposited. However, it needs high-vacuum equipment and careful preparation to avoid microscopic imperfections called "pinholes," which are especially common on rough or very porous surfaces [33].

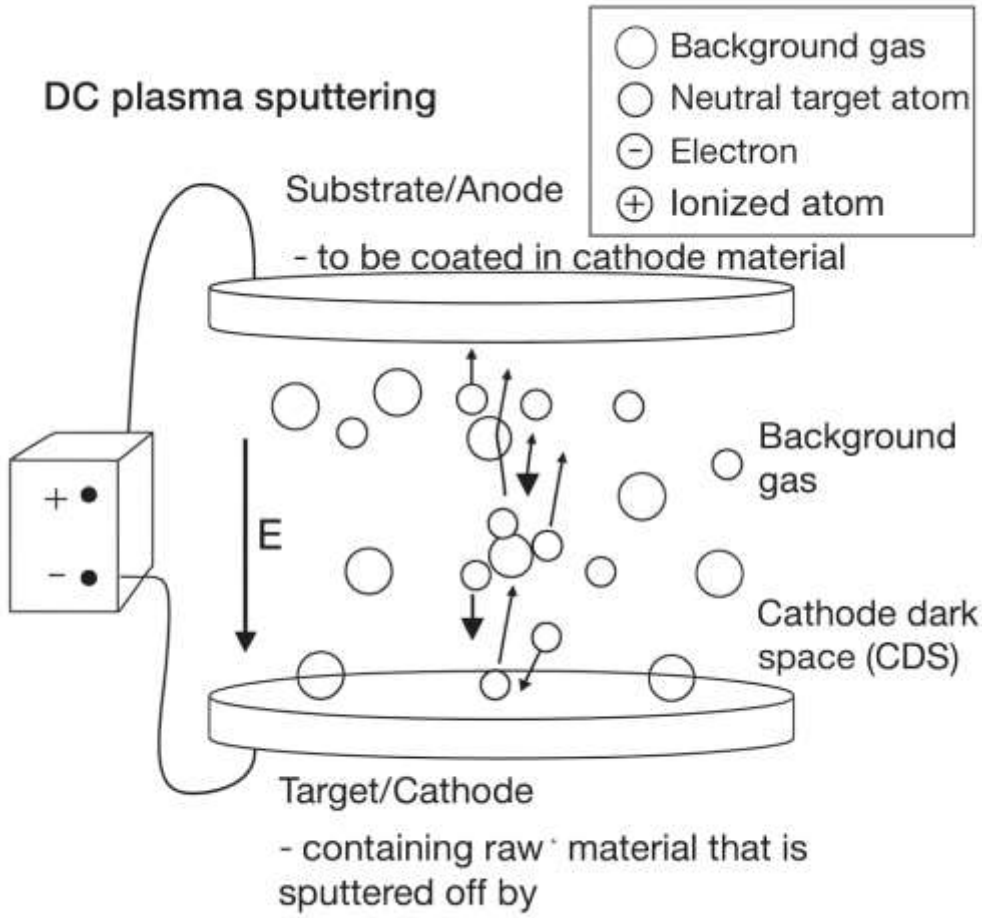

Figure 2.7: The target metal is sputtered using the argon ion [46].

2.3.1.3 Electroless plating

Electroless plating (ELP) is an autocatalytic process that deposits target metal evenly on a surface without needing external power, electrodes, or other machinery. Because reduction takes place on the surface itself, it can cover complicated shapes and internal pores. It can also minimize operational expenses compared to electroplating. However, ELP frequently has a high rejection rate because of pinholes, nodules, and other problems, which makes the overall cost go up [35].

2.3.2 Properties and Performance Characteristics

Palladium (Pd)-based membranes have become very promising materials for separating and purifying hydrogen because of their unique physical and chemical features. The main benefit of Pd is that it can break down molecular hydrogen into atomic species. This lets certain types of atoms pass through the metal lattice, which is what Sieverts' law says. Dense palladium membranes demonstrate elevated hydrogen

permeability across an extensive temperature spectrum, while exhibiting significant resistance to hydrogen embrittlement in comparison to body-cantered cubic metals [47,48].

Membrane	Preparation Method	δPd [μm]	T [°C]	ΔP [kPa]	H2 Permeability/Permeance	αH2/N2
Pd-Y	Cold-Rolling	80	400	25–300	3.43×10^{-8} (1)	N.D.
Pd-Ag	Cold-Rolling	76.2	400	≈90	$\approx 8 \times 10^{-9}$ (1)	N.D.
Pd-Ag-Y	Cold-Rolling	38	400	200	1.95×10^{-8} (1)	∞
Pd/γ-Al2O3	ELP	8.8	350	100	$\approx 4 \times 10^{-6}$ (2)	3.45
Pd-Au/α-Al2O3	ELP	8	400	50	3.87×10^{-3} (2)	500
Pd/Modified-PSS	ELP	7–8.53	320–380	202.6	$1.47–2.07 \times 10^{-6}$ (2)	92–∞
Pd/PSS	ELP-PP	20	395	200	$\approx 2.5 \times 10^{-4}$ (2)	≥1000
Pd-Ag/PSS	MS	10	450	200	3.4×10^{-5} (2)	39,000
Pd/Al2O3	ELP	5	350	30–100	4.9×10^{-9} (1)	7935–37,640
Pd/Ta	ELP	1	450	250	$5.9–12.2 \times 10^{-8}$ (1)	N.D.

Table 2.3: Pd-based Membrane Properties and Performance [47].

2.3.3 Applications in Real World uses

Pd-based membrane has numerous applications and the potential of this membrane in real world applications is getting superior gradually. Major industries including fuel cell manufacturing, cement production, and so will directly or indirectly are reliant on this technology.

2.3.3.1 Air Separation

Air separation technologies are crucial in industrial gas generation, with polymeric and cryogenic methods typically prevailing in the sector. Recent focus has shifted to palladium (Pd)-based membranes owing to their remarkable selectivity and catalytic characteristics. Pd membranes are especially beneficial for isolating hydrogen from air or other mixed streams, as they facilitate the dissociation and transport of hydrogen

atoms via the metallic lattice while efficiently excluding bigger diatomic molecules like nitrogen and oxygen. The minor kinetic diameter disparity between N_2 (3.64 Å) and O_2 (3.46 Å) complicates their separation with traditional size-sieving membranes. Pd-based membranes employ a solution-diffusion mechanism that selectively promotes hydrogen permeability, hence facilitating simultaneous H_2 recovery and purification in air separation processes. Palladium alloys, although not commonly employed for bulk O_2/N_2 separation, have shown potential to improve hydrogen rejection efficiency in hybrid air separation systems for oxy-fuel combustion and gas purification applications. Their durability under high operating temperatures and ability for near-infinite selectivity make them attractive for specialized applications where hydrogen impurities in air-derived streams pose challenges. Current research concentrates on alloying palladium with silver, copper, or gold to improve stability and reduce poisoning effects, hence broadening their applicability in air separation technologies.

2.3.3.2 CO_2 Separation

Palladium (Pd)-based membranes, although preliminary used for hydrogen purification, are also instrumental for CO_2 separation in pre-combustion capture processes. In contrast to polymeric membranes that directly separate CO_2 from gas mixtures like natural gas or flue gases, Pd membranes utilize their distinctive hydrogen selectivity. In integrated systems like steam reforming or water-gas shift (WGS) processes, Pd membranes selectively remove hydrogen from a CO_2-laden gas mixture, thereby indirectly facilitating CO_2 separation by concentrating CO_2 in the retentate. This dual functionality enhances hydrogen recovery while altering the chemical balance of reforming and water-gas shift processes, hence improving CO conversion and overall process efficiency.

Palladium-based alloys, such as Palladium–Silver and Palladium–Copper, are promptly utilized to enhance stability in carbon dioxide-rich environments and to mitigate embrittlement at elevated temperatures. These membranes are particularly appropriate for pre-combustion capture methodologies, wherein syngas is generated, and hydrogen is extracted for fuel or electricity production, resulting in a concentrated CO_2 stream for sequestration. Pd-based membranes, despite their limited use for post-combustion capture owing to low CO_2 selectivity, are receiving heightened attention in

hybrid topologies that integrate them with polymeric or ceramic membranes. This integration underscores their capacity to facilitate efficient CO_2 capture in hydrogen-focused energy systems.

2.3.4 Pd-Ag Membrane by SINTEF

Even though palladium-based membrane can achieve ultra-high selectivity of hydrogen, however the permeability of this dense type of membrane is low. Earlier we had to compromise permeability to get high purity. The underlying reason of lower permeability is its dense structure and the researchers realised that this issue can be dealt with by reducing the thickness of this membrane. Hence, it is called thin palladium-based or palladium alloy membrane. Also, the reason behind using alloy with palladium was to merely cut the cost as palladium is costly and a rare metal. In the academia it has been determined that 23 wt. % Ag makes the optimum alloy for hydrogen separation [49, 50].

2.4 Literature Gap

SINTEF assessed the inhibition of H_2S and flux recovery in thin Pd–Ag membranes and separately investigated the inhibition caused by light hydrocarbons. However, combined exposures, order-of-exposure effects, and effective regeneration protocols across different regimes remain underexplored. Furthermore, numerous datasets consist of hundreds of hours at the laboratory scale; there is a necessity for over 5,000 to 10,000 hours of operation under realistic pressure and temperature variations, as well as contaminant drifts, accompanied by standardized degradation metrics and recovery protocols [51]. SINTEF identifies the poor cost–performance of thin Pd–23 wt% Ag membranes as a significant barrier, noting that the consistent techno-economic analysis under actual duty cycles including capital expenditure, operational expenditure, regeneration, replacement is insufficiently reported [52].

3. Theory

3.1 Pd-H_2 System

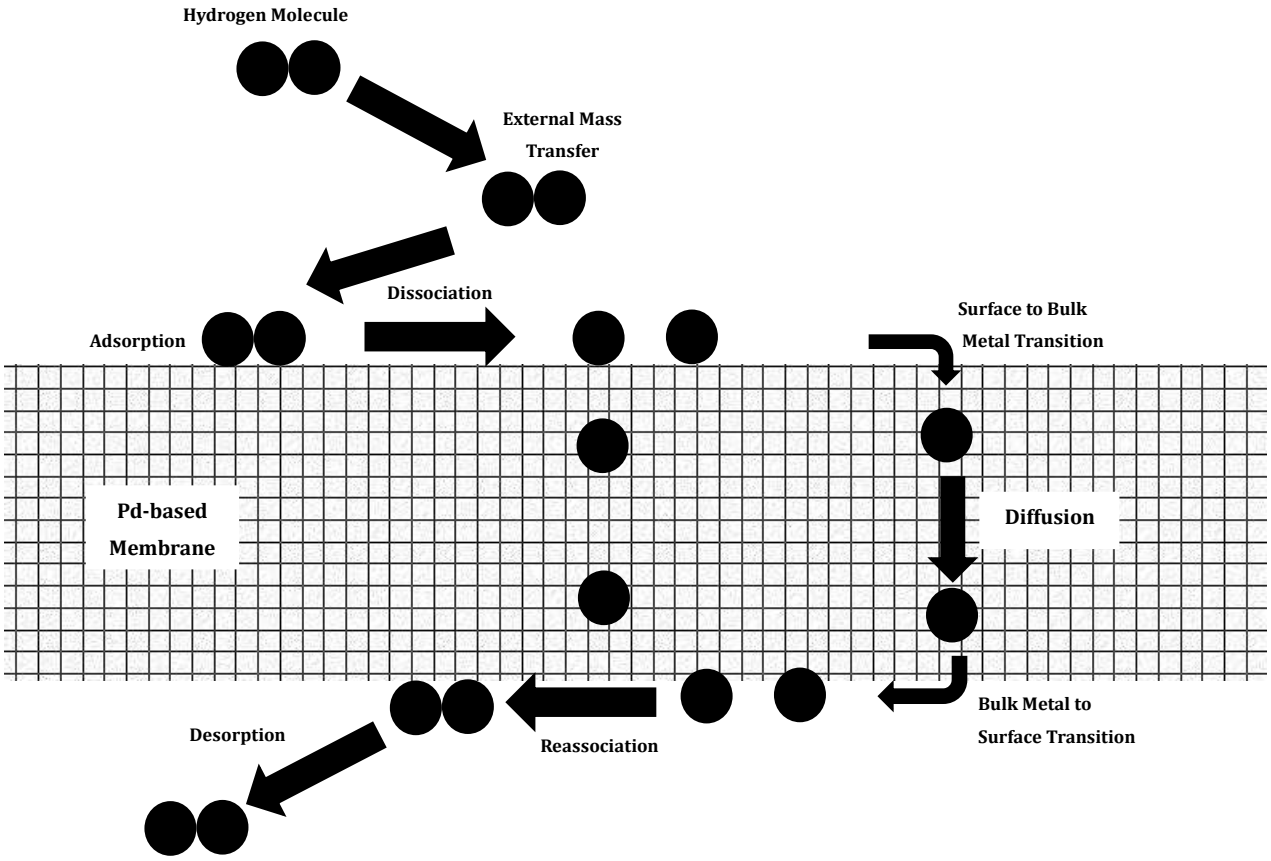

Figure 3.1: Solution-diffusion transport mechanism through Pd-based membrane adopted from [37,53].

Hydrogen permeation through Pd-based membrane can be modelled through solution-diffusion mechanism. As presented in the figure above, the transport mechanism can be described in the following steps:

a) Transport of molecular hydrogen from the bulk gas to the gas layer proximal to the surface.

b) Adsorption onto the surface accompanied by molecular dissociation.

c) Transport of hydrogen atom from the surface into the bulk metal.

d) Diffusion of atomic hydrogen through the bulk metal.

e) Transport of atomic hydrogen from the bulk metal to the surface on the permeate side

f) Reassociative desorption.

3.2 Fick's First Law

Assuming bulk diffusivity is constant, diffusion of hydrogen is rate limiting, and that the driving force for transport can be represented by the sorbed phase atomic hydrogen gradient, Fick's Law gives the steady state hydrogen flux [54]:

$$J_{H_2} = \frac{-DN_b}{2}\frac{dX}{dz}$$

Where,

J_{H_2} is hydrogen flux (mol/m2-s)

D is the hydrogen diffusivity in the bulk metal (m2/s),

X is the bulk composition of hydrogen inside the membrane (mol H/mol Pd)

Nb is the bulk metal Pd concentration (mol Pd/m3)

z is the spatial dimension along the thickness of the membrane

Also, according to Sievert's law hydrogen flux was found to be inversely proportional to thickness with an approximately square root dependence on H2 partial pressure. This behaviour is known as Sievert's law behavior. After applying Sievert's law on Fick's first law, the resultant equation is [54]:

$$J_{H_2} = \frac{P}{t}\left(p_1^n - p_2^n\right)$$

Where,

J_{H_2} is hydrogen flux (mol/m2-s)

P is permeability

t is thickness

p1 is partial pressure on the high-pressure side

p2 is partial pressure on the low-pressure side

If the adsorption equilibrium constant is assumed to be the same on both the feed side and the permeate side of the membrane, then the expression of equation above can be simplified in the Sieverts' Law format as follows [54]:

$$J_{H_2} = \frac{P}{t}\left(p_1^{0.5} - p_2^{0.5}\right)$$

Rate Limiting Step	Conditions
Diffusion	(i) Absence of mass transfer resistance (ii) Temperature above 573 K (iii) t ≤ 10μm (iv) Clean Pd
Desorption	Low Temperature
Adsorption	(i) low upstream H2 partial pressure (ii) Contamination
External mass transfer	(i) t ≤ 10 μm (ii) Low H2 partial pressure (iii) Porous support present
Fabrication Methods	(i) Film micro-structure, grain size, surface or grain boundary, contamination. (ii) t ≤ 10 μm

Table 3.1: Rate limiting steps in the hydrogen permeation through Pd-based membranes (Adopted from [53]).

It is established that if no external mass transfer resistance is present, practically diffusion limited permeation is expected for uncontaminated palladium-based membrane for temperature above 573 K with a membrane thickness down to 1 μm. However, as the membrane thickness descends down to critical thickness, the solid-state diffusion will become prompt enough that other rate processes including mass transfer, sorption and transition as well as surface topography will impact significantly, and eventually limit, the permeation rate. This certain phenomenon is called deviation from Sievert's law behavior [53].

3.3 Sieverts' Law and Arrhenius Plot

3.3.1 Background and Significance

As discussed before, dense Pd-based membranes facilitate the separation of H_2 through the solution–diffusion mechanism. H_2 dissociates on the feed-side surface, and atomic

H dissolves into the metal, diffusing through the lattice before recombining or desorbing on the permeate side. This process results in almost perfect H_2 selectivity through a defect free membrane [68]. The transfer mechanism can be represented through the following equation:

$$\frac{1}{2}\, H_2(g) \leftrightharpoons\ H_{(Dissolved)}$$

This equation establishes a relationship between gas-phase pressure and the chemical potential of dissolved hydrogen, forming the basis for the classical derivation of flux laws [66]. In scenarios where bulk diffusion is the rate-limiting factor and surface steps occur rapidly, the outcome is characterized by Richardson's/Sieverts-type permeation law, which exhibits a square-root dependence on pressure along with a permeability prefactor. This notion can be represented as:

$$J \propto\ P_{H_2}^{0.5}{}_{Feed} -\ P_{H_2}^{0.5}{}_{Permeation}\ \text{[66].}$$

In practical applications, real modules frequently encounter mixed feeds and gas-side mass-transfer effects, such as concentration polarization or adsorption, which can alter the pressure exponent from 0.5 and potentially skew transport parameters if not properly considered. This underscores the necessity of explicitly testing Sieverts' law in Pd(-Ag) systems.

In the dilute-solution limit for dissociative gases, Sieverts' law indicates that the concentration of dissolved hydrogen in a metal (e.g. Pd) is proportional to the square root of the hydrogen partial pressure. According to Sieverts' law:

$$C =\ K_s\sqrt{p_{H_2}}\ \text{[68].}$$

Where,
C is concentration or solubility
K_S is Sieverts' constant
p_{H2} is partial pressure of pure hydrogen

This equation is directly derived from the equilibrium equation of hydrogen diffusion, by comparing chemical potentials. Also, for ideal dilute solutions, determining activity

with concentration, it infers that solubility is proportional to the square root of permeability [66]. The square-root dependence indicates the dissociation of a diatomic hydrogen molecule into two hydrogen atoms before being dissolved into the lattice [69]. Deviations from the characteristics of $C \propto P^{0.5}$ occur at elevated H loadings (non-dilute behavior) or when surface/mass-transfer resistances are significant, necessitating more comprehensive analyses beyond the basic Sieverts model in permeation experiments.

3.3.2 Integration of Flick's Law and Sievert's Law

Under steady state conditions governed by bulk diffusion, the integration of Fick's law and Sieverts' law results in the established permeation expression.

$$J_{H_2} = \frac{DK_S}{t} \left(p_1^{0.5} - p_2^{0.5} \right) \text{ [68].}$$

From this relationship, we can derive that:

$$K_S = \frac{P}{D}$$

Where,
K_S is Sieverts' constant
P is Permeability
D is Diffusivity

If we would like to acquire diffusivity, from the above equation, we need permeability and Sievert constant. We have already got the permeability from our experiments. Furthermore, we will extract value of Sievert constant from the publication from Venvik et. al. [70].

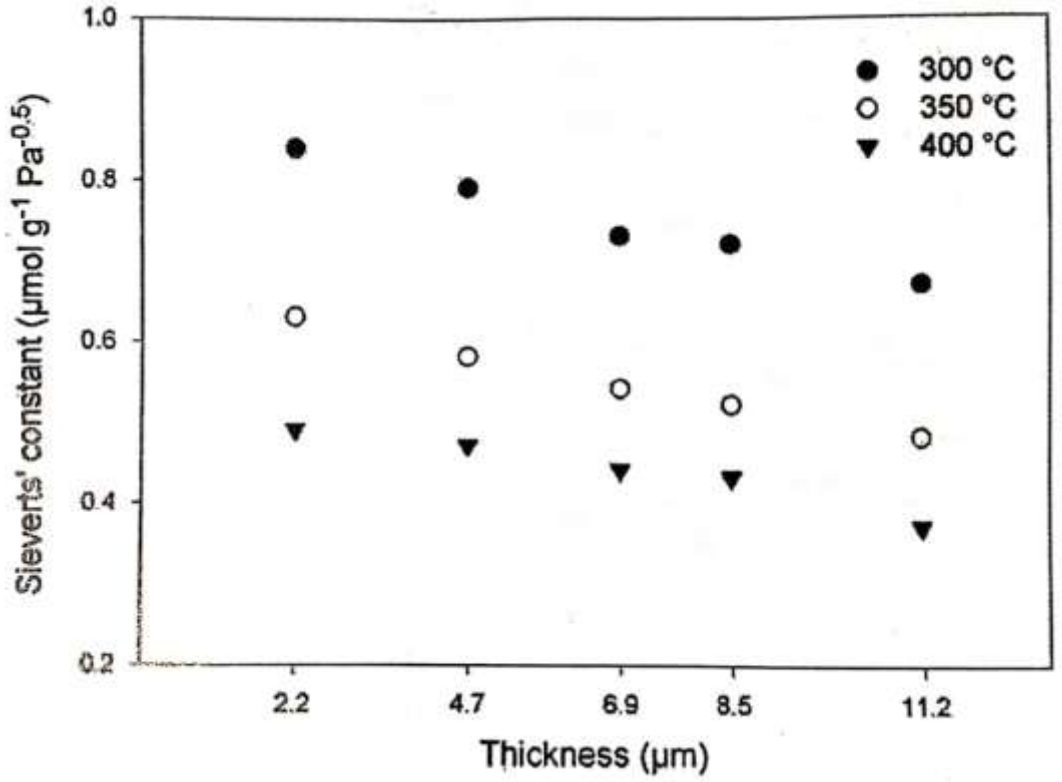

Figure 3.2: Sievert's constant as a function of the thickness of Pd77%Ag23% thin film membranes at various temperatures [70].

Hydrogen diffusivity in Pd-alloy membranes is thermally activated and is commonly described by an Arrhenius form:

$$D\ (T) = \ D_O e^{-E_D/RT}\ \text{[67].}$$

Where,

D is Diffusivity

D_O is Pre-exponential factor

E_D is activation energy for diffusion

R is gas constant

T is Temperature

Taking natural logs gives the linear relationship:

$$\ln D = \ln D_O - \frac{E_D}{RT}$$

4. Materials and Membranes

Palladium membranes have garnered increasing attention in recent years for hydrogen purification and H2 production via membrane reactors, attributed to their exceptional permeability and selectivity for H2. Pure Pd membranes frequently suffer from hydrogen embrittlement due to the ab phase transition of palladium hydride, which can take place at temperatures below the critical threshold of 293 °C and pressures below 2 MPa. Palladium is frequently alloyed with silver to prevent embrittlement, which also enhances hydrogen permeability by up to 70% relative to pure palladium. The optimal hydrogen permeability is achieved with a silver content of approximately 23 wt.% Ag (Pd77Ag23) [60-62]. During our experiments, we have evaluated the performance of two membranes, including a 10 μm membrane made by SINTEF Industry and a 5.5 μm membrane made by Hydrogen Mem Tech. SINTEF Industry used DC Magnetron Sputtering Method to make their 10 μm membrane on perfect silicon wafer whereas Hydrogen Mem Tech manufactured the 5.5 μm using Magnetron Sputtering on a glass plate.

4.1 Magnetron Sputtering

There are numerous methods described in the scientific literature for deposition of Pd and Pd-alloy layers onto substrates. Some of the prominent technologies are electroless plating (ELP), chemical vapor deposition (CVD) physical vapor deposition (PVD) including magnetron sputtering (PVD-MS). Magnetron sputtering can further be distributed into DC Magnetron Sputtering and RF Magnetron Sputtering. Based on the criteria of substrate, membrane synthesis technology can further be distributed into two types: Self-supported membrane and Supported membrane. Magnetron sputtering is a sub-type of sputtering method. The only difference is that there is a magnetron present behind the target metal that with maintain a magnetic field perpendicular to the electric field. The role of the magnetron is to create a spiral motion on the surface of the metals to keep the electrons attached a bit longer [55]. Magnetron sputtering is a very attractive deposition technique, as it delivers sub-micrometric homogeneous layers with a meticulous composition across the thickness, with apt Ag contents that is up to or higher than 23%. The advantages of this method include dense, uniform, and

high-purity films with good adhesion, control over film composition and properties as well as scalability and reproducibility [56].

4.1.1 Magnetron Sputtering on Si Wafer

According to Fernandez et al [56], a perfect silicon wafer is used as a temporary or permanent support in different industries including semiconductor processing, membrane manufacturing and advanced packaging. Its material and processing characteristics make it one of the most reliable supports in pd-based membrane manufacturing. It provides an abundantly fine and uniform surface for sputter-deposited Pd or Pd–Ag films. This smoothness is instrumental to ensuring spotless, super thin, homogeneous metal layers, which are crucial for high hydrogen permeability and selectivity in Pd-based membranes [57].

4.1.2 Magnetron Sputtering on Glass plate

Glass plate is a suitable support for thin film deposition of Pd based membrane, as it is flat, stable, and chemically inert. One of the major advantages of using glass substrates are typically being able to clean the organic residues of the surface using plasma cleaning or UV-ozone treatment, because of its diaphanous nature [59]. However, there are numerous drawbacks in using this type of support, such as porosity challenge, heat resistance lacking, weakness in durability, to name a few. The disadvantages of glass plate support will be discussed in detail in section 4.3.

4.2 Membrane by SINTEF Industry

The SINTEF Industry membrane was manufactured by DC-Magnetron Sputtering in two steps. First, a Pd/Ag23 wt.% target layer was deposited onto polished silicon single-crystal substrates, then the films are carefully peeled away from the silicon support and mounted to a porous stainless-steel support [56]. This enables the fabrication of defect-free high-flux membranes, approximately 2-3 μm in thickness, supported on macroporous substrates, suitable for operation at elevated pressures [51].

4.2.1 Topography of the membrane

The analysis of the Pd-Ag membrane thin films' surfaces was executed using atomic force microscopy (AFM). The results reveal that the grain size increased from 120 nm to 250–270 nm, as well as the film surface roughness rose from 4–5 nm to 10–12 nm as the temperature was elevated from approximately 360 K to 510 K. Following the determination of optimal conditions for achieving minimal grain size on silicon wafers, thin Pd-Ag films were deposited on various porous support. The porous supports significantly affect topography. Fine-pore supports (3–5 nm γ-Al_2O_3 or ZrO_2) produce dense columnar Pd–Ag films, whereas larger pore supports ($\geqslant$100 nm Al_2O_3) facilitate open columnar growth characterized by inter-grain voids. In the examined membranes, defects manifested as pinholes due to stress and creep, resulting in localized porosity that undermined selectivity. AFM analysis indicated that roughness increases with both deposition temperature and thickness: approximately 4–5 nm root mean square roughness observed at low temperatures (approximately 360–410 K). On the other hand, approximately 10–12 nm root mean square roughness observed at elevated temperatures ranging from 505 to 515 K [56,63].

4.2.2 Characteristics and Performance

The SINTEF Pd–23%Ag membrane, created through the sputtering of thin films onto silicon wafers and subsequently transferred to porous stainless-steel tubes, demonstrates both scalability and notable performance. The active layer, with a thickness of roughly 2 μm, attains hydrogen fluxes of up to 2477 $mL \cdot cm^{-2} \cdot min^{-1}$ (approximately 18.43 $mol \cdot m^{-2} \cdot s^{-1}$) at a temperature of 400 °C and a hydrogen feed pressure of 26 bar. Permeance is approximately constant at $\sim 1.5 \times 10^{-2}$ $mol \cdot m^{-2} \cdot s^{-1} \cdot Pa^{-0.5}$ across varying pressures, suggesting that transport adheres to Sieverts' law. Selectivity is notably high, exceeding 7500 at approximately 2 bar and around 2900 at 26 bar. Long-term trials demonstrated stable operation exceeding one year, with estimated lifetimes ranging from 1.6 to 2.5 years at 400 °C. [63].

4.3 Membrane by Hydrogen Mem-Tech

This particular membrane has been manufactured by Norwegian company Hydrogen Mem-Tech. It is synthesized via magnetron sputtering on a glass substrate. The

company website states that their membrane enables selective hydrogen separation with recovery rates of up to 99%, allowing for the synthesis of both industrial-grade and ultra-high-purity hydrogen from diverse feed gases. The design features modularity, compactness, and scalability, utilizing ultra-thin membranes affixed to substrate plates and organized in cassettes to promote efficient flow and seamless integration at minimal expense. The operation is straightforward and secure, featuring no moving components, no need for chemical cleaning, and a high tolerance for vibrations, which guarantees dependable performance with minimal maintenance and low noise levels [64]. Even though, this membrane is manufactured using the similar technology as SINTEF Industry, the substrate used in this case is different. Hence, there are some differences in case of characteristics and performance. We did not find any specific literature from the manufacturers about this specific membrane. So, we compared a similar membrane studied by Gobina et. al [58].

4.3.1 Topography of membrane

Pd–Ag membranes sputtered onto porous Vycor glass resulted in dense, continuous films measuring approximately 5–8 μm in thickness, characterized by fine submicron grains that coarsen with increasing thickness, as verified by SEM analysis. The deposition successfully occluded the approximately 40 Å pores of Vycor, creating a non-porous upper layer essential for attaining 100% hydrogen selectivity. Surface examination indicated a homogeneous, dense structure with negligible roughness variation (about 6.7%). The lack of nitrogen leakage further indicated well-packed grain boundaries devoid of pinholes or open defects. EPMA confirmed that the alloy composition (77:23 wt% Pd–Ag) remained intact, showing no evidence of contamination, peeling, or cracking, which indicates robust adhesion and long-term stability of the membranes [58].

4.3.2 Characteristics and Performance

Pd–Ag membranes on porous Vycor glass constitute a significant initial advancement in the field of hydrogen separation research. Pd–Ag alloy films, approximately 5–8 μm thick, were deposited via sputtering using Vycor tubes with pore sizes of around 40 Å. The membranes performed with total hydrogen selectivity, completely rejecting nitrogen, with hydrogen recovery achieving up to 90% at a pressure differential of 7

bar. The permeability inferred an Arrhenius relationship, with values approximately 2.3×10^{-5} $cm^3\cdot cm/(cm^2\cdot s\cdot atm^{0.5})$ at 780 K. The operation demonstrated stability during prolonged testing, with no instances of peeling or delamination noted. Vycor demonstrated significant thermal and chemical resistance, despite exhibiting modest flux relative to contemporary membranes [58].

4.4 Comparison between Glass membrane and Si Wafer Membrane

Characteristics/ Performance	Pd–Ag on Vycor glass (Gobina et al.)	Pd – 23%Ag (Si wafer → steel) (SINTEF)
Film thickness	5–8 μm (~6 μm)	~2 μm
Pressure tested	Δp up to 7 bar (measured)	2 bar and up to 26 bar feed H_2
Flux (as reported)	Flux not given directly (derived via Arrhenius)	At 400 °C, 26 bar: 2477 $mL\cdot cm^{-2}\cdot min^{-1}$ (STP) ≈ 18.43 $mol\cdot m^{-2}\cdot s^{-1}$ (SI) At 2 bar: ≈ 902 $mL\cdot cm^{-2}\cdot min^{-1}$ (calc.) ≈ 6.71 $mol\cdot m^{-2}\cdot s^{-1}$
Flux (Calculated)	$4.48\times10^{-2}\ {mol}/{m^2-s}$	$6.71\ {mol}/{m^2-s}$ (2 bar)
Permeance	5.361×10^{-5} $mol\cdot m^{-2}\cdot s^{-1}\cdot Pa^{-0.5}$ (calculated)	Permeance ≈ 1.5×10^{-2} $mol\cdot m^{-2}\cdot s^{-1}\cdot Pa^{-0.5}$
Selectivity	100% H_2 (no N_2 detected)	>7500 (99.99%) (2 bar) ~2900 (99.96%) (26 bar)

Table 4.1: Performance comparison between Pd–Ag on Vycor glass (Gobina et al.) and Pd–23%Ag (Si wafer → steel) (SINTEF) (Adopted from [58,63])

4.5 Conclusion

Comparing Pd–Ag membranes on Vycor glass with those developed by SINTEF on stainless steel supports reveals several differences. Even though the membrane on Vycor glass display perfect selectivity, however its permeance is much inferior compared to the SINTEF Industry membrane. Vycor glass support membrane exhibits fine porosity and a smooth surface, facilitating excellent adhesion for sputtered films and high-temperature resistance. However, its small pore size and fragile structure restrict mechanical robustness and large-scale applicability. The control of grain size is imprecise, and surface roughness may result in alteration of topography, thereby reducing flux. On the other hand, while SINTEF Industry membrane shows superior performance in the case of permeance, it yields a hydrogen with the purity of 99.99% (4.0) at 2 bar and 99.96% (3.6) at 26 bar. Even though this purity is not acceptable in semiconductor industry, this will be suitable for most of the industries including Fuel Cells. The SINTEF Industry membranes utilize porous stainless-steel supports, which enhance mechanical strength, pressure tolerance, and scalability. Thin films and controlled grain growth reduce roughness, while Pd–Ag provides chemical resistance to reactive gases. To sum up, SINTEF's design integrates durability, high flux, and industrial applicability, whereas Vycor support membrane demonstrates superior selectivity primarily at laboratory scales and moderate pressures [58,63].

5. Experimental

A set of experiments have been conducted to assess the characteristics and performance of a particular model of aforementioned SINTEF Industry membrane with a thickness of 10 μm as well as a Hydrogen Mem-tech Membrane with the thickness of 5.5 μm. To recap, the SINTEF Industry membrane has been manufactured through DC-Magnetron Sputtering on a temporary Si Wafer support. On the other hand, the Hydrogen Mem-Tech Membrane has been synthesized through Magnetron Sputtering method on a glass plate support. As we have already discussed the characteristics and performance of these membranes from literature, it will assist us while assessing the membranes reviewed by us and find the underlying causes why they behave the way they do.

5.1 Risk Analysis

The risks associated with experimental laboratory work were assessed, and the findings are presented in Appendix F. The risk analysis was distributed into three steps including bow-tie analysis, risk matrix and Failure Mode and Effects Analysis (FMEA). In summary, leakage, fire, and exposure to toxic and flammable substances (NH3, H2) were identified as the most probable occurrences and highest risks in this study. Then relevant measures have been taken to minimize the risk level to close to zero. Continuous leak testing was conducted prior to and during experiments to prevent these occurrences.

5.2 Experimental Setup

Our experiment starts with the mounting of the microchannel membrane reactor. In this section, it will be discussed how the microchannel membrane reactor is assembled followed by how lab view was set up to control the experiments. Furthermore, the equipment that have been used in the experiments will be described briefly.

5.2.1 Membrane Assembly

The assembly of the membrane module involves a precise, multi-step process aimed at ensuring structural stability, leak-tightness, and optimal performance during

operation. The procedure initiates with the precise alignment of the module's permeate side with the copper gasket, succeeded by the positioning of the channel layer to offer support and delineate the flow path [16]. All membranes were detached from the silicon wafer and mounted in a microchannel configuration, facilitating hydrogen permeation experiments with minimal gas transfer limitations. The effects of hydrogen depletion in the configuration are mitigated by the increased flow of hydrogen. High hydrogen concentration, combined with a small channel cross-section that restricts diffusion distance, effectively minimizes concentration polarization [37]. The placement of the feed side finalizes the layered structure, after which the module is secured with bolts that are evenly tightened using a hex key and wrench to endure high temperatures. Punched holes in the membrane were created using a copper wire to indicate the positions of the screws. The channel housing was positioned on top and secured by alternating the tightening of the screws to avoid straining the membrane. Excess membrane was excised and placed in a bottle as residue. Upon assembly, the module is affixed to the testing apparatus, with connections to the feed and permeate gas lines established using suitable wrenches to avoid stress on the fittings. Leak testing involves the introduction of inert gases, such as nitrogen or argon, under controlled conditions, ensuring that all valves are appropriately configured to prevent premature gas flow. The module integrates with mass flow controllers (MFCs) and is monitored through a computer interface to regulate gas flow rates and validate performance. This systematic method safeguards the integrity of the membrane assembly, reduces the likelihood of leakage or mechanical failure, and confirms the reliability of the configuration for future experimental testing [65].

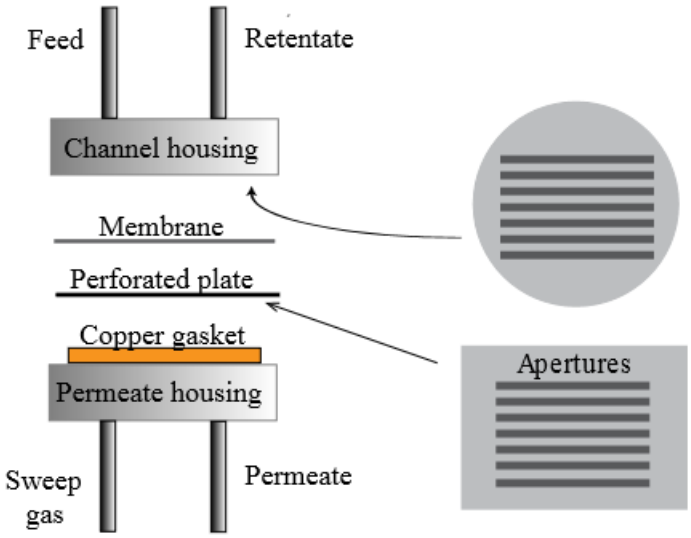

Figure 5.1: Microchannel parts and configuration

5.2.2 Lab View

LabVIEW was employed as the primary control and monitoring platform for the experimental setup. The software facilitated interaction with the mass flow controllers (MFCs) that manage nitrogen and hydrogen streams mainly on the feed side of the membrane module in the context of our experiment. A custom-designed virtual instrument (VI) was created to regulate flow rates, alternate gases, and record real-time data during testing. The graphical programming environment facilitated ongoing monitoring of pressure, temperature, and flow signals, thereby ensuring stable operating conditions and precise control of experimental parameters. LabVIEW facilitated automated data acquisition, reducing human error and allowing for synchronized recording of permeation performance alongside process conditions. The integration enhanced operational efficiency, increased reproducibility, and enabled swift modifications during leak testing and membrane performance assessment.

5.3.3 Gas Flow

The microchannel housing was positioned within a furnace in the hydrogen permeation apparatus. Mass flow controllers (MFCs) were employed to regulate the flow of all gases. The calibration of mass flow controllers for each gas was conducted utilizing a soap film meter. A Micro-GC (Agilent) was utilized to assess potential failure or leakage by introducing nitrogen. There was a needle valve placed between Micro GC and Retentate stream. No instances of N2 were observed during the experimentations. Therefore, the selectivity achieved was 100%.

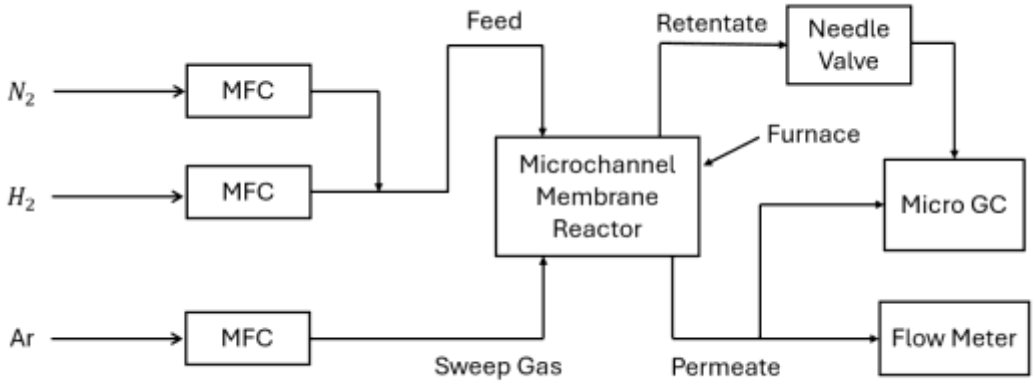

Figure 5.2: Gas flow of the microchannel membrane reactor system (Simplified, for detailed, refer Appendix E)

5.3 Heat Treatment

Heat treatments were performed on Pd–Ag23wt% membranes with thicknesses of 5.5 µm and 10 µm to enhance stability, reproducibility, and hydrogen permeation characteristics. Two treatment procedures were utilized.

5.3.1 Heat treatment in air (HTA)

Membranes were subjected to ambient air at a temperature of 350 °C. Prior to the introduction of air, hydrogen was removed from the system by passing nitrogen on the feed side and argon on the permeate side for a duration of 15 minutes. Air was introduced by opening the microchannel tubes, with each exposure maintained for one hour. After each step, nitrogen and argon were reintroduced for a duration of 15 minutes to eliminate oxygen prior to the reintroduction of hydrogen.

5.3.2 Heat treatment in H_2/N_2 atmosphere

A subsequent treatment was conducted at 350 °C using a controlled H_2/N_2 mixture with a total flow rate of 400 ml/min and a H2 and N2 volume ratio of 80:20. This treatment kept running until the permeation got stabilized. Exposing the membrane to a hydrogen/nitrogen atmosphere maintains a metallic and clean surface, which may influence the permeability of hydrogen.

5.4 Permeation Experiments

Experiments on hydrogen permeation were conducted to assess the transport properties of Pd-based membranes across various operating conditions. Measurements were conducted utilizing hydrogen and nitrogen mixtures under varying total flow rates, partial pressures, and temperatures, without the presence of sweep gas, to maintain clearly defined hydrogen partial pressures across the membrane. The temperature was controlled using an oven and while changing the temperature, a rate of 2 °C/ min was maintained so that any excessive stress is not applied to the membrane. The temperature was monitored using an N-type thermocouple positioned near the membrane housing. The permeance was assessed as a function of feed pressure and temperature, with multiple repetitions conducted during the experimental period to ensure reproducibility. As seen in the Figure 5.2, the permeance was measured using a flow meter. The unit that the permeance was measured in was mL/min. Later the measured permeance was converted into flux and permeability. Refer Appendix A for detailed calculations of Flux and Permeability.

5.4.1 Permeation Experiments of 10 μm Membrane

The 10 μm thick Pd-based membrane was investigated in a flat, self-supported configuration to assess the effect of thickness, pressure, and concentration polarization on hydrogen transport. Permeation behavior of pure hydrogen (purity 5.0) from a feed mixture of hydrogen and nitrogen through Pd77%Ag23% membranes was studied as a function of temperature, flow rate and partial pressure of hydrogen with no use of sweep gas. Experiments were conducted at specified temperatures of 300 °C, 350 °C and 400 °C. The 10 μm thick Pd–Ag23wt% membrane demonstrated stable and

reproducible results in permeation experiments following heat treatment in air and in H_2/N_2 (350 °C, H_2/N_2 = 320:80 ml/min).

Experiment	Thickness (μm)	Temperature	Total Flow	Flow Ratio (H2: N2)
1a	10	300	200	80:20
1b	10	350	200	80:20
1c	10	400	200	80:20
2a	10	300	400	80:20
2b	10	350	400	80:20
2c	10	400	400	80:20
3a	10	300	100	100% H2
3b	10	350	100	100% H2
3c	10	400	100	100% H2
4a	10	300	200	100% H2
4b	10	350	200	100% H2
4c	10	400	200	100% H2
5a	10	300	200	50:50
5b	10	350	200	50:50
5c	10	400	200	50:50

Table 5.1: Experiment Conditions in the case of 10 μm Membrane

5.4.2 Permeation Experiments of 5.5 μm Membrane

The 5.5 μm thick Pd-based membrane was assessed primarily to study hydrogen flux increase due to reduced thickness, as well as to examine tolerance against possible inhibiting species.

Experiment	Thickness (μm)	Temperature (℃)	Total Flow (H2+N2)	Flow Ratio (H2: N2)
6a	5.5	300	200	80:20
6b	5.5	350	200	80:20
6c	5.5	400	200	80:20
7a	5.5	300	400	80:20
7b	5.5	350	400	80:20
7c	5.5	400	400	80:20
8a	5.5	300	200	75:25
8b	5.5	350	200	75:25
8c	5.5	400	200	75:25
9a	5.5	300	400	75:25
9b	5.5	350	400	75:25
9c	5.5	400	400	75:25
10a	5.5	300	200	100% H2
10b	5.5	350	200	100% H2
10c	5.5	400	200	100% H2

Table 5.2: Experiment Conditions in the case of 5.5 μm Membrane

6. Results

6.1 Comparison to Literature

According to Vicinanza et al, the experimentally acquired permeability for 2.2 micron membrane ranges from $2.0*10^{-8}$ mol.m^{-1}s^{-1}Pa$^{-0.5}$ to $2.7*10^{-8}$ mol.m^{-1}s^{-1}Pa$^{-0.5}$ for different temperatures and heat treatment conditions [37]. However, from Mejdell et al, for the same thickness, the permeability ranges from $7.7*10^{-9}$ mol.m^{-1}s^{-1}Pa$^{-0.5}$ to $1.0*10^{-8}$ mol.m^{-1}s^{-1}Pa$^{-0.5}$. When the thickness is increased to 5 micron from 2.2 micron, the permeability goes as high as $1.6*10^{-8}$ mol.m^{-1}s^{-1}Pa$^{-0.5}$[16]. For our 5.5 micron membrane, the permeability ranges from $4.21*10^{-9}$ mol.m^{-1}s^{-1}Pa$^{-0.5}$ to $4.73*10^{-9}$ mol.m^{-1}s^{-1}Pa$^{-0.5}$. So, the experimental acquired permeability is only third of the literature reference value. From Vicinanza et al, the permeability for 11.1 micron membrane is $2.2*10^{-8}$ mol.m^{-1}s^{-1}Pa$^{-0.5}$[37]. However, for our 10 micron membrane the permeability ranges from $7.62*10^{-9}$ mol.m^{-1}s^{-1}Pa$^{-0.5}$ to $8.76*10^{-9}$ mol.m^{-1}s^{-1}Pa$^{-0.5}$. Compared to Vicinanza et al, the result is one third, whereas compared to Mejdell et al, our permeability is pretty close.

Membrane Thickness	Vicinanza et. al [37] (mol.m^{-1}s^{-1}Pa$^{-0.5}$)	Mejdell et. al [16] (mol.m^{-1}s^{-1}Pa$^{-0.5}$)	This study (mol.m^{-1}s^{-1}Pa$^{-0.5}$)
2.2 μm	$8.2*10^{-9}$ - $1.1*10^{-8}$	$7.7*10^{-9}$ - $1.0*10^{-8}$	-
4.7 μm	$1.3*10^{-8}$ - $1.7*10^{-8}$	-	-
5 μm	-	$1.4*10^{-8}$ - $1.6*10^{-8}$	-
5.5 μm	-	-	$4.21*10^{-9}$ – $4.73*10^{-9}$
8.5 μm	$1.6*10^{-8}$ - $2.1*10^{-8}$	-	-
10 μm	-	-	$7.62*10^{-9}$ – $8.76*10^{-9}$
11.2 μm	$2.2*10^{-8}$	-	-

Table 6.1: Comparison of the results of this study with Vicinanza et. al [37] and Mejdell et. al [16].

6.2 Gas mixture effects

6.2.1 Total Flow Dependency

At this section, effects arising from H_2-N_2 mixtures as well as the behaviour of hydrogen alone have been analysed. The dependency of hydrogen permeability through the 10 µm thin Pd-Ag membrane on total flow of hydrogen and nitrogen has been studied at different temperatures including 300 °C, 350 °C, and 400 °C. This analysis has been made for different H_2/N_2 flow ratio including 80:20, 100% Hydrogen and 50:50. The reported permeability values reflect the average across various binary mixtures under each condition. At 400 °C, it has been found that the dependence of hydrogen permeability on total flow is insignificant that indicates of no influence of external mass transport on hydrogen transport. At 80: 10 ratio, the permeability has shown decreasing trend with increasing total flow. On the other hand, for 100% hydrogen, there was barely any dependence of permeability with total flow.

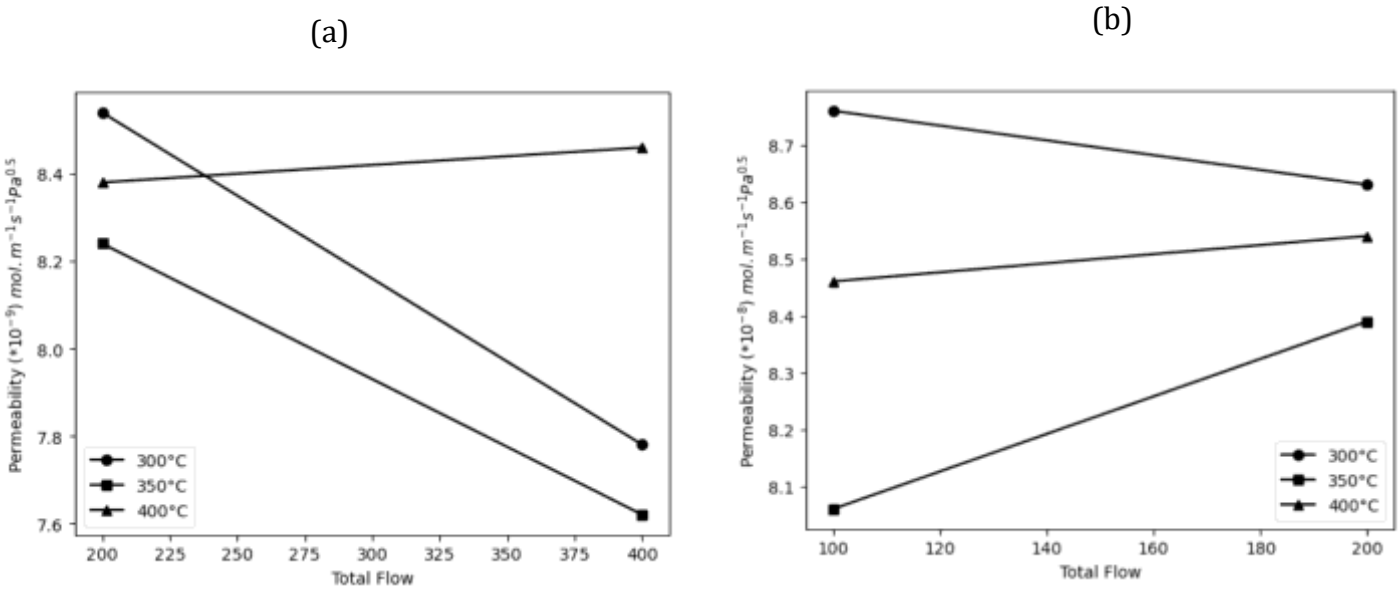

Figure 6.1: Total Flow Dependency of 10 µm Membrane (a) For 80:20 Flow Ratio, (b)For 100:0 Flow Ratio

For the thin 5.5 µm Pd-Ag membrane, an opposite trend is observed. The hydrogen permeability acquired for this membrane showed an increasing trend with increasing total flow rate across all operating temperatures. The increase rate of permeability is

approximately identical across all operating temperatures. This pattern of behaviour indicates that for thinner membranes, increased feed velocities alleviate concentration polarisation at the membrane surface, thus augmenting the effective driving force for hydrogen permeation. To summarize, while the 10micron membrane is primarily influenced by bulk transport within the metallic layer, but the 5.5 μm membrane is significantly impacted by boundary-layer phenomena, rendering flow management a crucial element for performance optimisation.

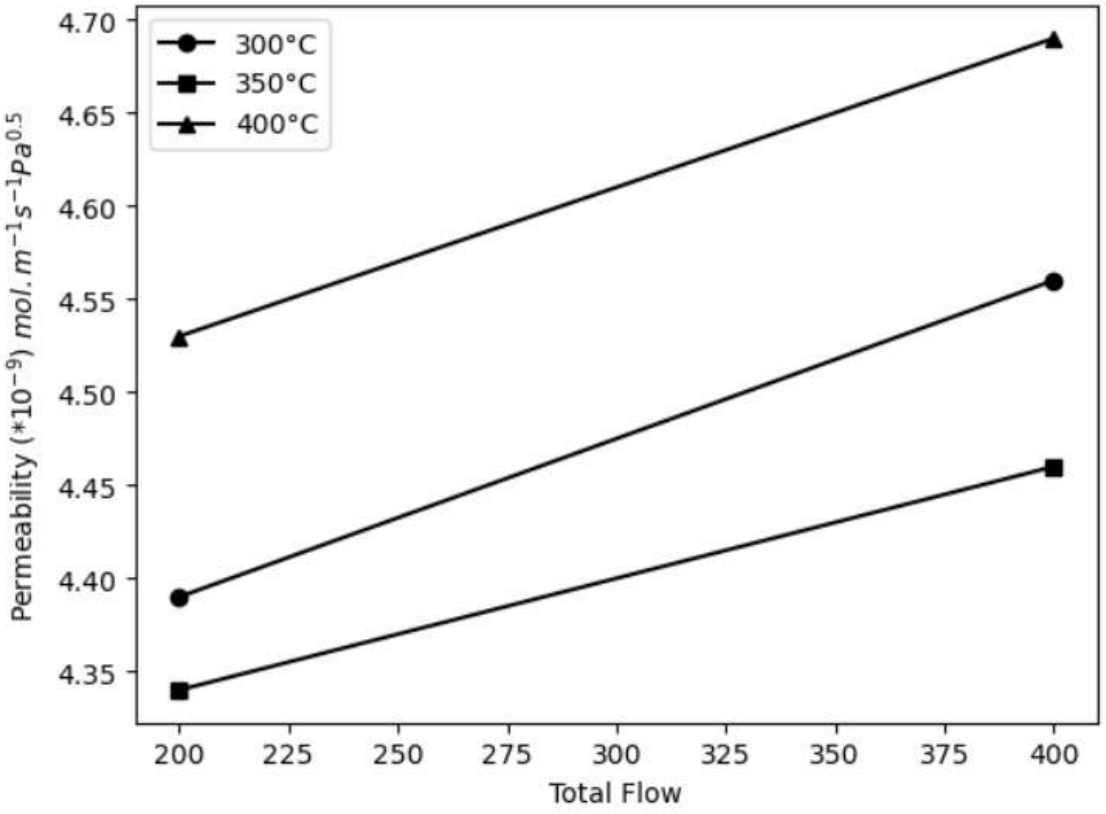

Figure 6.2: Total Flow Dependency of 5.5 μm Membrane

6.2.2 Depletion and Concentration Dependency

This study examines the relationship between hydrogen permeability and hydrogen concentration in a 10 μm thin Pd-Ag membrane at temperatures of 300 °C, 350 °C, and 400 °C. For 10 μm membrane, hydrogen permeability showed an increasing trend across all the temperatures with an increasing hydrogen concentration. However, the effect is more pronounced for 300 degree celcius. Therefore, for 10 μm membrane, the dependence on hydrogen concentration is evident across all temperatures. like the 5.5

μm membrane, for the 10 μm membrane, hydrogen concentrations had less impact on hydrogen permeation at higher temperatures compared to that of lower temperatures.

This study examines the relationship between hydrogen permeability and hydrogen concentration in a 5.5 μm thin Pd-Ag membrane at temperatures of 300 °C, 350 °C, and 400 °C. The effect of hydrogen concentration on permeability in the 5.5 μm Pd-based membrane was evaluated by averaging data from different total flow rates. Across all the temperature points, permeability displayed an increasing trend with increasing hydrogen concentration. However, the effect is more pronounced for 300 degree Celsius compared to other temperatures.

(a) (b)

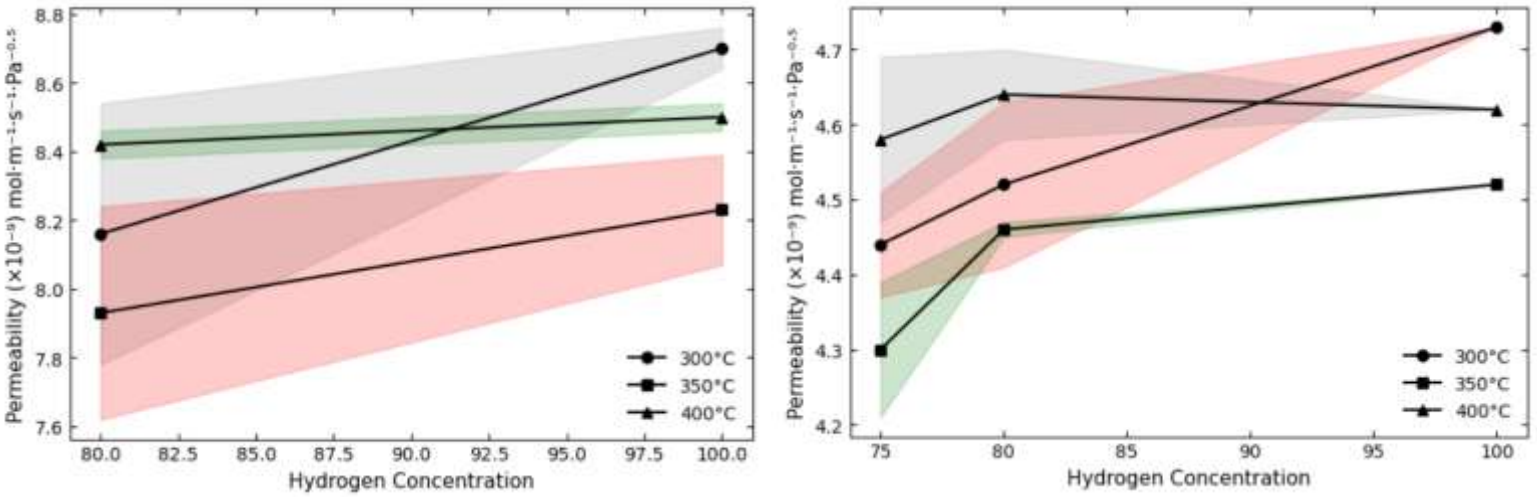

Figure 6.3: Hydrogen Concentration effect (Along with deviation range) on (a) 10 μm membrane, (b) 5.5 μm Membrane.

6.3 Temperature Dependence

From Vicinanza et al, the relation between permeability and temperature is increasing. So, with increasing temperature, the permeability increases from $2.22*10^{-8}$ $mol.m^{-1}s^{-1}Pa^{-0.5}$ to $2.27*10^{-8}$ $mol.m^{-1}s^{-1}Pa^{-0.5}$. However, for our experiment, we do not see a similar

trend. Because, for 350 degree Celsius, we see a decreasing trend and increasing trend for 400 degree Celsius.

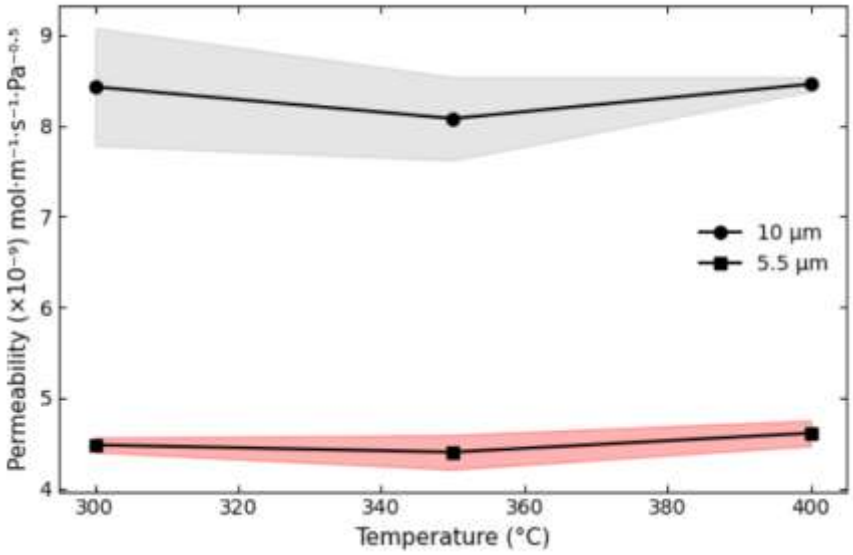

Figure 6.4: Temperature Dependence (Along with deviation range) on (a) 10 µm membrane, (b) 5.5 µm Membrane.

6.4 Hydrogen Solubility and Diffusivity in Pd-Ag Membrane

As part of our next study, the natural logarithm of diffusivity and the correspondent inverse temperature will be plotted to evaluate a linear dependency of both membranes in accordance with Sieverts' law. This type of validation is crucial for verifying whether the rate-limiting step is bulk diffusion through the metal lattice rather than surface adsorption or desorption processes as well as mass transfer. The synthesis mode, surface architecture and flaws could be identified as the underlying reason of the deviations from linearity. If linearity with accordance with Sievert's law is identified for a membrane, it assures that the permeability values that are produced are reproducible and may be reliable in the design and performance assessment of hydrogen separation membranes.

Under steady state conditions governed by bulk diffusion, the integration of Fick's law and Sieverts' law results in the established permeation expression.

Permeability, P= $K_S D$

$Density, \rho$= 12.0e6

Diffusivity, D= $\frac{P}{K_S \rho * 10^{-6}}$

Diffusivity, D= $\frac{P}{12 * K_S}$

From the equation P= $K_S D$, we can get diffusivity (D) by inserting the values of permeability and sievert constant into the equation. From figure 3.2, we can extract the values of sievert constant and the values of diffusivity at specific membrane thickness and particular temperature. Afterwards, with these values, we could do our calculations.

6.3.1 5.5 µm Membrane

Temperature (K)	Sievert Constant (Ks) ($\mu mol/gPa$^0.5)	Permeability (mol/msPa^0.5)	D	ln D
573	0.77	4.50e-9	1.36e-16	-36.53
623	0.57	4.39e-9	1.95e-16	-36.17
673	0.45	4.68e-9	2.84e-16	-35.80

Table 6.2: Values for 5.5 µm membrane of Sievert constant and diffusivity adopted from figure 3.2

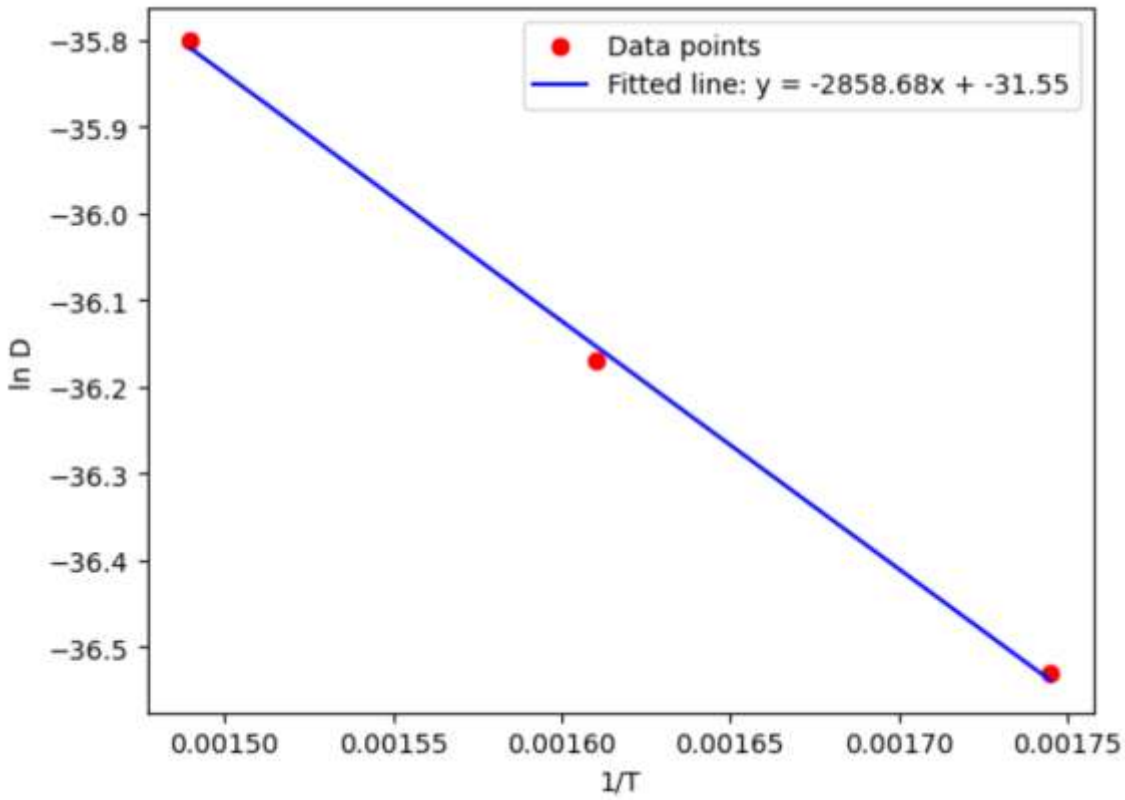

Figure 6.5: ln D Vs 1/T Plot for 5.5 µm Membrane.

Y= -2858.68X-31.55

R2= 0.9977

Ea=23.76 kJ/mol

6.3.2 10 µm Membrane

Temperature (K)	Sievert Constant (Ks) ($\mu mol/gPa$^0.5)	Permeability (mol/msPa^0.5)	D	ln D
573	0.7	7.78e-9	2.58e-16	-35.89
623	0.55	7.62e-9	3.50e-16	-35.59
673	0.4	8.46e-9	5.78e-16	-35.09

Table 6.3: Values for 10 µm membrane of Sievert constant and diffusivity adopted from figure 3.2

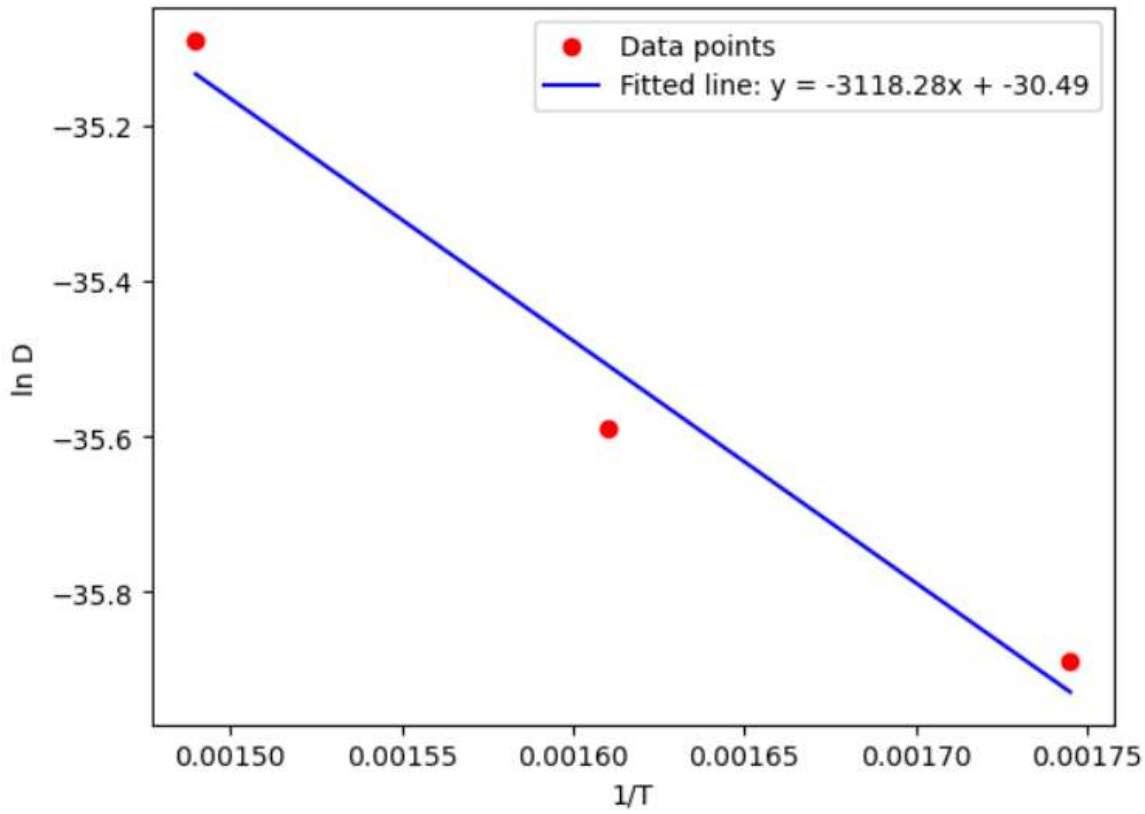

Figure 6.6: ln D Vs 1/T Plot for 10 µm Membrane.

Y=-3118.28x-30.49

R^2= 0.969

Ea= 25.92 kJ/mol

From this calculation, we got to know an intrinsic characteristic of both membranes. In the case of both membranes, they show temperature dependency. Therefore, it suggests that both membranes follow Fick's law and Sievert's law.

6.5 Anomaly of 5.5 µm membrane

In this section, a very peculiar anomaly regarding the 5.5 µm membrane will be discussed. As mentioned earlier, this particular membrane has been manufactured by Norwegian company Hydrogen Mem-Tech. It is synthesized through Magnetron sputtering on glass plate substrate. According to the company website, their manufactured membrane provides selective hydrogen separation with recovery rates reaching 99%, facilitating the production of both industrial-grade and ultra-high-purity hydrogen from various feed gases. As, this variant of the membrane is a thinner version of Pd based membrane, we expected a more superior result in terms of hydrogen flux and permeability. As speculated, the hydrogen flux output from this membrane was superior to that of the 10 µm membrane. We began the experiment with 320 ml/min hydrogen and 80 ml/min nitrogen feed at 300 °C temperature. As expected, we got a high hydrogen flux. Subsequently, we increased the membrane temperature to 400 °C. Initially, we saw an increased hydrogen flux at the increased temperature. Therefore, we were waiting for the flux to get stabilized. However, gradually but effectively, we could see a trend of hydrogen flux decrease. For the next 417 hours, we ran the experiment in order for the flux value to get stabilized. When the flux was stabilized after long 417 hours, we decided to move on to the next experiment which was with 160 ml/min hydrogen and 40 ml/min nitrogen in the feed at 400 °C. Even though, the flux for this membrane seemed to be twice as much as the 10 µm membrane. Eventually, it went down to approximately the same level as the 10 µm membrane. Even though, it is mentioned in the company website that the selectivity of the membrane is 99%, we can only speculate that the high selectivity could have been acquired at the cost of hydrogen flux. This can further backed by the analysis we did in chapter 4. From table 4.1, we can see that the membrane based on glass substrate had superior selectivity. However, it had much poorer flux. As, our 5.5 µm membrane is based on glass substrate, we can understand why we are getting such anomaly.

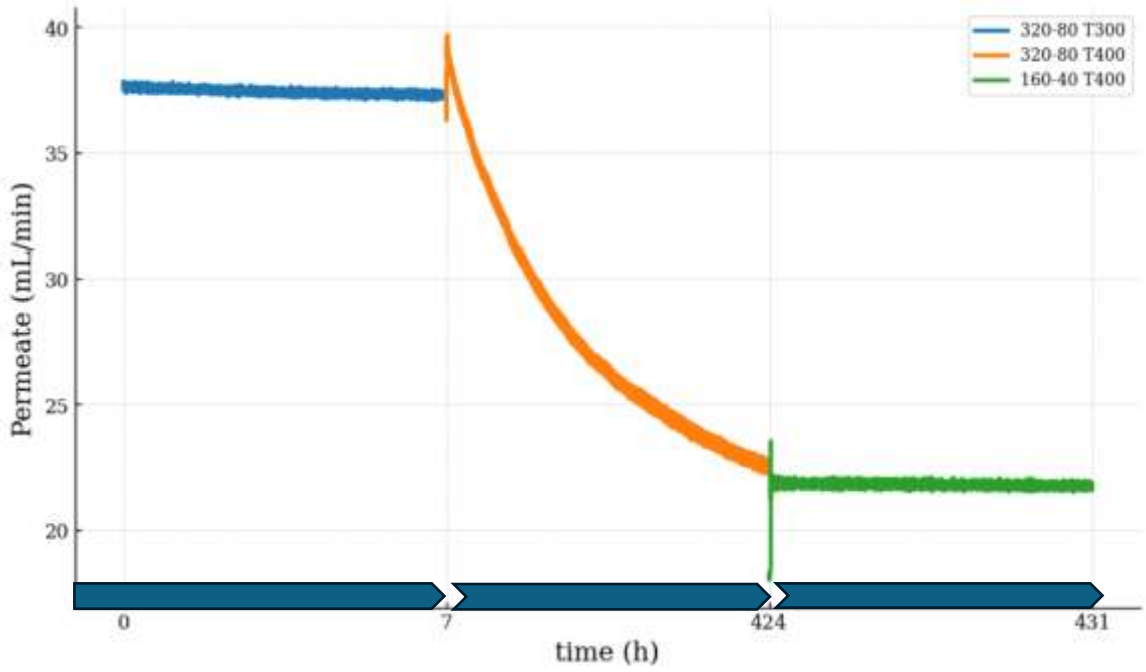

Figure 6.7: Alteration of behaviour of 5.5 µm Membrane

From the image below, it is evident that the 5.5-micron membrane has curled up. This was unusual behaviour, indications some tension in the structure which might have something to do with the anomaly behaviour. To further verify, we wanted to do MS-AES analysis. The initial hypothesis about this anomaly was an impurity in the fabrication, most likely related to cadmium but this was not found or verified. We have requested the raw data, but due to some issues in sample digestion, our lab engineer has been reluctant to just send them.

Figure 6.8: Curled up 5.5 µm Membrane

7. Discussion

7.1 Performance Analysis

To begin the performance analysis of both membranes we can take the comparison of chapter 4 as an analogy. From chapter 4, we have come to know that although the membrane on Vycor glass has excellent selectivity, its permeance is significantly inferior to that of the SINTEF Industry membrane. We have mentioned earlier that the Vycor glass support membrane is the closest to our 5.5 μm membrane from literature whereas the SINTEF Industry membrane from the chapter 4 is exactly same as the 10 μm membrane we have used for our experimentation. Vycor glass support membrane has fine porosity and a smooth surface, promoting superior adherence for sputtered films and resistance to high temperatures. Nonetheless, its diminutive pore size and delicate structure limit mechanical durability and extensive use. The regulation of grain size is inaccurate, and surface roughness may lead to change of topography, thus diminishing flux. On the other hand, while SINTEF Industry membrane shows superior performance in the case of permeance, it yields a hydrogen with high purity. Thin coatings and regulated grain development diminish roughness, but Pd–Ag offers chemical resistance against reactive gases.

7.2 Determination of Rate Limiting Step

7.2.1 5.5 μm Membrane

Based on our experiments, the permeance we acquired is much less compared to literature. However, this membrane follows Sievert's law. Consequently, it is not sensitive to total flow rate. According to table 3.1, when the membrane thickness is less than or equal to 10 μm as well as the cleanliness of the membrane is impeccable, the rate limiting step is usually bulk diffusion. However, when we account for the results acquired from the hydrogen permeation, the results are at least half as expected. The reason could have something to do with the surface topography, which will be discussed in later section.

7.2.2 10 μm Membrane

In the case of 10 μm membrane, R is approx. 0.97. So, we have concluded that rather than bulk diffusion, surface phenomena or mass transfer is the rate limiting step for this membrane. From table 3.1, it is indicated that the reason behind deviation from linearity might be due to contamination of membrane. However, the flux from this membrane is excellent with perfect selectivity. This aspect of the membrane will be discussed in the next section.

7.3 Discussion of Abnormal Phenomena of 5.5 μm Membrane

It is very crucial that we determine the underlying reasons behind this permeation alteration phenomena. One of the reasons can be shift of rate limiting step. From, all the analysis we have concluded that for this membrane, bulk diffusion is the rate limiting step. However, it is possible that the rate limiting step has been altered gradually. Furthermore, phenomena like Ag surface segregation or Mechanical stress on the membrane resulting in wrinkling or deviating the structural integrity of the membrane has enabled the alteration.

7.4 Limitation of Experimentation

The major limitation of the study was not to find a definitive factor behind the functional anomaly of the 5.5 μm membrane. Besides, the possibility of microstructural evolution can be another limitation. Furthermore, the resistance due to the substrate has not been accounted for. Finally, a spectroscopy study of 5.5 μm membrane is crucial to define its phenomena.

8. Conclusion

The dependence of hydrogen permeability on total flow is opposite for both 5.5 μm and 10 μm membrane. Whereas 10 μm membrane showed a decreasing trend, 5.5 μm membrane showed decreasing trend. However, the effect of total flow for 10 μm membrane was insignificant at higher temperature. Moreover, 10 μm membrane did not show any dependence on total flow at 100% hydrogen concentration. In the case of hydrogen concentration, permeability showed a steady increasing trend for both 5.5 μm and 10 μm membrane. Thickness dependence for both membrane at 300 °C, 350 °C and 400 °C is identical in terms of gradient. However, due to the surface anomaly the thickness dependence does not follow the literature trend. In terms of temperature stability, the 10 μm membrane has always been consistent and reliable. However, since the issue in 5.5 μm has started when the temperature went from 300 °C to 400 °C, it can be said that the temperature stability of the 5.5 μm membrane is not that great. But overall, there was something in the fabrication of this membrane that went wrong.

To sum up, the membranes synthesized through magnetron sputtering method has been proven to be superior in hydrogen separation. However, whereas the flux and the selectivity of 10 μm membrane is feasible and its technology ready level is very high, the flux of 5.5 μm membrane has been measured to be poor instead of the selectivity to be very high. The 10 μm membrane design integrates durability, high flux, and industrial applicability, whereas 5.5 μm membrane demonstrates superior selectivity primarily at laboratory scales and moderate pressures. Overall, this anomaly can be described as a fault in the fabrication, leading to unexpectedly low flux. However, if we could address the issue of 5.5 μm membrane, this could perform much better than the 10 μm membrane.

Finally, the performance of 10 μm membrane has been proven to be superior, consistent, reproducible and feasible. On contrary, 5.5 μm membrane require further study to define its issues and rectify them.

References

[1] Yuping Shang, Shenghu Sang, Aviral Kumar Tiwari, Salahuddin Khan, Xin Zhao. Impacts of renewable energy on climate risk: A global perspective for energy transition in a climate adaptation framework [J]. Applied Energy 362 (2024), 122994.

[2] K. R. Shivanna. Climate change and its impact on biodiversity and human welfare [J]. Indian National Science Academy (2022) 88:160–171.

[3] The Surprising Reason Your Groceries Are More Expensive [A]. TIME, 2025.

[4] Damian Carrington. 'No country is safe': deadly Nordic heatwave supercharged by climate crisis, scientists say [A]. The Guardian, 2025.

[5] Keshani Attanayake, Isuru Wickramage, Udul Samarasinghe, Yasangi Ranmini, Sandali Ehalapitiya, Ruwan Jayathilaka, Shanta Yapa. Renewable energy as a solution to climate change: Insights from a comprehensive study across nations [J]. Plos One, June 20, 2024.

[6] Tze-Zhang Ang, Mohamed Salem, Mohamad Kamarol, Himadry Shekhar Das, Mohammad Alhuyi Nazari, Natarajan Prabaharan. A comprehensive study of renewable energy sources: Classifications, challenges and suggestions [J]. Energy Strategy Reviews 43 (2022), 100939.

[7] Md Monjur Hossain Bhuiyan, Zahed Siddique. Hydrogen as an alternative fuel: A comprehensive review of challenges and opportunities in production, storage, and transportation [J]. International Journal of Hydrogen Energy, 102 (2025): 1026–1044.

[8] Ramesh Bhandari, Niroj Adhikari. A comprehensive review on the role of hydrogen in renewable energy systems [J]. International Journal of Hydrogen Energy 82 (2024) 923–951.

[9] Damien Guilbert, Gianpaolo Vitale. Hydrogen as a Clean and Sustainable Energy Vector for Global Transition from Fossil-Based to Zero-Carbon [J]. Clean Technologies, 2021, 3, 881–909.

[10] Joseph Nyangona, Ayesha Darekarb. Advancements in hydrogen energy systems: A review of levelized costs, financial incentives and technological innovations [J]. Innovation and Green Development 3 (2024) 100149.

[11] bp

[12] A. J. Dessler, D. E. Overs, W. H. Appleby. The Hindenburg Fire: Hydrogen or Incendiary Paint? [J]. Buoyant Flight (2005), 52(2–3).

[13] Release and Ignition of Hydrogen Following Collision of a Tractor-Semitrailer with Horizontally Mounted Cylinders and a Pickup Truck Near Ramona, Oklahoma, May 1, 2001. National Transportation Safety Board (NTSB); Report number NTSB/HZM-02/02

[14] Hao Li, Xuewen Cao, Yang Liu, Yanbo Shao, Zilong Nan, Lin Teng, Wenshan Peng, and Jiang Bian. Safety of hydrogen storage and transportation: An overview on mechanisms, techniques, and challenges [J]. Energy Reports, 8 (2022): 6258–6269.

[15] Muhammad Aziz, Ammonia as Effective Hydrogen Storage: A Review on Production, Storage and Utilization, Energies, 2020.

[16] Astrid Lervik Mejdell. Properties of 1-5 μm Pd/Ag23wt.% membranes for hydrogen separation. Doctoral theses at NTNU, 2009:76.

[17] Seyedehhoma Ghavam, Maria Vahdati, I. A. Grant Wilson, Peter Styring. Sustainable Ammonia ProductionProcesses. Frontiers in Energy Research, (9), 2021: 580808.

[18] Véronique Dias, Maxime Pochet, Francesco Contino, Hervé Jeanmart. Energy and Economic Costs of Chemical Storage. Front. Mech. Eng. 2020, 6, 21.

[19] Lin Ye, Richard Nayak-Luke, René Bañares-Alcántara, Edman Tsang. Reaction: "Green" Ammonia Production. Chem, 3(5), 2017: 712-714.

[20] Jose´ Luis Aprea. Quality specification and safety in hydrogen production, commercialization and utilization [J]. International journal of hydrogen energy, 39 (2014): 8604-8

[21] Marco Succi, Giorgio Macchi, and Sarah Riddle Vogt. High-purity Hydrogen: Guidelines to Select the Most Suitable Purification Technology. Entegris, Inc.

[22] Mauro Luberti, Hyungwoong Ahn. Review of Polybed pressure swing adsorption for hydrogen purification. International Journal of Hydrogen Energy. 47 (20), 2022: 10911-10933

[23] Werner Liemberger, Markus Groß, Martin Miltner, Michael Harasek. Experimental analysis of membrane and pressure swing adsorption (PSA) for the hydrogen separation from natural gas. Journal of Cleaner Production. Volume 167, 20 November 2017, Pages 896-907

[24] Majid Aasadnia, Mehdi Mehrpooya, Bahram Ghorbani. A novel integrated structure for hydrogen purification using the cryogenic method. Journal of Cleaner Production. Volume 278, 1 January 2021, 123872.

[25] Dixit V. Bhalani, Bogyu Lim. Hydrogen Separation Membranes: A Material Perspective. Molecules 2024, 29, 4676.

[26] Dedy Kristanto, Yulius Deddy Hermawan, Hariyadi, Yusmardhany Yusuf. Integrated simulation system of CO2 gas injection application for enhanced oil recovery in the oil field. Journal of Petroleum Exploration and Production Technology. https://doi.org/10.1007/s13202-020-00955-9

[27] Frederico Relvas, Roger D. Whitley, Carlos Silva, Adelio Mendes. Single-Stage Pressure Swing Adsorption for Producing Fuel Cell Grade Hydrogen. Ind. Eng. Chem. Res. 2018, 57, 5106−5118.

[28] Ryan Baker, Jiujun Zhang. Proton exchange membrane or polymer electrolyte membrane (pem) fuel cells. 2011. Electrochemistry Encyclopedia of The Electrochemistry Society. https://knowledge.electrochem.org/encycl/art-f04-fuel-cells-pem.htm

[29] Majid Aziz, Archis Amrite, Utsav Raj Aryal, Ajay K. Prasad. Electrochemical Hydrogen Separation and Compression. Journal of Applied Electrochemistry. https://doi.org/10.1007/s10800-025-02312-2

[30] H.K. Lee a, H.Y. Choi, K.H. Choi, J.H. Park, T.H. Lee. Hydrogen separation using electrochemical method. Journal of Power Sources 132 (2004) 92–98.

[31] Tom Skoczylas. Securing high-purity hydrogen. Compound Semiconductor magazine, Volume 24, Issue 8.

[32] P. Bernardo, E. Drioli, G. Golemme. Membrane Gas Separation: A Review/State of the Art. Industrial & Engineering Chemistry Research. 2009, Vol 48, Issue 10.

[33] Pratibha Pandey, R.S. Chauhan. Membranes for gas separation. Progress in Polymer Science. Volume 26, Issue 6, August 2001, Pages 853-893.

[34] Nathan W. Ockwig, Tina M. Nenoff. Membranes for Hydrogen Separation. Chem. Rev. 2007, 107, 4078-4110.

[35] Neha Pal, Madhu Agarwal, Karishma Maheshwari, Yogendra Singh Solanki. A review on types, fabrication and support material of hydrogen separation membrane. Materials Today: Proceedings 28 (2020) 1386–1391.

[36] Christopher Stafford. Polymer Membranes. National Institute of Standards and Technology. US Department of Commerce. https://www.nist.gov/programs-projects/polymer-membranes

[37] Nicla Vicinanza. An investigation of fundamental phenomena affecting the performance of sputtered Pd-alloy thin film membranes for hydrogen separation. Doctoral Theses at NTNU, 2014

[38] S. M. Saufi, A. F. Ismail. Fabrication of carbon membranes for gas separation––a review. Carbon 2004, 42, 241.

[39] Min Deng, Jing Wei, Wentao Du, Zikang Qin, Zimei Zhang, Lin Yang, Lu Yao, Wenju Jiang, Bo Tang, Xiaohua Ma, and Zhongde Dai. High-Performance Carbon Molecular Sieve Membranes Derived from a PPA-Cross-Linked Polyimide Precursor for Gas Separation. ACS Applied Materials & Interfaces 2024, 16, 44927–44937.

[40] A. Bartoletti, E. Mercadelli, A. Gondolini, V. Saraceni, A. Fasolini, J. De Maron, F. Basile, A. Sanson. Nanostructured ceramic membranes for hydrogen separation. Separation and Purifcation Technology 372 (2025) 133436.

[41] Xiao Ma, Pengli Chen, Ming Zhong, Feng Zhang, Weihong Xing. Tight Ultrafiltration Ceramic Membrane for Separation of Dyes and Mixed Salts (both NaCl/Na2SO4) in Textile Wastewater Treatment. Industrial & Engineering Chemistry Research. Vol 56/Issue 24 (2017).

[42] Hang Yin, Alex C.K. Yip. A Review on the Production and Purification of Biomass-Derived Hydrogen Using Emerging Membrane Technologies. Catalysts. Volume 7, Issue 10. DOI: 10.3390/catal7100297

[43] F.A. Lewis. The palladium-hydrogen system, a survey of hydride formation and the effects of hydrogen contained within the metal lattices, Platin. Met. Rev. 26 (1982) 20–27.

[44] W. J. Koros, R. Mahajan. Pushing the limits on possibilities for large scale gas separation: Which strategies? J. Membr. Sci. 2000, 175, 181–196.

[45] MKS Instruments Handbook: Semiconductor Devices & Process Technology. https://www.mks.com/n/cvd-physics.

[46] Prof. Igor Lubomirsky. Dielectrics, Electromechanics, Ion-Conductors. https://www.weizmann.ac.il/MCMS/igorl/equipment/sputter.

[47] Nadia Cerone, Giuseppe Domenico Zito, Carmine Florio, Laura Fabbiano, Francesco Zimbardi. Recent Advancements in Pd-Based Membranes for Hydrogen Separation. Membranes for Hydrogen Separation. Energies 2024, 17, 4095.

[48] Julio J. Conde, Marta Maroño & José María Sánchez-Hervás. Pd-Based Membranes for Hydrogen Separation: Review of Alloying Elements and Their Influence on Membrane Properties. Separation & Purification Reviews, 46:2, 152-177.

[49] Ekain Fernandez, Jose Angel Sanchez-Garcia, Jose Luis Viviente, Martin van Sint Annaland, Fausto Gallucci, and David A. Pacheco Tanaka. Morphology and N2 Permeance of Sputtered Pd-Ag Ultra-Thin Film Membranes. Molecules 2016, 21, 210.

[50] H. Klette, R. Bredesen. Sputtering of very thin palladium-alloy hydrogen separation membranes. Membrane Technology. Volume 2005, Issue 5, May 2005, Pages 7-9.

[51] T.A. Peters, T. Kaleta, M. Stange, R. Bredesen. Hydrogen transport through a selection of thin Pd-alloy membranes: Membrane stability, H2S inhibition, and flux recovery in hydrogen and simulated WGS mixtures. Catalysis Today. Volume 193, Issue 1, 15 October 2012, Pages 8-19.

[52] Rune Bredesen, Thijs Peters, Marit Synnøve Sæverud Stange. Thin Pd-23w%Ag membranes for hydrogen separation.

[53] Timothy L. Ward, Tien Dao. Model of hydrogen permeation behavior in palladium membranes. Journal of Membrane Science 153 (1999) 211-231.

[54] Abdulrahman Alraeesi, and Tracy Gardner. Assessment of Sieverts Law Assumptions and 'n' Values in Palladium Membranes: Experimental and Theoretical Analyses. Membranes. 2021, 11, 778.

[55] H. D. Tonga, A. H. J. van den Berga, J. G. E. Gardeniers, H. V. Jansen, F. C. Gielens, and M. C. Elwenspoek. Preparation of palladium–silver alloy films by a dual-sputtering technique and its application in hydrogen separation membrane. Thin Solid Films 479 (2005) 89– 94.

[56] Ekain Fernandez, Jose Angel Sanchez-Garcia, Jose Luis Viviente, Martin van Sint Annaland, Fausto Gallucci, David Alejandro Pacheco Tanaka. Morphology and N2 Permeance of Sputtered Pd-Ag Ultra-Thin Film Membranes. Molecules 2016, 21, 210; doi:10.3390/molecules21020210.

[57] Tong Duy Hien. Microfabricated Palladium-Based Membranes for Hydrogen Separation. University of Twente Doctoral Thesis.

[58] E. Gobina, R. Hughes, D. Monaghan and D. Arnel. High-Temperature Selective Membranes for Hydrogen Separation. Asia-Pacific Journal of Chemical Engineering (1994).

[59] Samco Incorporated, UV-Ozone Cleaning Systems, Samco Inc., [Online]. Available: https://www.samcointl.com/products/surface-treatment/uv-ozone-cleaning-systems/

[60] F. A. Lewis, The palladium-hydrogen system: Structures near phase transition and critical points, International Journal of Hydrogen Energy, vol. 20, no. 7, pp. 587–592, 1995. DOI: 10.1016/0360-3199(94)00113-E.

[61] Steve N. Paglieri and J. Douglas Way, Innovations in Palladium Membrane Research, Separation and Purification Methods, vol. 31, no. 1, pp. 1–169, 2002. DOI: 10.1081/SPM-120006115.

[62] Fabio Gallucci, Eduardo Fernandez, Pablo Corengia, and Martijn V. Annaland, Recent advances on membranes and membrane reactors for hydrogen production, Chemical Engineering Science, vol. 92, pp. 40–66, 2013. DOI: 10.1016/j.ces.2013.01.008.

[63] Thijs Peters, Marit Stange and Rune Bredesen. Development Of Thin Pd-23% Ag/Stainless Steel Composite Membranes for Application in Water Gas Shift Membrane Reactors. Carbon Dioxide Capture for Storage in Deep Geologic Formations - Results from the CO2 Capture Project. Chapter 12. Page: 135-155.

[64] Hydrogen Mem-Tech AS. https://hydrogen-mem-tech.com/product/

[65] Bengt Arild Johannesen. Microchannel Membrane Reactor for production of pure Hydrogen: Inhibition effects on thin self-supported Pd/Ag membranes. Doctoral Theses at NTNU, 2014.

[66] Y. Yang, G. Wang, L. Zhang, S. Zhang, and L. Lin. Recent Advances in Palladium-Based Membranes for Hydrogen Separation: Materials, Fabrication, and Challenges. Processes, vol. 12, no. 2855, pp. 1–47, 2024. doi: 10.3390/pr1222855

[67] S. Sivashanmugam, A. Basile, and A. Iulianelli. Analyzing Sieverts' Law Assumptions for Mixed Feeds Permeation in Pd and Pd–Ag Foils. Membranes, vol. 11, no. 778, pp. 1–23, 2021. doi: 10.3390/membranes11110778

[68] S. Sivashanmugam, A. Basile, and A. Iulianelli. Hydrogen Permeation Studies through Pd and Pd–Ag Membranes: Effect of Pressure and Temperature on Sieverts' Law Validity. Separation and Purification Technology, vol. 25, no. 2, pp. 123–137, 2005. doi: [10.1016/S1383-5866(05)00045-2]

[69] S. Sivashanmugam, A. Basile, and A. Iulianelli. Hydrogen Transport through Palladium Membranes: Deviations from Sieverts' Law. Journal of Membrane Science, vol. 241, no. 1, pp. 157–166, 2004. doi: [10.1016/j.memsci.2004.05.030]

[70] Nicla Vicinanza, Ingeborg-Helene Svenum, Live Nova Naess, Thijs A. Peters, Rune Bredsen, Anne Borg, Hilde J. Venvik. Thickness dependent effects of solubility and surface phenomena on the hydrogen transport properties of sputtered Pd77%Ag23% thin film membranes. Journal of Membrane Science 476 (2015), 602-608

Appendix

Appendix A

In this section, it will be discussed how the raw data were processed and converted into flux and permeability. The details raw data will be found in Appendix E. Let's first have a look at the raw data:

Experiment	Thickness (μm)	Temperature	Total Flow	Flow Ratio (H2: N2)	Flow Rate (mL/ min)	p_H2_feed (Pa)
1a	10	300	200	80:20	22.32	164000
1b	10	350	200	80:20	21.55	164000
1c	10	400	200	80:20	21.90	164000
2a	10	300	400	80:20	20.33	164000
2b	10	350	400	80:20	19.93	164000
2c	10	400	400	80:20	22.10	164000
3a	10	300	100	100:0	36.42	205000
3b	10	350	100	100:0	33.52	205000
3c	10	400	100	100:0	35.18	205000
4a	10	300	200	100:0	35.87	205000
4b	10	350	200	100:0	34.87	205000
4c	10	400	200	100:0	35.52	205000
5a	10	300	200	50:50	0	105000
5b	10	350	200	50:50	0	105000
5c	10	400	200	50:50	0	105000

Fig: Raw data for the 10 μm membrane

Experiment	Thickness (μm)	Temperature (℃)	Total Flow (H2+N2)	Flow Ratio (H2: N2)	Flow Rate (mL/min)	p_H2_feed (Pa)
6a	5.5	300	200	80:20	20.8	164000
6b	5.5	350	200	80:20	20.01	164000
6c	5.5	400	200	80:20	21.24	164000
7a	5.5	300	400	80:20	21.41	164000
7b	5.5	350	400	80:20	20.89	164000
7c	5.5	400	400	80:20	22.27	164000
8a	5.5	300	200	75:25	17.64	153750
8b	5.5	350	200	75:25	17.87	153750
8c	5.5	400	200	75:25	18.33	153750
9a	5.5	300	400	75:25	18.48	153750
9b	5.5	350	400	75:25	17.81	153750
9c	5.5	400	400	75:25	18.79	153750
10a	5.5	300	200	100:0	35.74	205000
10b	5.5	350	200	100:0	34.70	205000
10c	5.5	400	200	100:0	34.96	205000

Fig: Raw data for the 5.5 μm membrane

The hydrogen flow through the Pd-based membrane is given in the unit of mL/min. We need to convert that into mol/s first.

$1\ mL/min = 1\ cm^3/min$

So, $x\ mL/min = x\ cm^3/min$

Again, $x\ cm^3/min = \frac{x}{60}\ cm^3/s$

Let's consider hydrogen an ideal gas.

$1\ cm^3 = \frac{1}{22414}\ mol$

$\frac{x}{60} = cm^3/s = \frac{x}{60*22414}\ mol/s$

Now, if we divide the above term with membrane area, we will get flux.

The membrane area is 2.4 cm^2 or 0.00024 m^2

So, Flux, J= $\frac{x}{60*22414*0.00024} \frac{mol}{m^2 s}$

Flux calculation:

Flux, J=$\frac{x}{60*22414*0.00024}$ $mol\ /\ (m\text{^}2\ s)$

Let's multiply membrane thickness with the above term and we get:

Flux * Membrane thickness = $\frac{x*t*10^{-6}}{60*22414*0.00024}$ mol/ms

For 10 μm thickness:

Flux * Membrane thickness = $\frac{x*10*10^{-6}}{60*22414*0.00024}$ mol/ms

For 4 μm thickness:

Flux * Membrane thickness =$\frac{x*4*10^{-6}}{60*22414*0.00024}$ mol/ms

Now, if we divide this term with difference of square root of the feed pressure and the permeate pressure of hydrogen, we get the permeability.

Before doing that, we must know that the total pressure at feed side was 2.05 bar or 205000 Pa. Total pressure at permeate side was 1.05 bar or 105000 Pa. In our calculation, we just accounted for the partial pressure of hydrogen. At the feed side, we calculated the partial pressure based on the total feed pressure and composition of the flow. For the permeate side, since 100% of the flow is hydrogen, the total permeate pressure was accounted for in our calculation.

For instance,

In the case of 1a, the composition of total flow was H_2:N_2=80:20 and the total feed pressure was 2.05 bar. So, the partial pressure of hydrogen was 2.05*0.8= 1.64 bar = 164000 Pa

Permeability Calculation:

For 10 μm thickness:

Permeability, P = $\frac{x*10*10^{-6}}{60*22414*0.00024\ (P_1^{0.5} - P_2^{0.5})}\ mol/msPa^{0.5}$

For 5.5 μm thickness:

Permeability, P = $\frac{x*5.5*10^{-6}}{60*22414*0.00024\ (P_1^{0.5} - P_2^{0.5})}\ mol/msPa^{0.5}$

Here,

P_1 = Partial pressure of hydrogen at feed side

P_2 = Partial pressure of hydrogen at permeate side

For 10 micron Membrane:

Table: Values of Flux and Permeability for 10 micron Membrane

Experiment	Thickness (μm)	Temperature	Total Flow	Flow Ratio (H2: N2)	Flow Rate (mL/min)	p_H2_feed (Pa)	Flux (mol/m2.s)	Permeability
1a	10	300	200	80:20	22.32	164000	0.691532	8.54E-09
1b	10	350	200	80:20	21.55	164000	0.066767	8.24E-09
1c	10	400	200	80:20	21.90	164000	0.067852	8.38E-09
2a	10	300	400	80:20	20.33	164000	0.062987	7.78E-09
2b	10	350	400	80:20	19.93	164000	0.061748	7.62E-09
2c	10	400	400	80:20	22.10	164000	0.068471	8.46E-09
3a	10	300	100	100:0	36.42	205000	0.112839	8.76E-09
3b	10	350	100	100:0	33.52	205000	0.103853	8.06E-09
3c	10	400	100	100:0	35.18	205000	0.108997	8.46E-09
4a	10	300	200	100:0	35.87	205000	0.111135	8.63E-09
4b	10	350	200	100:0	34.87	205000	0.108036	8.39E-09
4c	10	400	200	100:0	35.52	205000	0.110050	854E-09
5a	10	300	200	50:50	0	105000	0	0
5b	10	350	200	50:50	0	105000	0	0
5c	10	400	200	50:50	0	105000	0	0

For 5.5 micron Membrane:

Experiment	Thickness (μm)	Temperature (℃)	Total Flow (H2+N2)	Flow Ratio (H2: N2)	Flow Rate (mL/min)	p_H2_feed (Pa)	Flux	Permeability
6a	5.5	300	200	80:20	20.8	164000	0.064444	4.37E-09
6b	5.5	350	200	80:20	20.01	164000	0.061996	4.21E-09
6c	5.5	400	200	80:20	21.24	164000	0.065807	4.47E-09
7a	5.5	300	400	80:20	21.41	164000	0.066334	4.50E-09
7b	5.5	350	400	80:20	20.89	164000	0.064723	4.39E-09
7c	5.5	400	400	80:20	22.27	164000	0.068998	4.68E-09
8a	5.5	300	200	75:25	17.64	153750	0.054653	4.41E-09
8b	5.5	350	200	75:25	17.87	153750	0.055366	4.47E-09
8c	5.5	400	200	75:25	18.33	153750	0.056791	4.58E-09
9a	5.5	300	400	75:25	18.48	153750	0.057256	4.62E-09
9b	5.5	350	400	75:25	17.81	153750	0.055180	4.45E-09
9c	5.5	400	400	75:25	18.79	153750	0.058216	4.70E-09
10a	5.5	300	200	100:0	35.74	205000	0.110732	4.73E-09
10b	5.5	350	200	100:0	34.70	205000	0.107510	4.59E-09
10c	5.5	400	200	100:0	34.96	205000	0.108315	4.62E-09

Table: Values of Flux and Permeability for 5.5 micron Membrane

Appendix B

Temperature (K)	Sievert Constant (Ks) ($\mu mol/gPa$^0.5)	Permeability (mol/msPa^0.5)
573	0.77	4.50e-9
623	0.57	4.39e-9
673	0.45	4.68e-9

Table: Values for 4 μm membrane of Sievert constant adopted from figure 3.2 and Experimental Values of Permeability (for H_2:N_2 = 320:80)

Temperature (K)	Sievert Constant (Ks) ($\mu mol/gPa$^0.5)	Permeability (mol/msPa^0.5)
573	0.7	7.78e-9
623	0.55	7.62e-9
673	0.4	8.46e-9

Table: Values for 10 μm membrane of Sievert constant adopted from figure 3.2 and Experimental Values of Permeability

Determination of Equation

For gas transport through a metal:

$$P=D\times S$$

Here,

P= Permeability $[mol/(m \cdot s \cdot Pa^{0.5})]$

D= Diffusivity $[m^2/s]$

S= Solubility

Sievert's law gives:

$$C = K_S P_{H_2}^{0.5}$$

Here,

C = concentration of dissolved hydrogen [μmol / g]

K_s = Sievert constant

P_{H_2} = Partial Pressure of H_2

So the solubility per volume (not per mass) is obtained by multiplying by the density (ρ):

$$S=Ks\times\rho$$

So, finally: $D = \frac{P}{K_S * \rho}$

Determination of density:

The Ideal Gas Law in terms of molar density:

$$PV = nRT$$
$$\rho_m = \frac{n}{V} = \frac{P}{RT}$$

At 300°C

- Temperature: $T = 300 + 273.15 = 573.15\,\text{K}$
- Calculation:

$$\rho_m = \frac{2.05 \times 10^5}{(8.314) \times (573.15)} = \frac{205000}{4764.6} = 43.02\,\text{mol/m}^3$$

At 350°C

- Temperature: $T = 350 + 273.15 = 623.15\,\text{K}$
- Calculation:

$$\rho_m = \frac{2.05 \times 10^5}{(8.314) \times (623.15)} = \frac{205000}{5181.1} = 39.57\,\text{mol/m}^3$$

At 400°C

- Temperature: $T = 400 + 273.15 = 673.15\,\text{K}$
- Calculation:

$$\rho_m = \frac{2.05 \times 10^5}{(8.314) \times (673.15)} = \frac{205000}{5597.5} = 36.62\ \text{mol/m}^3$$

Determination of diffusivity for 4 µm membrane:

The equation:

$D = \frac{P}{K_S * \rho}$

For 573° C, $D = \frac{4.50e-09}{0.8e6*43.02}$ = 1.36e-16

For 623° C, $D = \frac{4.39e-09}{0.57e6*39.57}$ = 1.95e-16

For 673° C, $D = \frac{4.68e-09}{0.45e6*36.62}$ = 2.84e-16

Determination of ln D for 5.5 µm membrane:

For 573° C, $\ln D =$ ln (1.36e-17) = -36.53

For 623° C, $\ln D =$ ln (1.95e-16) = -36.17

For 673° C, $\ln D =$ ln (2.84e-16) = -35.80

Temperature (K)	Sievert Constant (Ks) ($\mu mol/gPa$^0.5)	Permeability (mol/msPa^0.5)	D	ln D
573	0.77	4.50e-9	1.36e-16	-36.53
623	0.57	4.39e-9	1.95e-16	-36.17
673	0.45	4.68e-9	2.84e-16	-35.80

Table: Values for 5.5 µm membrane of Sievert constant adopted from figure 3.2, Experimental Values of Permeability, Calculated values of Diffusivity and natural logarithmic values of diffusivity

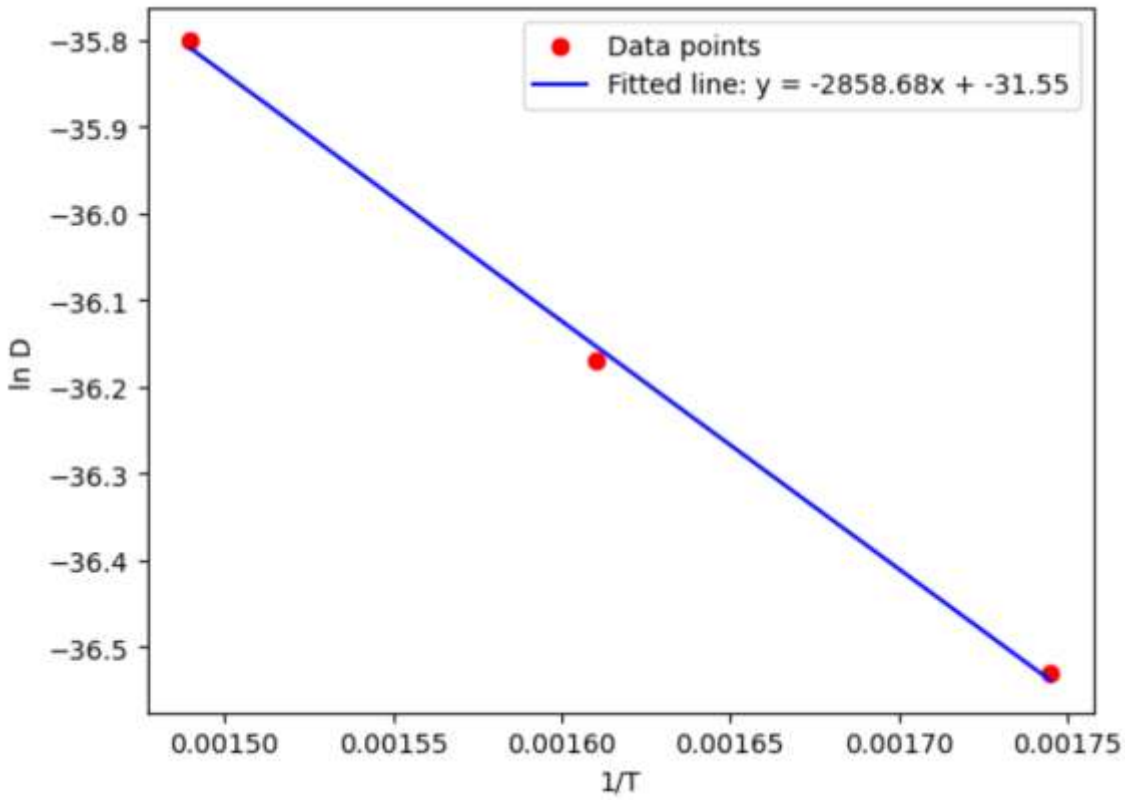

Fig: ln D Vs 1/T for 5.5 micron membrane

Linearity of 4 µm membrane:

$R^2 = 1 - \frac{SS_{res}}{SS_{tot}}$

$SS_{res} = \Sigma (y - y_{fit})^2$

$SS_{tot} = \Sigma (y - \bar{y})^2$

$y_{fit} = mx + b$

$\bar{y} = \frac{y_1+y_2+y_3}{3}$

From the graph, we get that, y= -2858.68x-31.55

Given,

X_1= 0.00149
X_2=0.00161
X_3=0.001745

y_1= -35.80
y_2=-36.17
y_3=-36.53

y_{fit},1= -2858.68*0.00149-31.55= -35.81
y_{fit},2= -2858.68*00.161-31.55= -36.15
y_{fit},3= -2858.68*0.001745-31.55= -36.54

$$\bar{y} = \frac{-(35.80+36.17+36.53)}{3} = -36.17$$

$$SS_{res} = (-35.80 + 35.81)^2 + (-36.17 + 36.15)^2 + (-36.53 + 36.54)^2$$

$$SS_{res} = 0.0006$$

$$SS_{rot} = (-35.80 + 36.17)^2 + (-36.17 + 36.17)^2 + (-36.53 + 36.17)^2$$

$$SS_{rot} = 0.2665$$

$$R^2 = 1 - \frac{0.0006}{0.2665}$$

$$R^2 = 0.9977 = 99.77\%$$

Determination of diffusivity for 10 µm membrane:

The equation:

$$D = \frac{P}{K_S * \rho}$$

For 573° C, $D = \frac{7.78e-09}{0.7e6*43.02}$ = 2.58e-16

For 623° C, $D = \frac{7.62e-09}{0.55e6*39.57}$ = 3.50e-16

For 673° C, $D = \frac{8.46e-09}{0.4e6*36.62}$ = 5.78e-16

Determination of ln D for 10 µm membrane:

For 573° C, $\ln D = \ln$ (2.58e-16) = -35.89

For 623° C, $\ln D = \ln$ (3.50e-16) = -35.59

For 673° C, $\ln D = \ln$ (5.78e-16) = -35.09

Temperature (K)	Sievert Constant (Ks) ($\mu mol/gPa$^0.5)	Permeability (mol/msPa^0.5)	D	ln D
573	0.7	7.78e-9	2.58e-16	-35.89
623	0.55	7.62e-9	3.50e-16	-35.59
673	0.4	8.46e-9	5.78e-16	-35.09

Table: Diffusivity value for 10 micron membrane

Table: Values for 10 µm membrane of Sievert constant adopted from figure 3.2, Experimental Values of Permeability, Calculated values of Diffusivity and natural logarithmic values of diffusivity

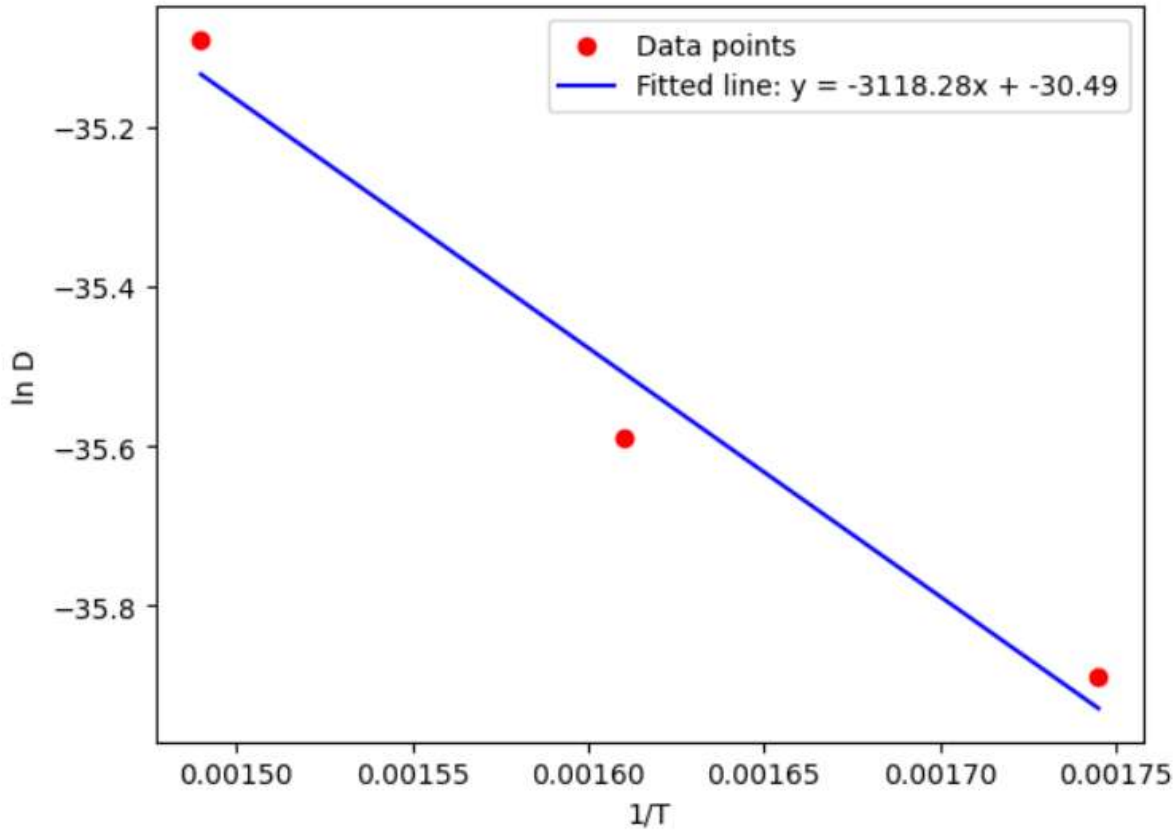

Figure: ln D Vs 1/T

Linearity of 4 µm membrane:

$$R^2 = 1 - \frac{SS_{res}}{SS_{tot}}$$

$$SS_{res} = \Sigma (y - y_{fit})^2$$

$SS_{tot} = \Sigma\,(y - \bar{y})^2$

$y_{fit} = mx + b$

$\bar{y} = \frac{y_1+y_2+y_3}{3}$

From the graph, we get that, y= -3118.28x-30.49

Given,

X_1= 0.00149
X_2=0.00161
X_3=0.001745

y_1= -35.09
y_2=-35.59
y_3=-35.89

y_{fit},1= -3118.28*0.00149-30.49=-35.136
y_{fit},2= -3118.28*0.00161-30.49=-35.51
y_{fit},3= -3118.28*0.001745-30.49=-35.93

$\bar{y} = \frac{-(35.09+35.59+35.89)}{3}$ = -36.52

$SS_{res} = (-35.09 - 35.136)^2 + (-35.59 - 35.51)^2 + (-35.89 - 36.93)^2$

$SS_{res} = 0.010116$

$SS_{rot} = (-35.09 + 35.52)^2 + (-35.59 + 35.52)^2 + (-35.89 + 35.52)^2$

$SS_{rot} = 0.3267$

$R^2 = 1 - \frac{0.0.0.16}{0.3267}$

$R^2 = 0.969 = 96.90\%$

Appendix C

Codes for Flow Rate and Concentration

```
import matplotlib.pyplot as plt
```

Code-1:

```
x1 = [80, 100]
y1 = [8.16e-9, 1.384e-8]

x2 = [80, 100]
y2 = [7.93e-9, 1.309e-8]

x3 = [80, 100]
y3 = [8.42e-9, 1.353e-8]

x_scale = 1
y_scale = 1e9



x1s = [val * x_scale for val in x1]
y1s = [val * y_scale for val in y1]

x2s = [val * x_scale for val in x2]
y2s = [val * y_scale for val in y2]

x3s = [val * x_scale for val in x3]
y3s = [val * y_scale for val in y3]

fig, ax = plt.subplots(facecolor="white")
ax.set_facecolor("White")



plt. plot(x1s, y1s, color="black", marker='o', label="300°C")
plt.plot(x2s, y2s, color="black", marker='s', label="350°C")
plt.plot(x3s, y3s, color="black", marker='^', label="400°C")



plt.title("")
plt.xlabel("Total Flow")
plt.ylabel("Permeability ($*10^{-9}$) $mol.m^{-1}s^{-1}Pa^{0.5}$")
```

```
plt.grid(False)
plt.legend()
plt.show()
```

Code-2

```
import matplotlib.pyplot as plt

x1 = [200, 400]
y1 = [8.54e-9, 7.78e-9]

x2 = [200, 400]
y2 = [8.24e-9, 7.62e-9]

x3 = [200, 400]
y3 = [8.38e-9, 8.46e-9]


x_scale = 1
y_scale = 1e9


x1s = [val * x_scale for val in x1]
y1s = [val * y_scale for val in y1]

x2s = [val * x_scale for val in x2]
y2s = [val * y_scale for val in y2]

x3s = [val * x_scale for val in x3]
y3s = [val * y_scale for val in y3]

fig, ax = plt.subplots(facecolor="white")
ax.set_facecolor("White")


plt.plot(x1s, y1s, color="black", marker='o', label="300°C")
plt.plot(x2s, y2s, color="black", marker='s', label="350°C")
plt.plot(x3s, y3s, color="black", marker='^', label="400°C")


plt.title("")
```

```
plt.xlabel("Total Flow")
plt.ylabel("Permeability ($*10^{-9}$) $mol.m^{-1}s^{-1}Pa^{0.5}$")



plt.grid(False)
plt.legend()
plt.show()
```

Code for Permeance Decrease analysis for 4 micron membrane

```
import pandas as pd
import matplotlib.pyplot as plt
import numpy as np

files = [
    "2025-06-09_222644_2um_HMT_postHTA1_320-80 T300.txt",
    "2025-06-12_151212_2um_HMT_postHTA1_320-80 T400.txt",
    "2025-06-29_115416_2um_HMT 160-40 T400.txt",
]

labels = {
    "2025-06-09_222644_2um_HMT_postHTA1_320-80 T300.txt": "320-80 T300",
    "2025-06-12_151212_2um_HMT_postHTA1_320-80 T400.txt": "320-80 T400",
    "2025-06-29_115416_2um_HMT 160-40 T400.txt":           "160-40 T400",
}



USECOLS = [2, 10, 12, 18, 33, 34]
NAMES   = ['time (s)', 'membrane T', 'Oven T', 'H2 flow',
           'Permeate (mL/min)', 'Retentate (mL/min)']

limits = {
    "2025-06-09_222644_2um_HMT_postHTA1_320-80 T300.txt": (   5000,
26000, 35, 42),
    "2025-06-12_151212_2um_HMT_postHTA1_320-80 T400.txt": (0, 1450000,
15, 42),
    "2025-06-29_115416_2um_HMT 160-40 T400.txt":           (   0, 26000,
18, 25),
}

target_duration_h = 2.0
```

```
parts = []
offset_h = 0.0

for f in files:
    df = pd.read_table(f, decimal=',', header=0, encoding='latin',
                       usecols=USECOLS, names=NAMES)

    df = df[['time (s)', 'Permeate (mL/min)']].copy()
    df['time (s)'] = pd.to_numeric(df['time (s)'], errors='coerce')
    df['Permeate (mL/min)'] = pd.to_numeric(df['Permeate (mL/min)'],
errors='coerce')
    df = df.dropna(subset=['time (s)', 'Permeate (mL/min)'])

    # --- crop using per-file limits ---
    x_min, x_max, y_min, y_max = limits.get(f, (None, None, None, None))
    if x_min is not None:
        df = df[df['time (s)'] >= x_min]
    if x_max is not None:
        df = df[df['time (s)'] <= x_max]
    if y_min is not None:
        df = df[df['Permeate (mL/min)'] >= y_min]
    if y_max is not None:
        df = df[df['Permeate (mL/min)'] <= y_max]

    if df.empty:
        print(f"Skipped (no rows after cropping): {f}")
        continue


    t0 = df['time (s)'].min()
    df['time_norm (s)'] = df['time (s)'] - t0


    actual_duration_s = df['time_norm (s)'].max()
    if actual_duration_s > 0:
        scale_factor = (target_duration_h * 3600.0) / actual_duration_s
    else:
        scale_factor = 1.0
    df['time_scaled (h)'] = df['time_norm (s)'] * scale_factor / 3600.0


    df['time_concat (h)'] = df['time_scaled (h)'] + offset_h
```

```
    offset_h += target_duration_h


    df['segment'] = labels[f]
    parts.append(df)

if not parts:
    raise RuntimeError("No data to plot (all parts were skipped).")

final_df = pd.concat(parts, ignore_index=True)


plt.rcParams.update({
    'font.family': 'serif',
    'font.size': 14,
    'axes.labelsize': 16,
    'axes.titlesize': 18,
    'xtick.labelsize': 12,
    'ytick.labelsize': 12,
    'axes.linewidth': 1,
    'xtick.direction': 'in',
    'ytick.direction': 'in',
})


segment_order = [labels[f] for f in files]
color_list = ["#1f77b4", "#ff7f0e", "#2ca02c"]
color_map = dict(zip(segment_order, color_list))

fig, ax = plt.subplots(figsize=(10, 6))


for seg_name in segment_order:
    seg = final_df[final_df['segment'] == seg_name]
    if seg.empty:
        continue
    ax.plot(seg['time_concat (h)'], seg['Permeate (mL/min)'],
            linewidth=2.5, label=seg_name, color=color_map.get(seg_name,
'black'))

ax.set_xlabel('time (h)')
ax.set_ylabel('Permeate (mL/min)')
```

```
ax.set_title('')

scaled_ticks = [0, 2, 4, 6]
real_labels  = [0, 7, 424, 431]
ax.set_xticks(scaled_ticks)
ax.set_xticklabels([str(l) for l in real_labels])

ax.grid(True, which='both', linestyle='--', linewidth=0.5, alpha=0.7)
ax.spines['top'].set_visible(False)
ax.spines['right'].set_visible(False)
ax.tick_params(axis='both', which='both', width=1)
ax.legend(fontsize=10)

plt.tight_layout()
plt.show()
```

Code for Linearity Analysis

```
import numpy as np
import matplotlib.pyplot as plt



x = np.array([0.00149, 0.00161, 0.001745])
y = np.array([-36.11, -36.54, -36.89])

m, c = np.polyfit(x, y, 1)

print(f"Slope (m): {m}")
print(f"Intercept (c): {c}")

y_fit = m * x + c

plt.scatter(x, y, color='red', label='Data points')
plt.plot(x, y_fit, color='blue', label=f'Fitted line: y = {m:.2f}x +
{c:.2f}')
plt.xlabel('1/T')
plt.ylabel('ln D')
plt.legend()
plt.grid(False)
plt.show()
```

Appendix D

Raw Data

The title of each experiment is given on the top-middle of each figure. The common structure of the title: hydrogen flow rate-nitrogen flow rate, temperature. For instance: 320-80 T400. Here 320 (mL/m) represents the flow rate of hydrogen, 80 (mL/m) represents the flow rate of nitrogen. Moreover, T400 (400 $°C$) represents the temperature of membrane

5.5 μm membrane

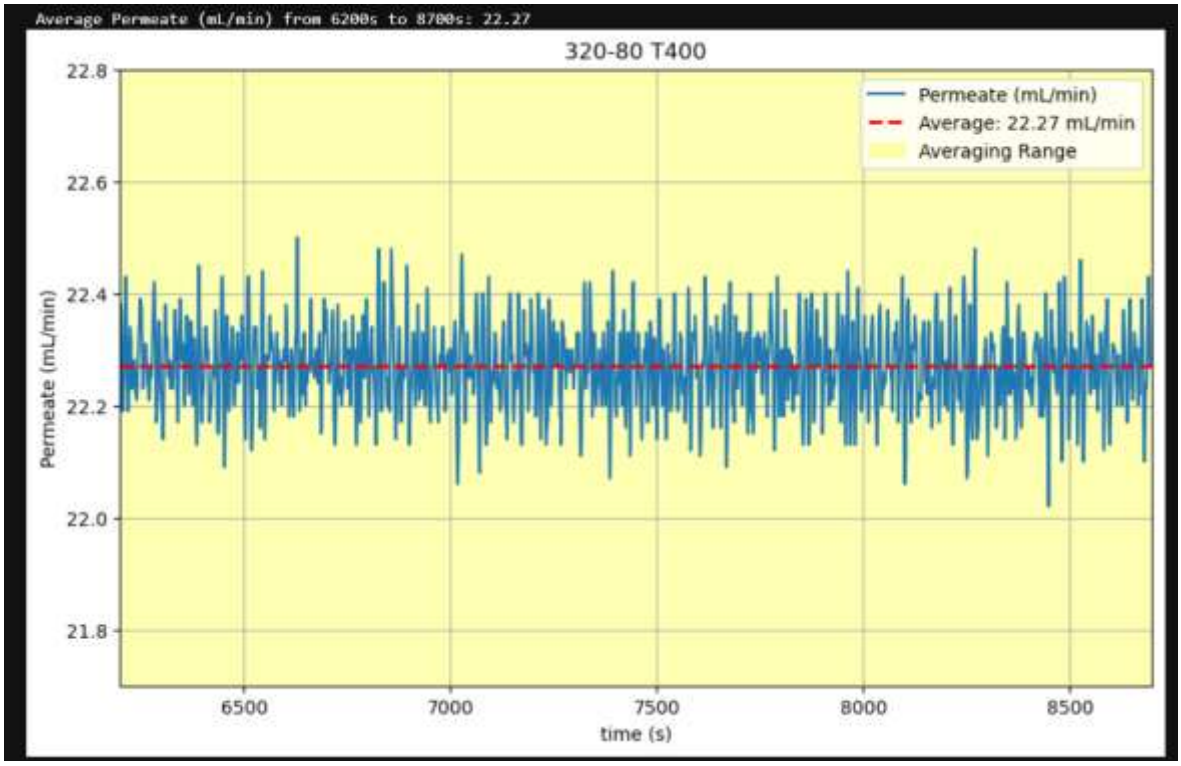

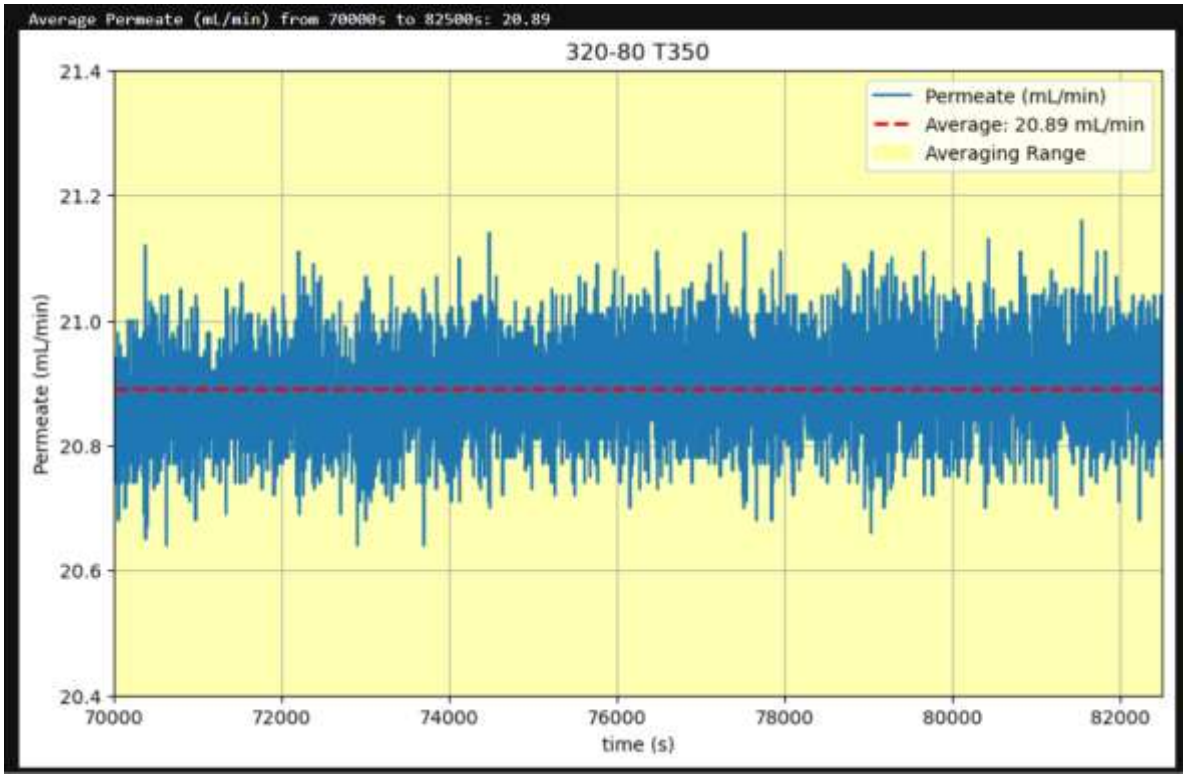
Average Permeate (mL/min) from 70000s to 82500s: 20.89
320-80 T350
Permeate (mL/min)
Average: 20.89 mL/min
Averaging Range
Permeate (mL/min)
time (s)
21.4
21.2
21.0
20.8
20.6
20.4
70000
72000
74000
76000
78000
80000
82000

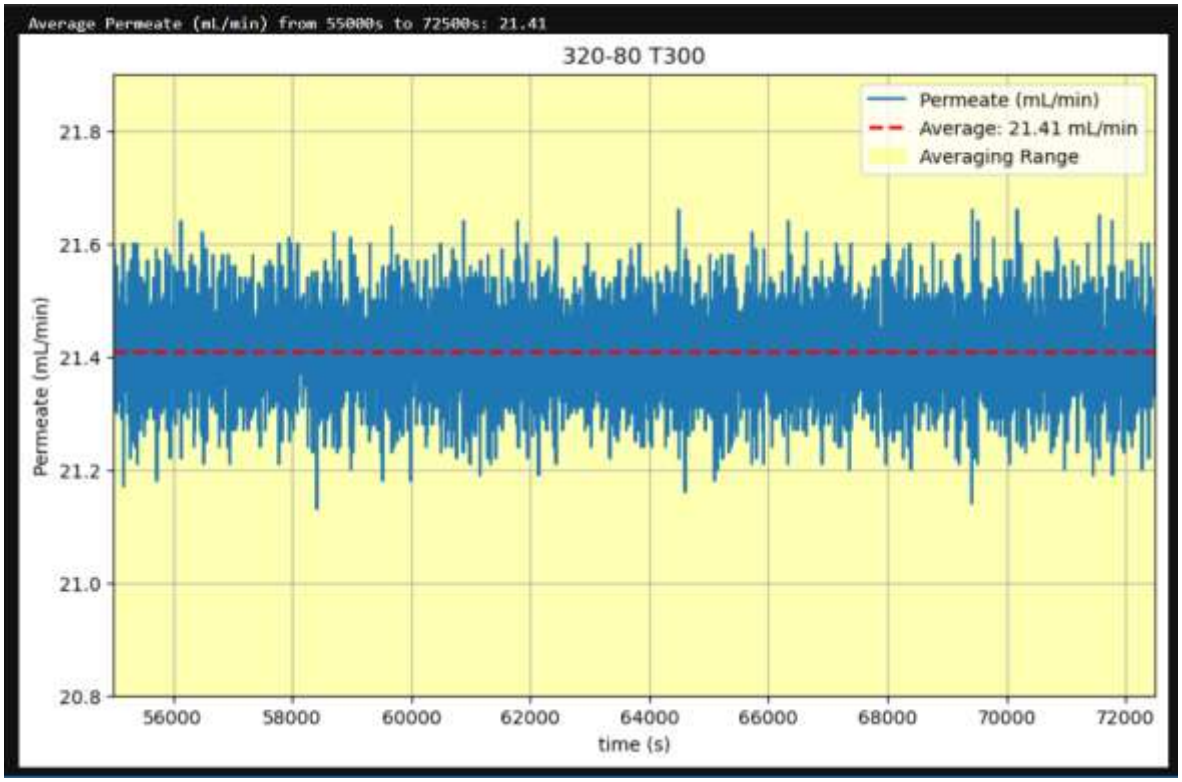
Average Permeate (mL/min) from 55000s to 72500s: 21.41
320-80 T300
Permeate (mL/min)
Average: 21.41 mL/min
Averaging Range
Permeate (mL/min)
time (s)
21.8
21.6
21.4
21.2
21.0
20.8
56000
58000
60000
62000
64000
66000
68000
70000
72000

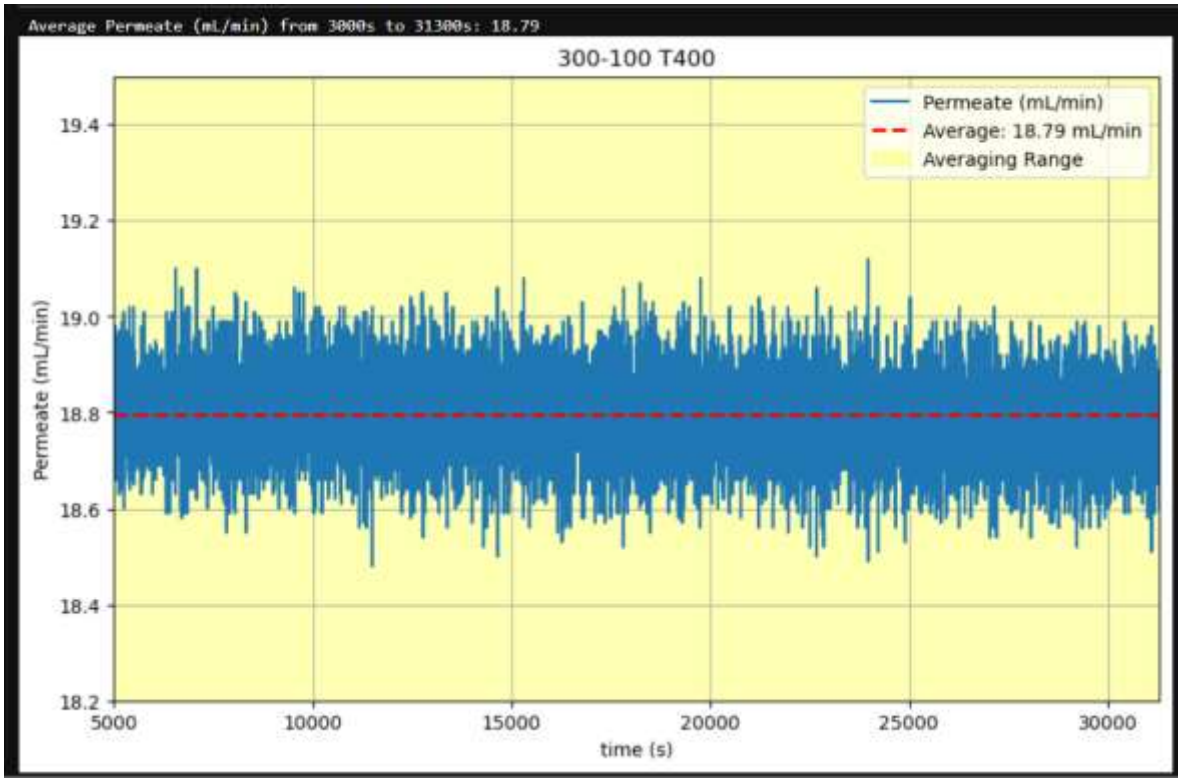
Average Permeate (mL/min) from 3000s to 31300s: 18.79
300-100 T400
Permeate (mL/min)
Average: 18.79 mL/min
Averaging Range
Permeate (mL/min)
time (s)
19.4
19.2
19.0
18.8
18.6
18.4
18.2
5000
10000
15000
20000
25000
30000

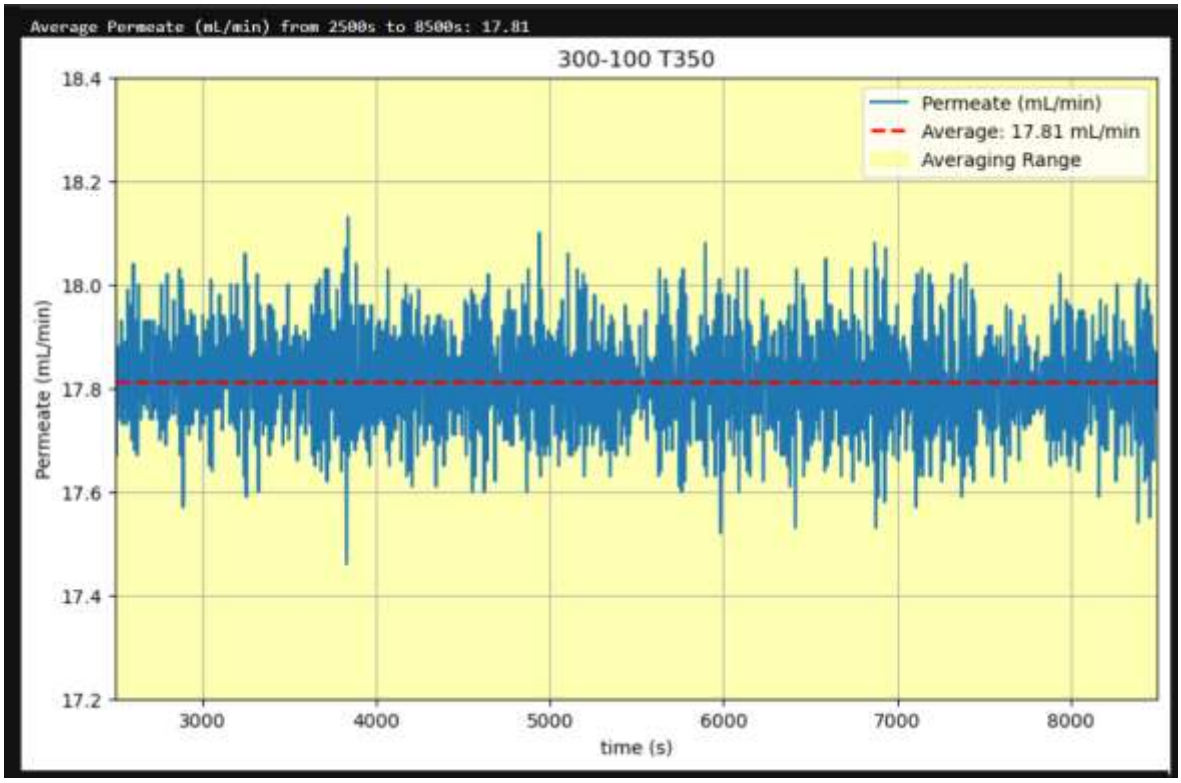
Average Permeate (mL/min) from 2500s to 8500s: 17.81
300-100 T350
Permeate (mL/min)
Average: 17.81 mL/min
Averaging Range
Permeate (mL/min)
time (s)
18.4
18.2
18.0
17.8
17.6
17.4
17.2
3000
4000
5000
6000
7000
8000

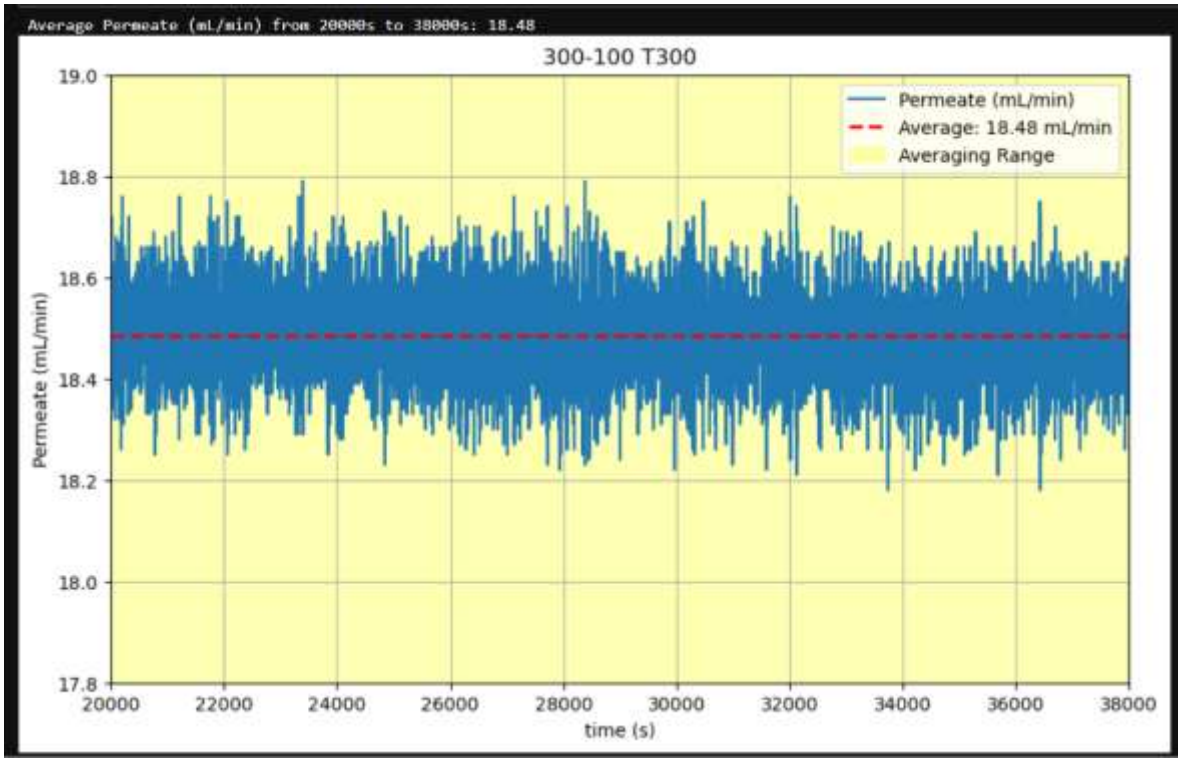
Average Permeate (mL/min) from 20000s to 38000s: 18.48
300-100 T300
Permeate (mL/min)
Average: 18.48 mL/min
Averaging Range
Permeate (mL/min)
time (s)
19.0
18.8
18.6
18.4
18.2
18.0
17.8
20000
22000
24000
26000
28000
30000
32000
34000
36000
38000

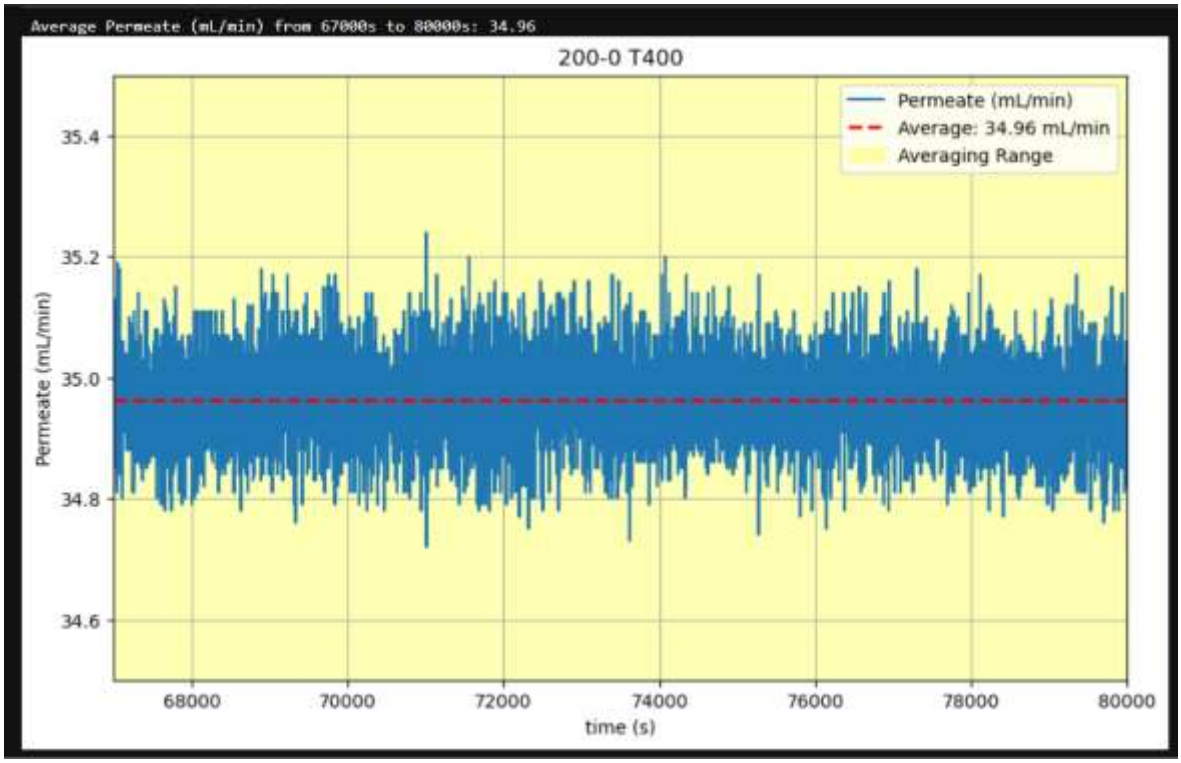
Average Permeate (mL/min) from 67000s to 80000s: 34.96
200-0 T400
Permeate (mL/min)
Average: 34.96 mL/min
Averaging Range
Permeate (mL/min)
time (s)
35.4
35.2
35.0
34.8
34.6
68000
70000
72000
74000
76000
78000
80000

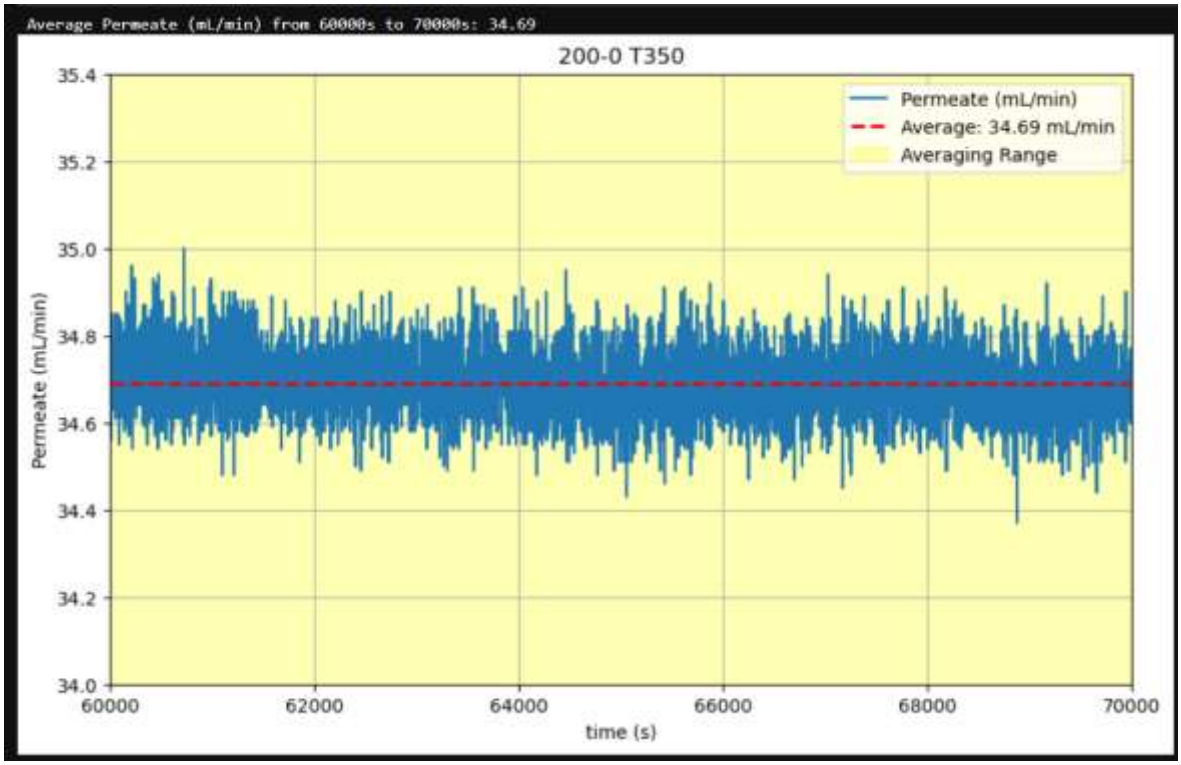
Average Permeate (mL/min) from 60000s to 70000s: 34.69
200-0 T350
Permeate (mL/min)
Average: 34.69 mL/min
Averaging Range
Permeate (mL/min)
time (s)
35.4
35.2
35.0
34.8
34.6
34.4
34.2
34.0
60000
62000
64000
66000
68000
70000

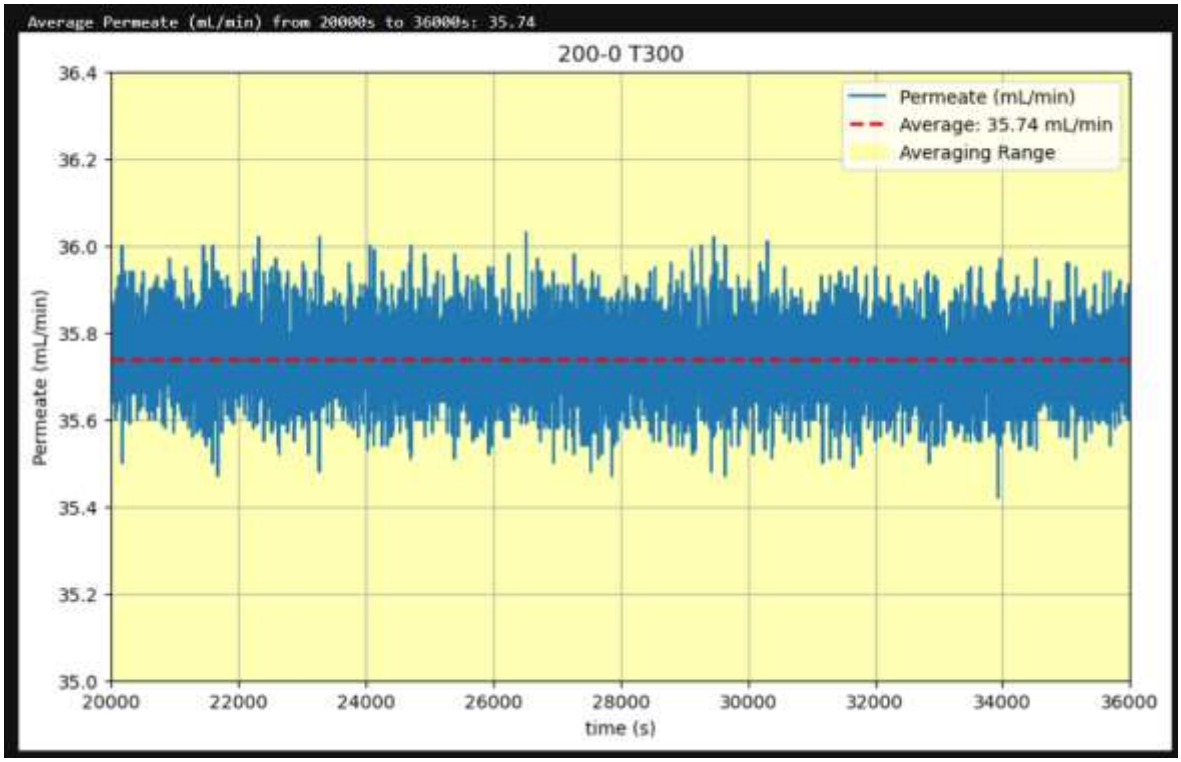
Average Permeate (mL/min) from 20000s to 36000s: 35.74
200-0 T300
Permeate (mL/min)
Average: 35.74 mL/min
Averaging Range
Permeate (mL/min)
time (s)
36.4
36.2
36.0
35.8
35.6
35.4
35.2
35.0
20000
22000
24000
26000
28000
30000
32000
34000
36000

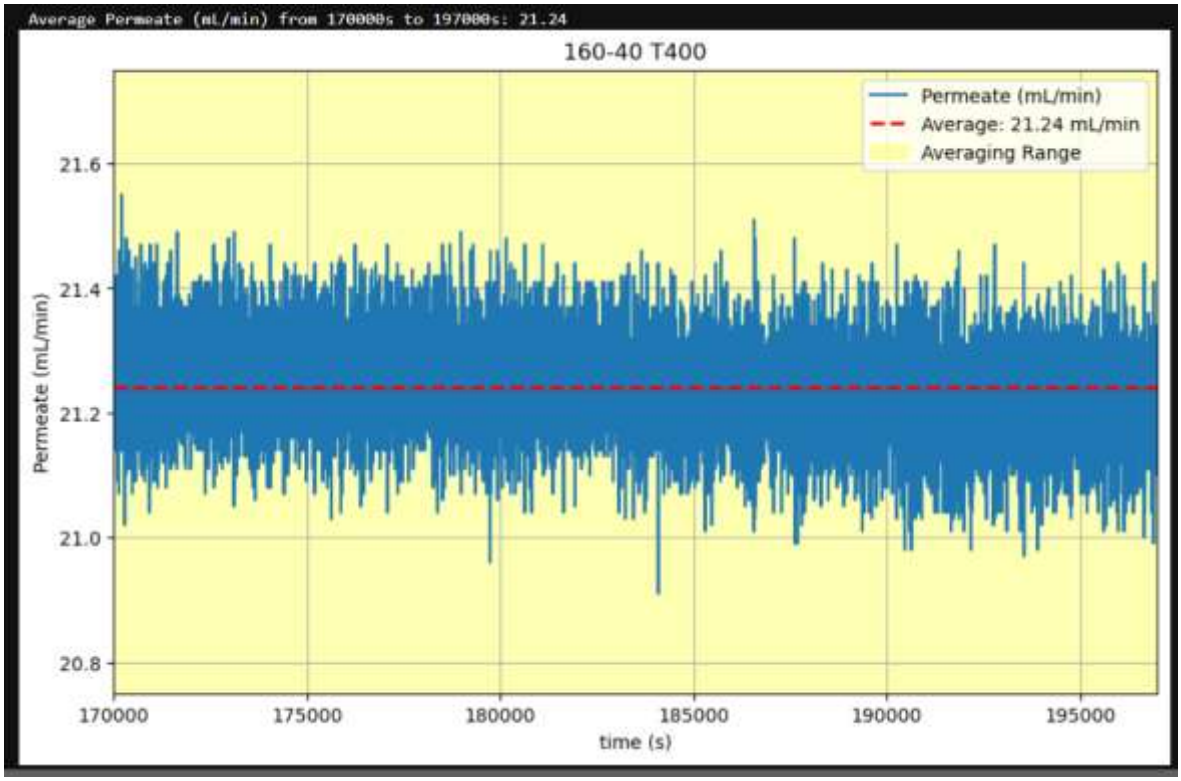
Average Permeate (mL/min) from 170000s to 197000s: 21.24
160-40 T400
Permeate (mL/min)
Average: 21.24 mL/min
Averaging Range
Permeate (mL/min)
time (s)
21.6
21.4
21.2
21.0
20.8
170000
175000
180000
185000
190000
195000

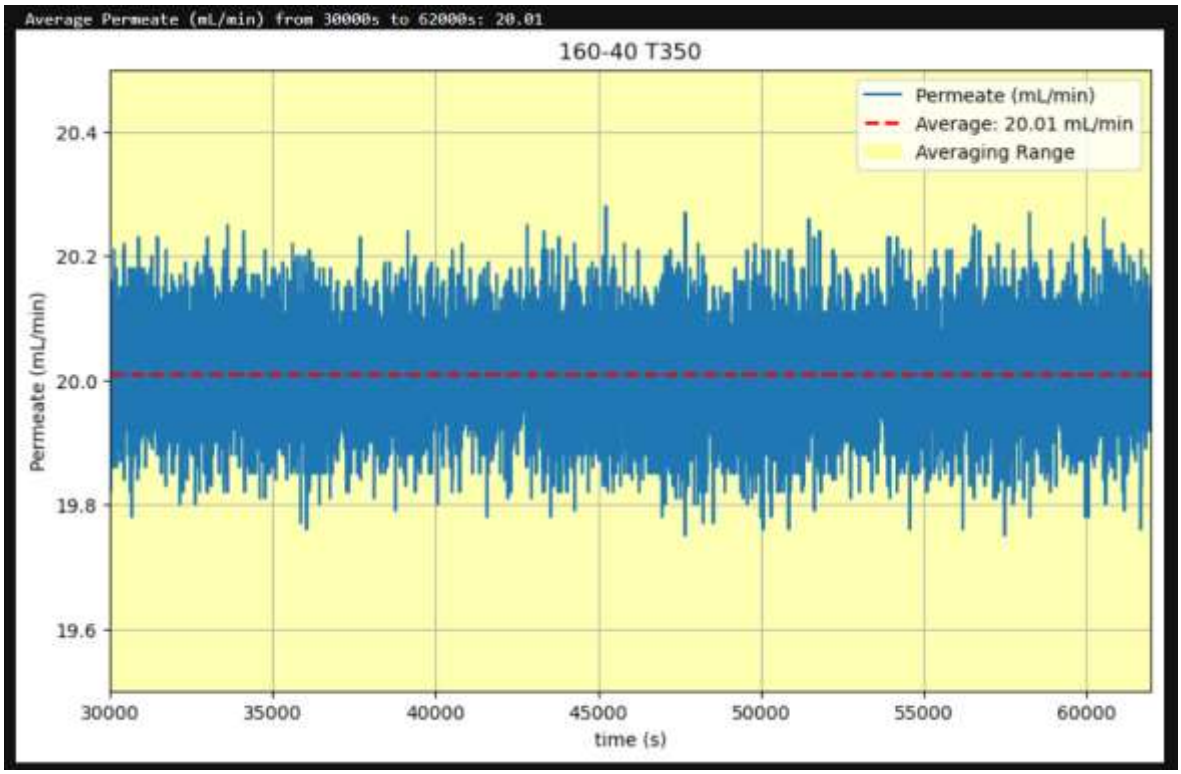
Average Permeate (mL/min) from 30000s to 62000s: 20.01
160-40 T350
Permeate (mL/min)
Average: 20.01 mL/min
Averaging Range
Permeate (mL/min)
time (s)
20.4
20.2
20.0
19.8
19.6
30000
35000
40000
45000
50000
55000
60000

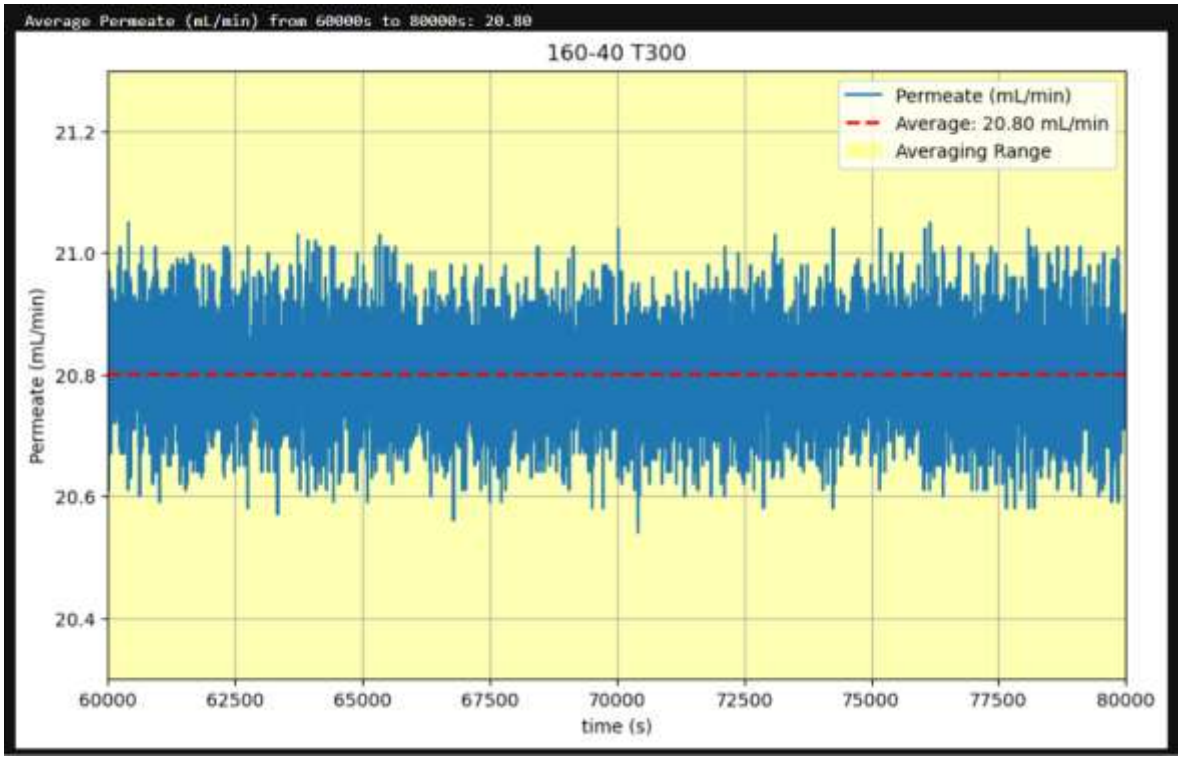
Average Permeate (mL/min) from 60000s to 80000s: 20.80
160-40 T300
Permeate (mL/min)
Average: 20.80 mL/min
Averaging Range
Permeate (mL/min)
21.2
21.0
20.8
20.6
20.4
60000
62500
65000
67500
70000
72500
75000
77500
80000
time (s)

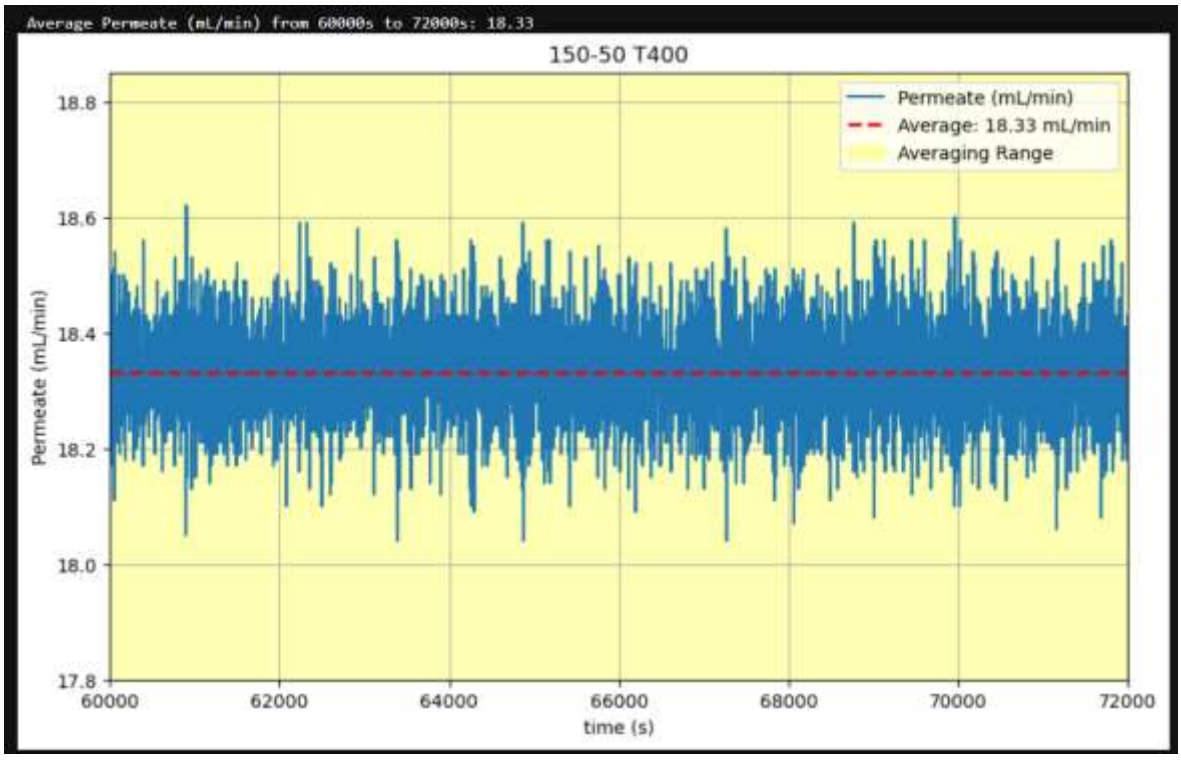
Average Permeate (mL/min) from 60000s to 72000s: 18.33
150-50 T400
Permeate (mL/min)
Average: 18.33 mL/min
Averaging Range
Permeate (mL/min)
18.8
18.6
18.4
18.2
18.0
17.8
60000
62000
64000
66000
68000
70000
72000
time (s)

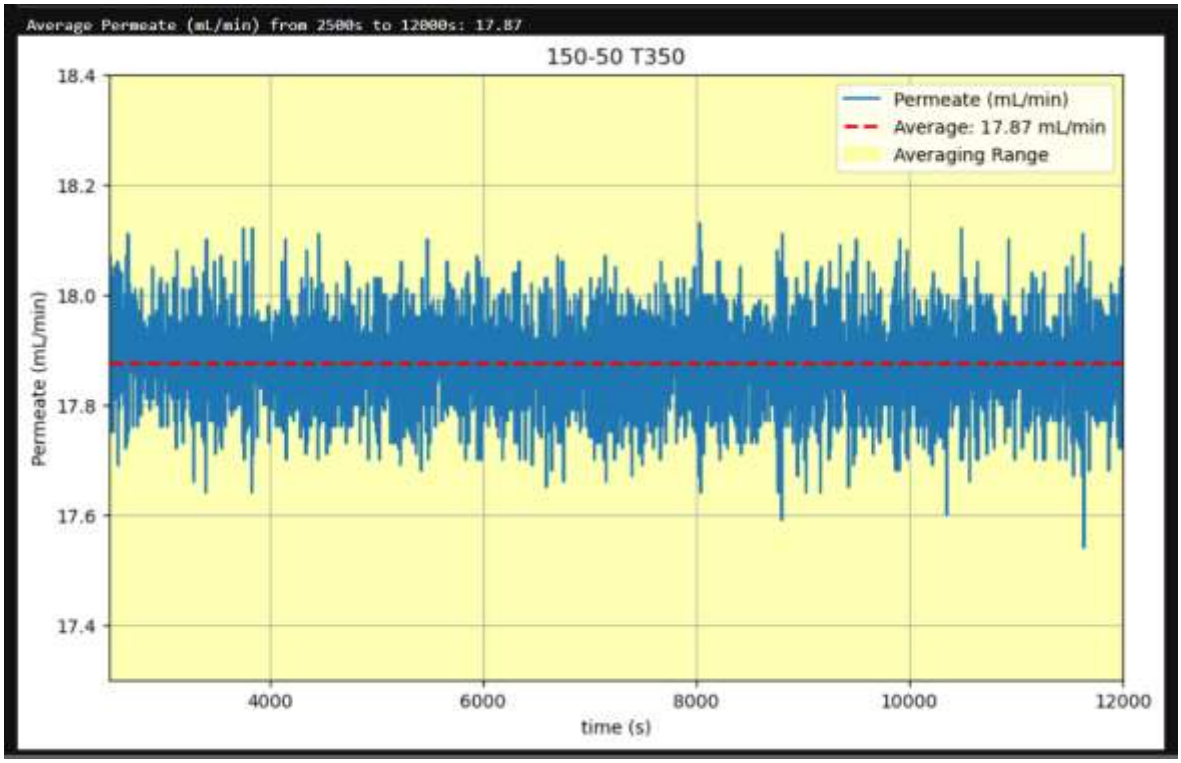
Average Permeate (mL/min) from 2500s to 12000s: 17.87
150-50 T350
Permeate (mL/min)
Average: 17.87 mL/min
Averaging Range
Permeate (mL/min)
time (s)
18.4
18.2
18.0
17.8
17.6
17.4
4000
6000
8000
10000
12000

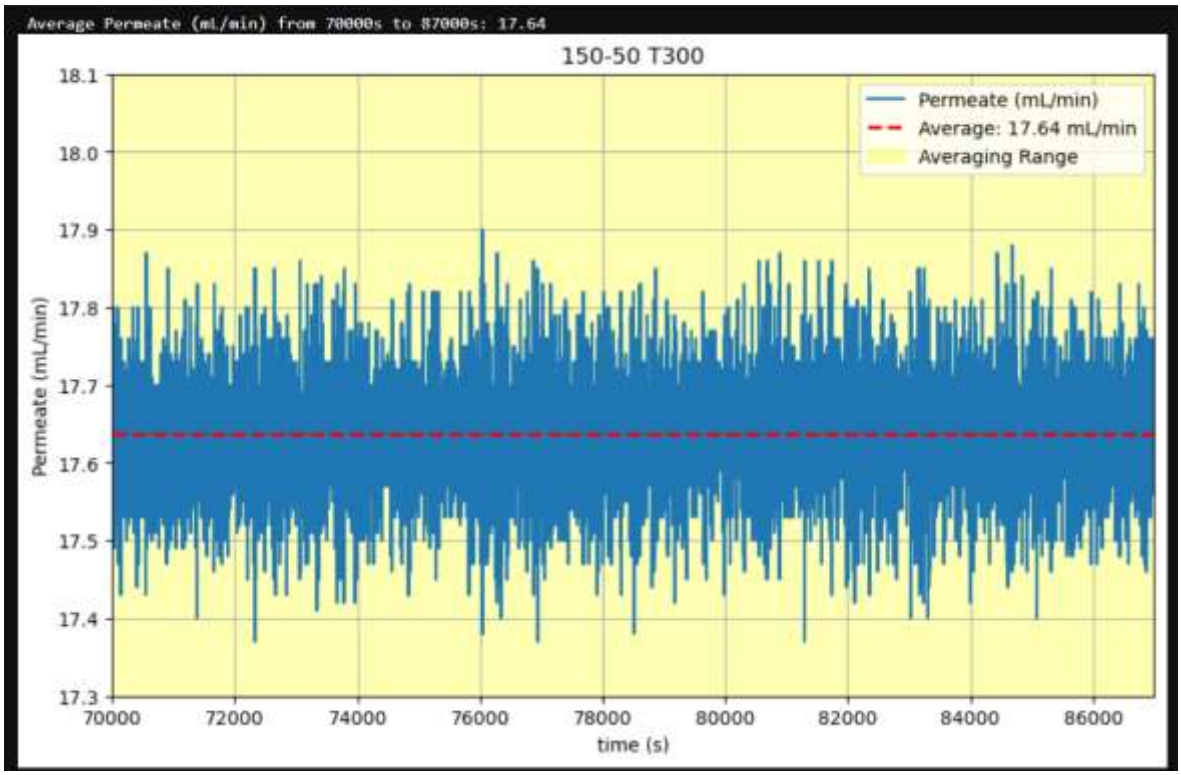
Average Permeate (mL/min) from 70000s to 87000s: 17.64
150-50 T300
Permeate (mL/min)
Average: 17.64 mL/min
Averaging Range
Permeate (mL/min)
time (s)
18.1
18.0
17.9
17.8
17.7
17.6
17.5
17.4
17.3
70000
72000
74000
76000
78000
80000
82000
84000
86000

10 μm membrane:

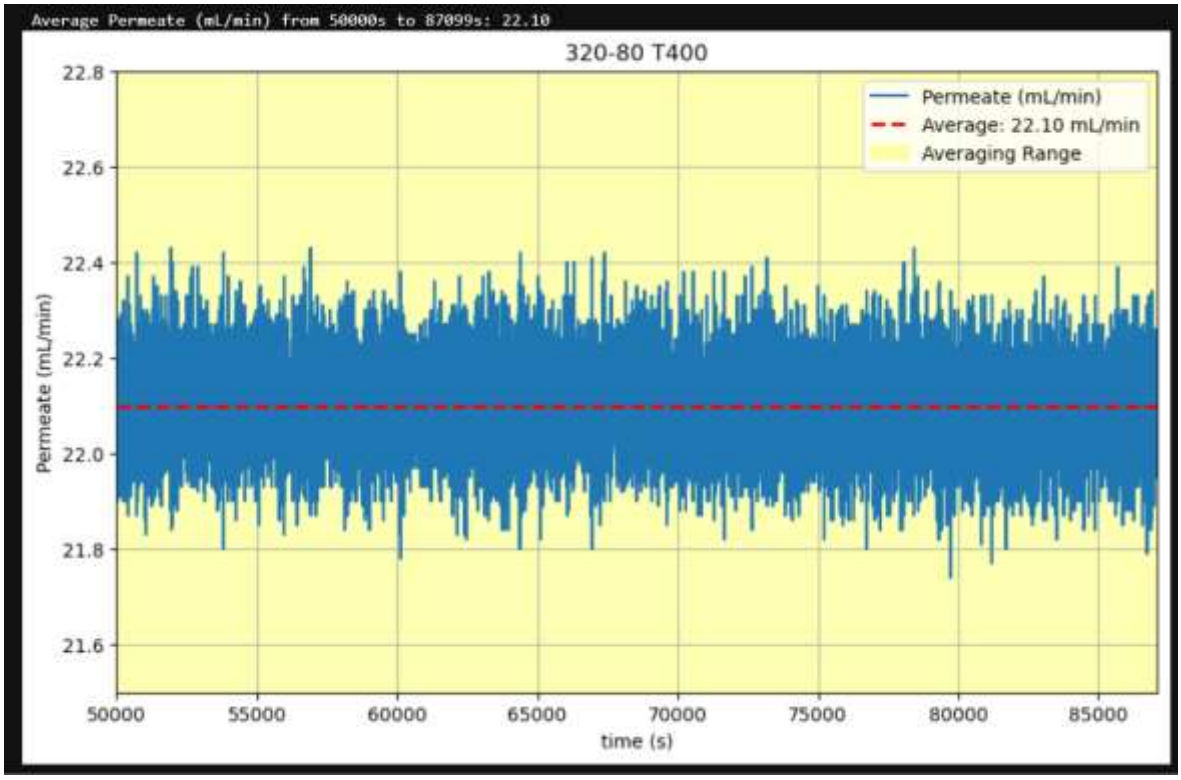

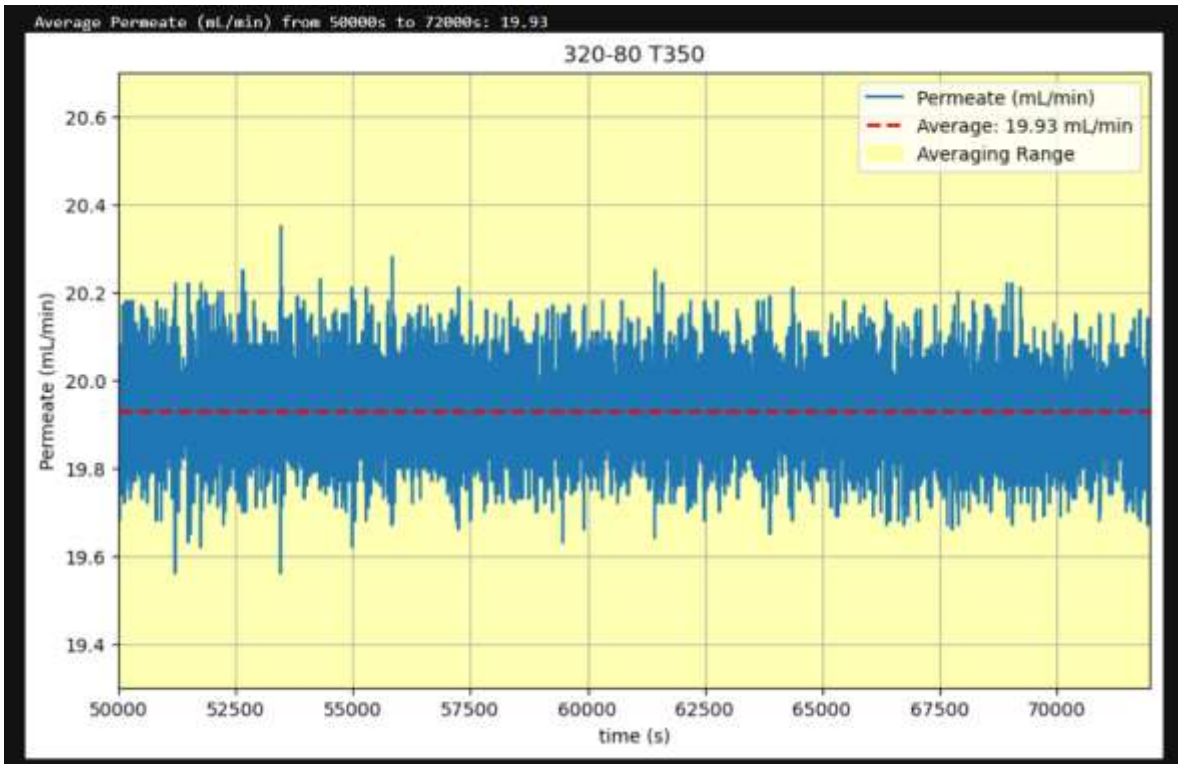

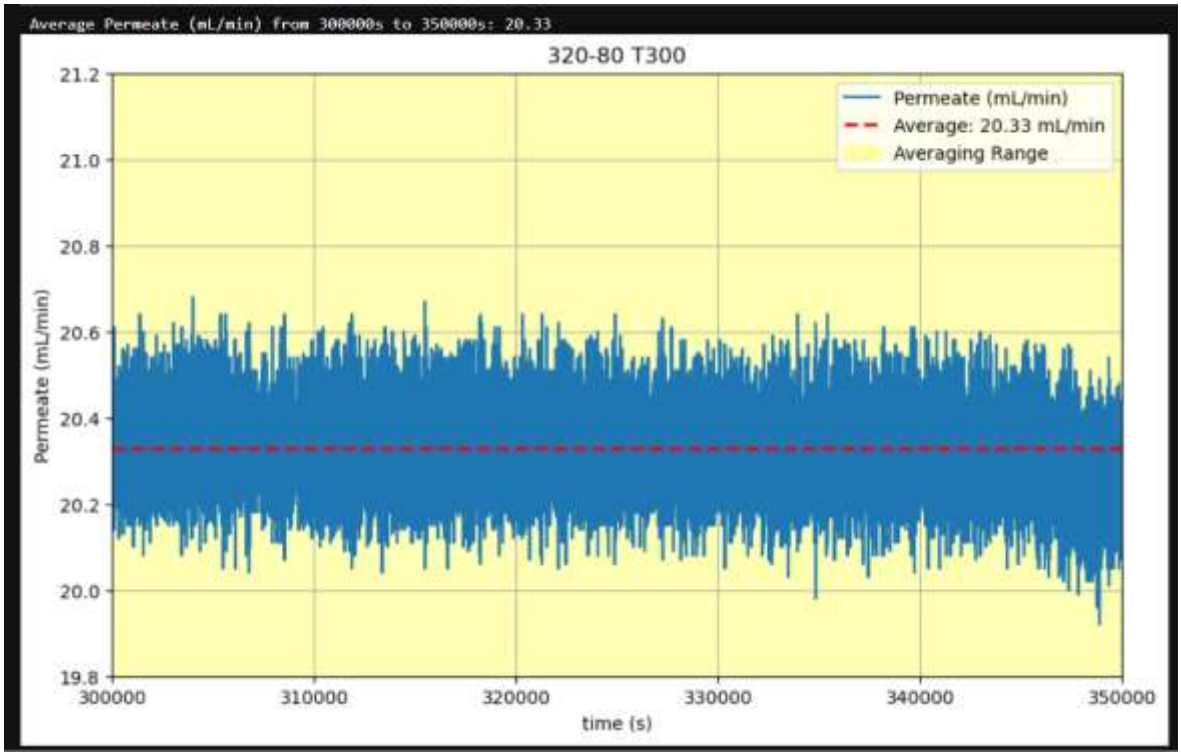
Average Permeate (mL/min) from 300000s to 350000s: 20.33
320-80 T300
Permeate (mL/min)
Average: 20.33 mL/min
Averaging Range
Permeate (mL/min)
time (s)
21.2
21.0
20.8
20.6
20.4
20.2
20.0
19.8
300000
310000
320000
330000
340000
350000

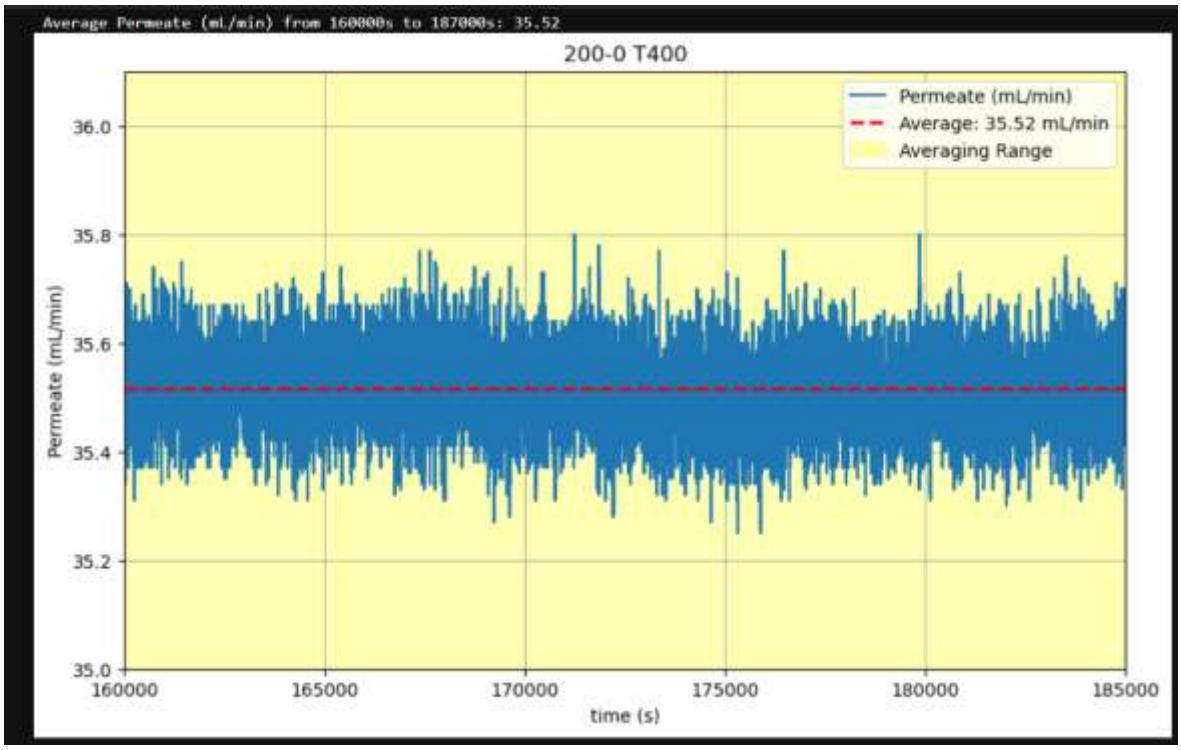
Average Permeate (mL/min) from 160000s to 187000s: 35.52
200-0 T400
Permeate (mL/min)
Average: 35.52 mL/min
Averaging Range
Permeate (mL/min)
time (s)
36.0
35.8
35.6
35.4
35.2
35.0
160000
165000
170000
175000
180000
185000

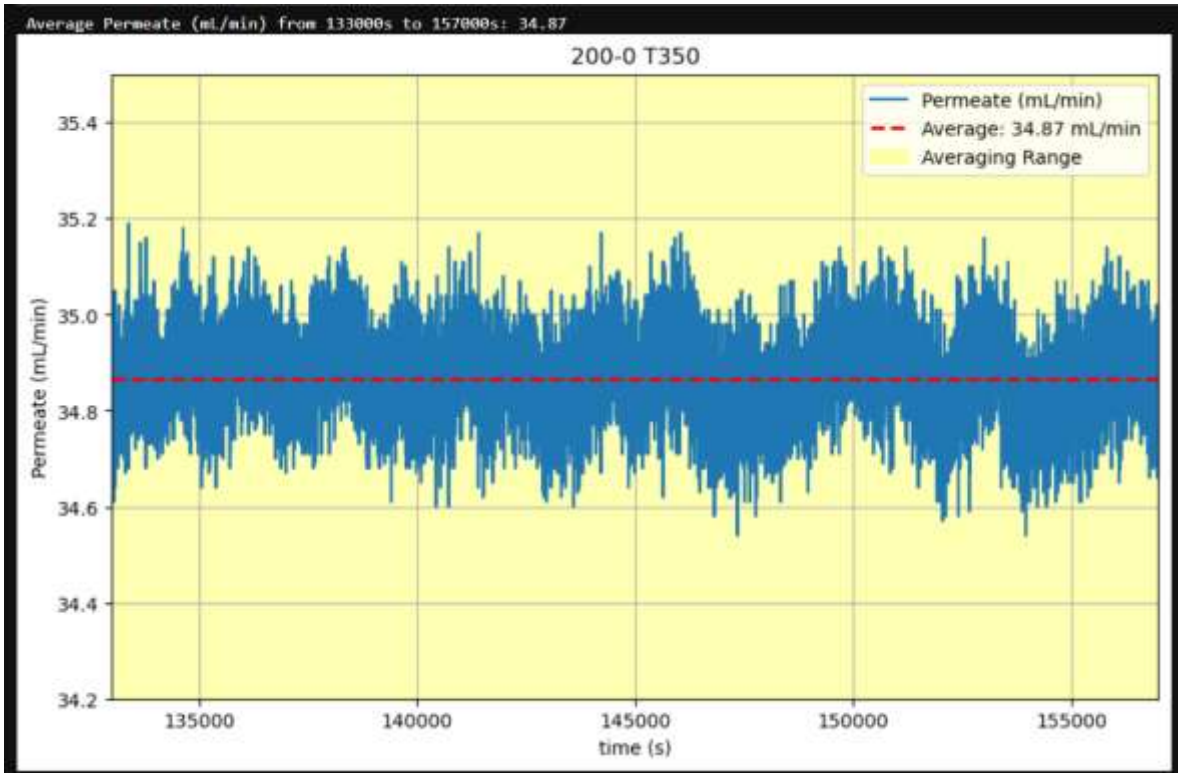
Average Permeate (mL/min) from 133000s to 157000s: 34.87
200-0 T350
Permeate (mL/min)
Average: 34.87 mL/min
Averaging Range
Permeate (mL/min)
time (s)
35.4
35.2
35.0
34.8
34.6
34.4
34.2
135000
140000
145000
150000
155000

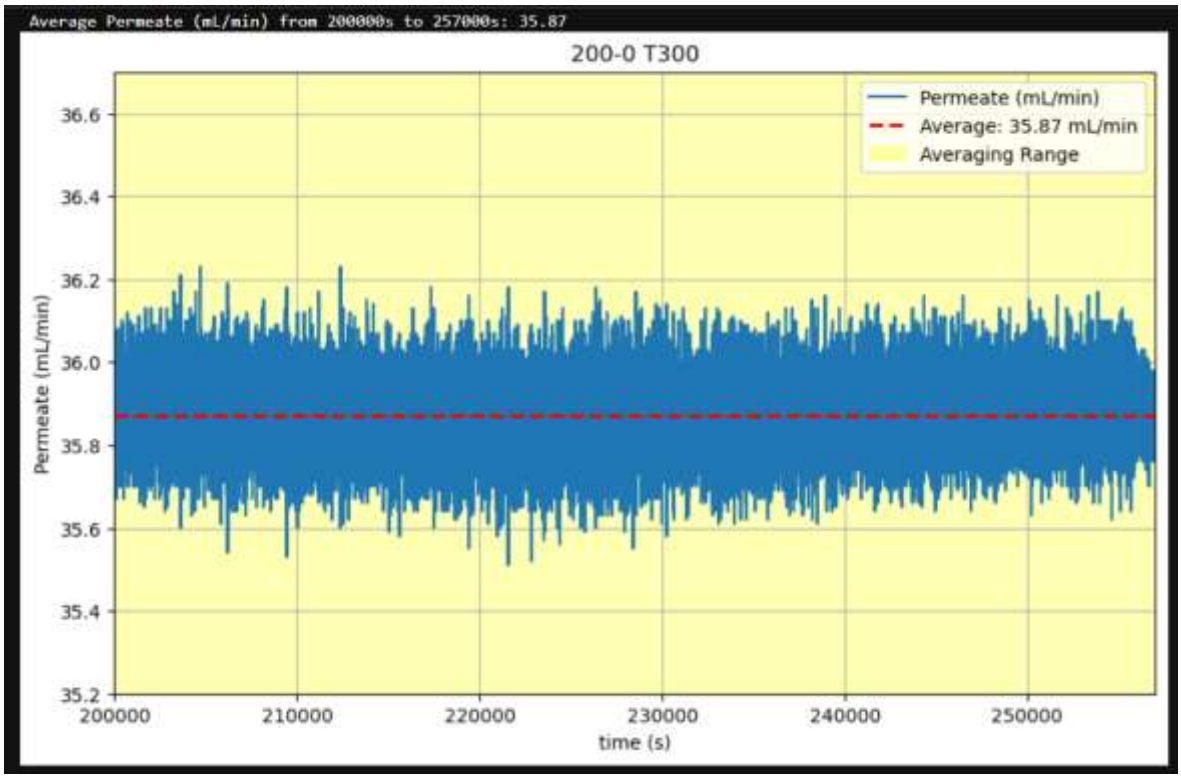
Average Permeate (mL/min) from 200000s to 257000s: 35.87
200-0 T300
Permeate (mL/min)
Average: 35.87 mL/min
Averaging Range
Permeate (mL/min)
time (s)
36.6
36.4
36.2
36.0
35.8
35.6
35.4
35.2
200000
210000
220000
230000
240000
250000

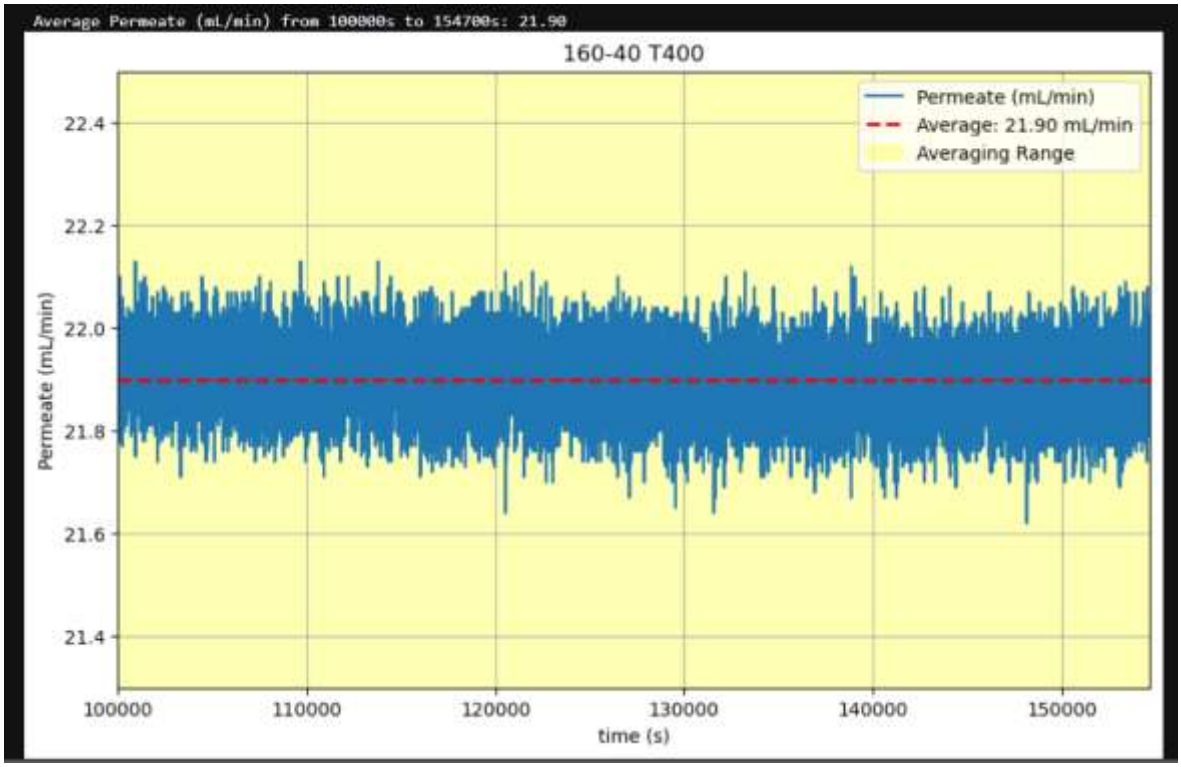
Average Permeate (mL/min) from 100000s to 154700s: 21.90
160-40 T400
Permeate (mL/min)
Average: 21.90 mL/min
Averaging Range
Permeate (mL/min)
time (s)
22.4
22.2
22.0
21.8
21.6
21.4
100000
110000
120000
130000
140000
150000

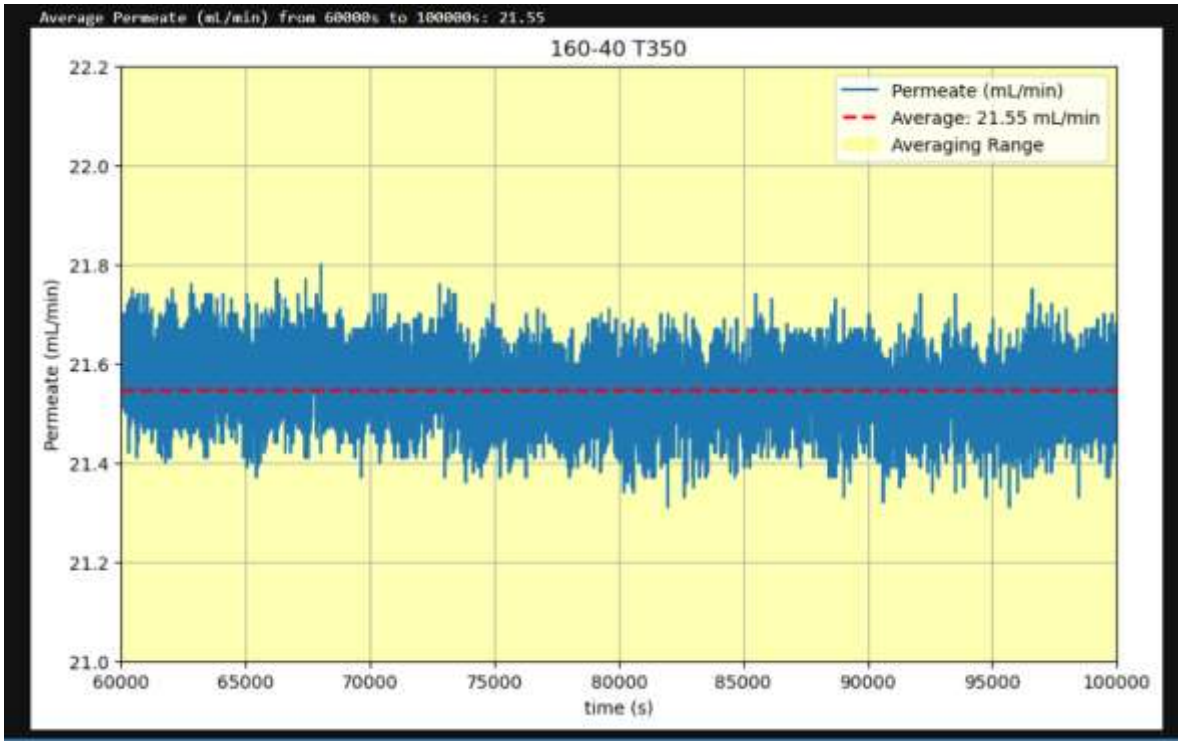
Average Permeate (mL/min) from 60000s to 100000s: 21.55
160-40 T350
Permeate (mL/min)
Average: 21.55 mL/min
Averaging Range
Permeate (mL/min)
time (s)
22.2
22.0
21.8
21.6
21.4
21.2
21.0
60000
65000
70000
75000
80000
85000
90000
95000
100000

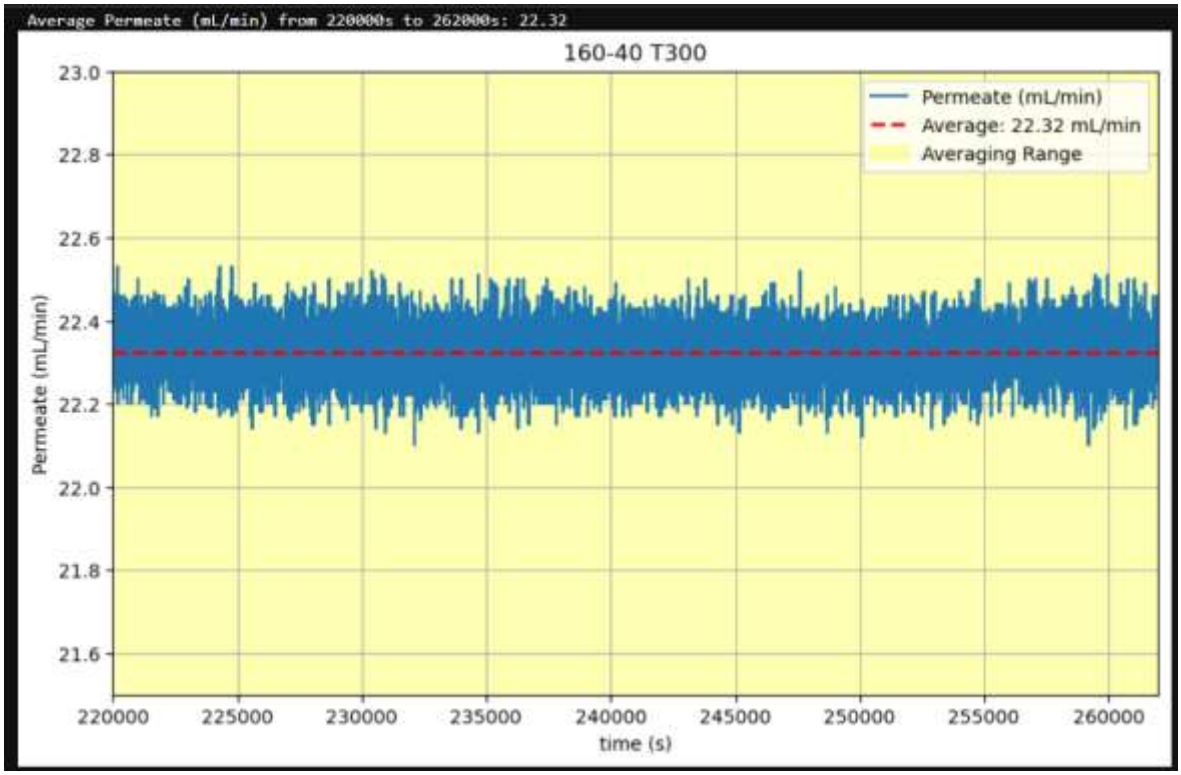
Average Permeate (mL/min) from 220000s to 262000s: 22.32
160-40 T300
Permeate (mL/min)
Average: 22.32 mL/min
Averaging Range
Permeate (mL/min)
time (s)
23.0
22.8
22.6
22.4
22.2
22.0
21.8
21.6
220000
225000
230000
235000
240000
245000
250000
255000
260000

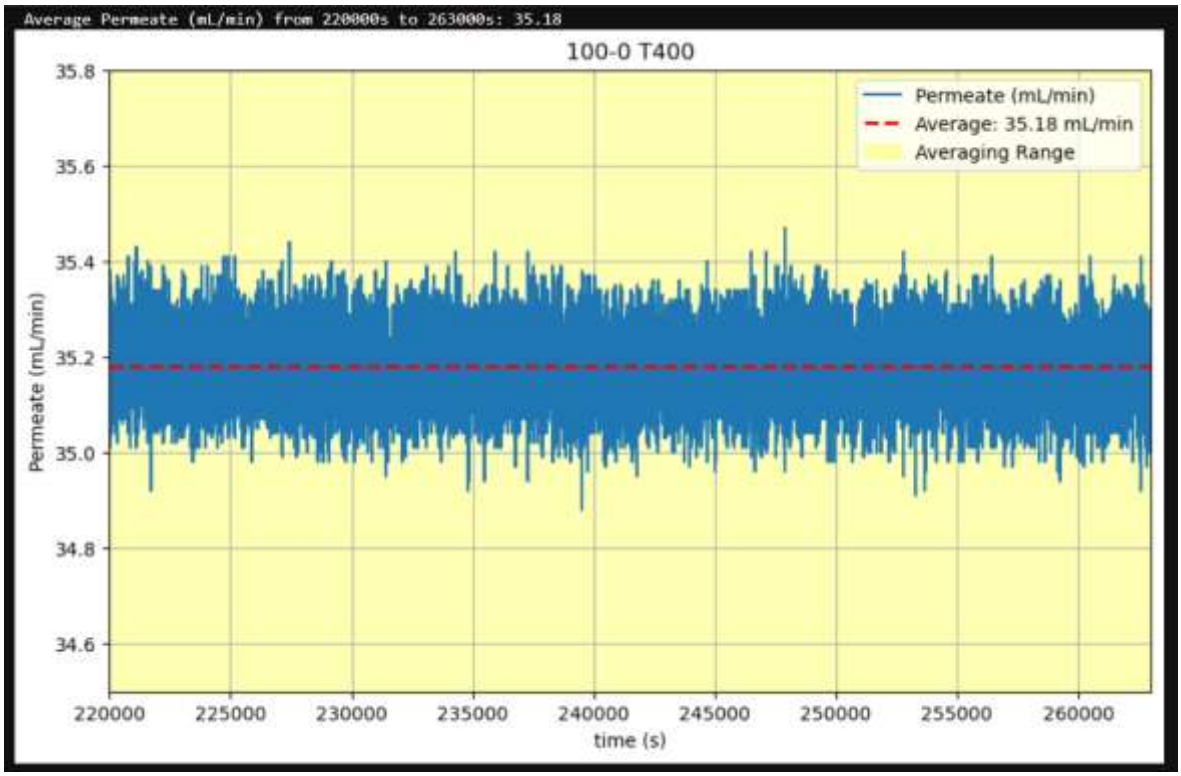
Average Permeate (mL/min) from 220000s to 263000s: 35.18
100-0 T400
Permeate (mL/min)
Average: 35.18 mL/min
Averaging Range
Permeate (mL/min)
time (s)
35.8
35.6
35.4
35.2
35.0
34.8
34.6
220000
225000
230000
235000
240000
245000
250000
255000
260000

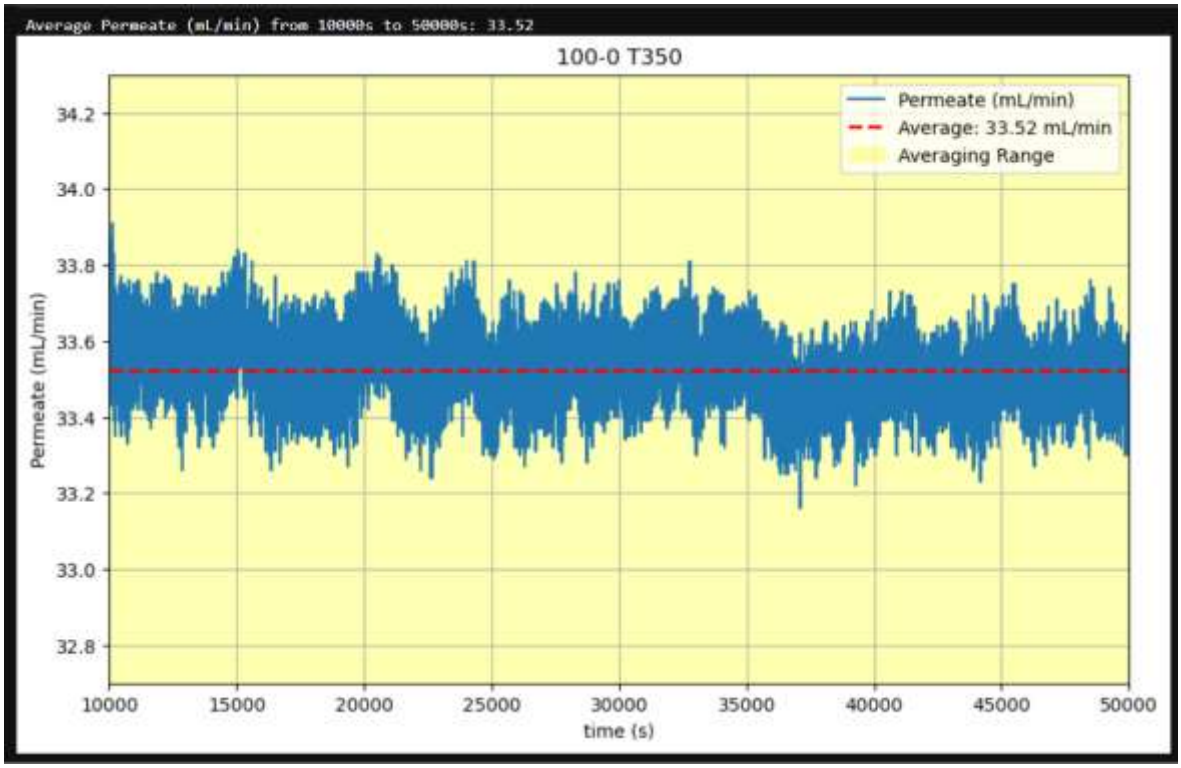
Average Permeate (mL/min) from 10000s to 50000s: 33.52
100-0 T350
Permeate (mL/min)
Average: 33.52 mL/min
Averaging Range
Permeate (mL/min)
time (s)

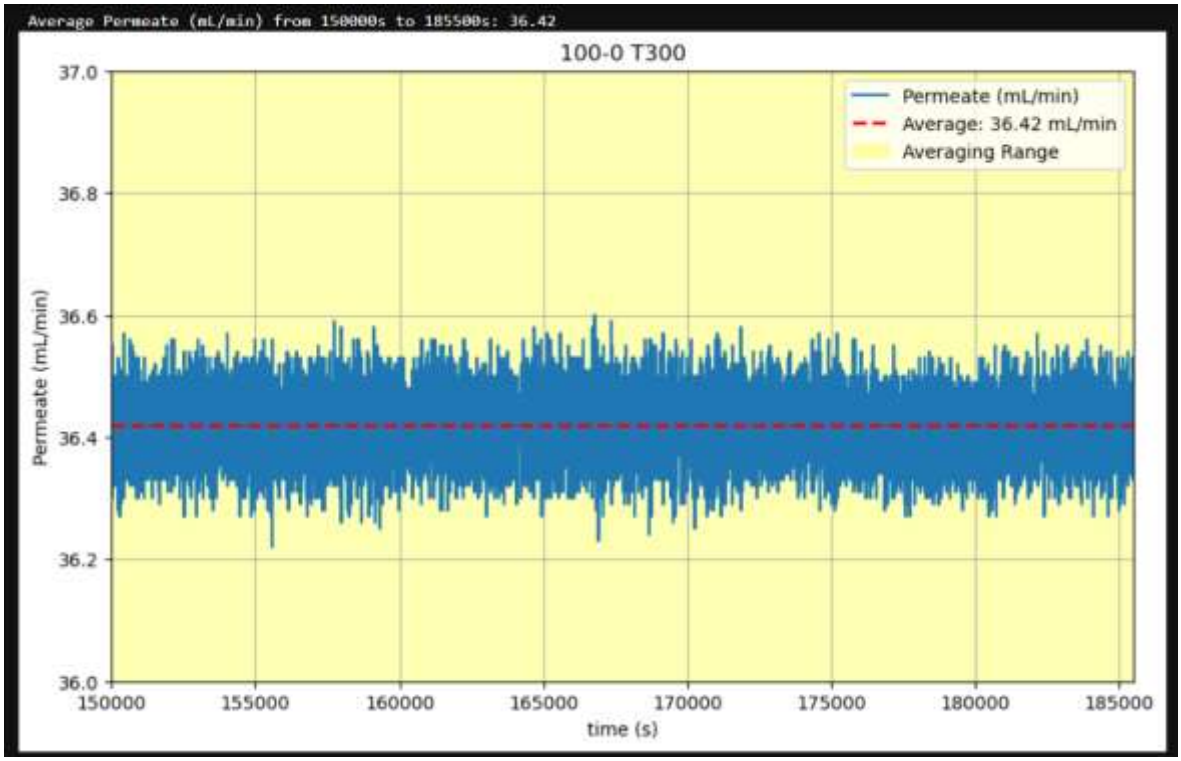
Average Permeate (mL/min) from 150000s to 185500s: 36.42
100-0 T300
Permeate (mL/min)
Average: 36.42 mL/min
Averaging Range
Permeate (mL/min)
time (s)

Appendix E

Gas Flow

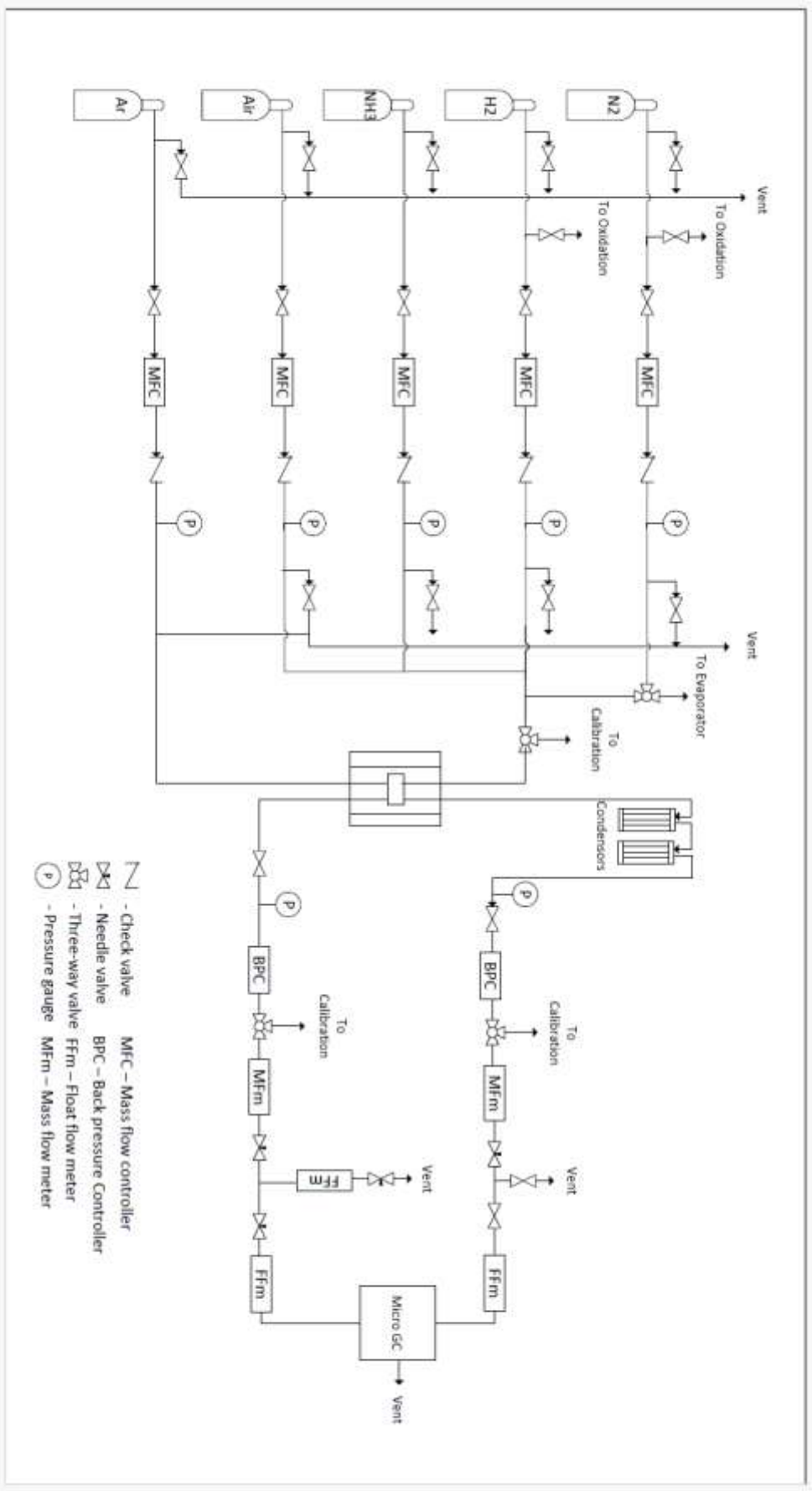

Appendix F

HSE Risk Assessment

NV-IKP, Catalysis, Student, 2025, Sheikh Md Rashedul Alam Sa

Risk-ID: 9760	**Reported by:** Sheikh Md Rashedul Alam Sayem	**Reported:** 26.03.2025
Status: Review round	**Responsible for risk:** Sheikh Md Rashedul Alam Sayem	**Deadline for closing:** 25.05.2025
Reported from unit: Fakultet for ingeniørvitenskap	**Assigned unit:** Fakultet for ingeniørvitenskap	**Form:** Risikovurdering HMS

Risk element

"Fra enhet": Angir enhet til den som oppretter risikovurderingen.
"Til enhet": Angir enhet som omfattes av risikovurderingen. Denne kan endres.
"Risikoansvarlig": Angir den som oppretter risikovurderingen. Denne personen har redigeringstilgang.

HMS Risikovurdering

NTNU

Innledning

Tittel	NV-IKP, Catalysis, Student, 2025, Sheikh Md Rashedul Alam Sa
Kategori	Laboratorie / verksted
Prosjektnr., arbeidsnr., emnekode, annet	TPK-4950
Deltakere i risikovurderingen	Hilde Johnsen Venvik Willow Nadine Dew Estelle Marie Madeleine Vanhaecke
☐ *Legg til eksterne deltakere (fritekst)*	
Kommentar	
Sted	kjmihallen ,Hall D, 2nd floor
Leserettighet	Kun risikoansvarlig (den som oppretter risikovurderingen)

Bakgrunn

Bakgrunn for risikovurdering Ny arbeidsoppgave/prosess/aktivitet.

Arbeidsbeskrivelse

Evaluating performance of Pd Membrane for hydrogen separation from ammonia mixture. In our project, we will observe the perr and inhibition of ammonia that is considered as a hindrance to hydrogen permiability. Later we will analyze the materials of the r understand the phenomenon better.

Avgrensninger / forutsetninger

1. Pd membranes are prone to hydrogen embrittlement, especially at lower temperatures or under cyclic loading conditions. This failure of the membrane over time. We are not exploring how to optimize on it.2. Palladium is an expensive material, which can m applications economically challenging.

Last opp relevant dokumentasjon

h2_sds.pdf

https://hydrogeni.no/research/cost-effecti ble-production/

nh3_sds.pdf

Rig_2.9_Oxidation_MembraneNov2024.pdf

Det anbefales mellomlagring underveis. Lagreknapp nederst i skjemaet

Identifiser uønskede hendelser og vurder risiko

Åpne NTNUs HMS-retningslinjer og pros

Arbeidsmiljøfaktorer	Kjemisk og biologisk
Aktivitet 1	Handling ammonia gas or ammonia-containing mixtures during experiments
Uønsket hendelse 1	Ammonia Exposure
Eksisterende tiltak	Suction Point, personal protective equipment (PPE) like gloves, goggles, and respirators, Leak test before experimentation, NH3 bottle is inside the rig where ventilation takes place every 2 minutes, ammonia sensors for leak detection and proper ventilation systems
Sannsynlighet	Lite sannsynlig
Konsekvens	Menneske - Kritisk Omdømme - Farlig
	Øk./materiell - Farlig Ytre miljø - Farlig
Begrunnelse	Ammonia is highly toxic and corrosive, posing significant health and safety risks
Kommentar / forslag til nye tiltak	

☑ Legg til ny uønsket hendelse

Uønsket hendelse 2	Membrane Fouling
Eksisterende tiltak	N/A
Sannsynlighet	Sannsynlig
Konsekvens	Menneske - Ingen/liten fare  Omdømme - Ingen/liten fare
	Øk./materiell - Farlig Ytre miljø - Farlig
Begrunnelse	Fouling reduces membrane performance and increases operational costs
Kommentar / forslag til nye tiltak	

☐ Legg til ny uønsket hendelse

☑ Legg til ny aktivitet

Aktivitet 2	Handling Hydrogen Gas
Uønsket hendelse 1	Hydrogen Embrittlement
Eksisterende tiltak	Use of Pd alloys (e.g., Pd-Ag) to reduce embrittlement, periodic inspection of membranes
Sannsynlighet	Sannsynlig
Konsekvens	Menneske - Ikke aktuell Omdømme - Ingen/liten fare
	Øk./materiell - Farlig Ytre miljø - Farlig
Begrunnelse	Hydrogen embrittlement is a known issue with Pd membranes, especially under cyclic loading.
Kommentar / forslag til tiltak	Monitor membrane integrity regularly, use hydrogen sensors, and explore alternative membrane materials.

☑ Legg til ny uønsket hendelse

Uønsket hendelse 2	Fire or Explosion
Eksisterende tiltak	Use of flame arrestors, explosion-proof equipment, and hydrogen sensors
Sannsynlighet	Lite sannsynlig

Konsekvens	Menneske - Katastrofalt		Omdømme - Katastrofalt
	Øk./materiell - Kritisk		Ytre miljø - Farlig
Begrunnelse			
Kommentar / forslag til tiltak			

☐ Legg til ny uønsket hendelse

☑ Legg til ny aktivitet

Aktivitet 3	Membrane Installation		
Uønsket hendelse 1	Membrane Damage		
Eksisterende tiltak	Use of protective gloves and tools, and careful handling procedures		
Sannsynlighet	Mindre sannsynlig		
Konsekvens	Menneske - Ikke aktuell		Omdømme - Ingen/liten fare
	Øk./materiell - Farlig		Ytre miljø - Farlig
Begrunnelse	Pd membranes are expensive and delicate, making them prone to damage during installation. But, It does not concern HSE safety code.		
Kommentar / forslag til tiltak	Train personnel on proper handling techniques, use specialized tools for installation, and inspect membranes before installation.		

☑ Legg til ny uønsket hendelse

Uønsket hendelse 2	High-Temperature Exposure		
Eksisterende tiltak	Use of heat-resistant gloves and tools.		
Sannsynlighet	Mindre sannsynlig		
Konsekvens	Menneske - Kritisk		Omdømme - Ingen/liten fare
	Øk./materiell - Ingen/liten fare		Ytre miljø - Ingen/liten fare
Begrunnelse			
Kommentar / forslag til tiltak			

☑ Legg til ny uønsket hendelse

Uønsket hendelse 3	Gas Leaks		
Eksisterende tiltak	Use of gaskets, seals, and leak detection methods		
Sannsynlighet	Sannsynlig		
Konsekvens	Menneske - Farlig		Omdømme - Ingen/liten fare
	Øk./materiell - Ingen/liten fare		Ytre miljø - Farlig
Begrunnelse	Suction Point, personal protective equipment (PPE) like gloves, goggles, and respirators, Leak test before experimentation, Gas sensors		
Kommentar / forslag til tiltak	i		

☑ Legg til ny uønsket hendelse

Uønsket hendelse 4	Contamination
Eksisterende tiltak	Cleaning the reactor before installation

Sannsynlighet	Sannsynlig		
Konsekvens	Menneske - En viss fare		Omdømme - En viss fare
	Øk./materiell - Farlig		Ytre miljø - En viss fare
Begrunnelse	It does not concern the HSE Safety Code		
Kommentar / forslag til tiltak	Implement strict cleaning protocols		

☐ Legg til ny uønsket hendelse

☑ Legg til ny aktivitet

Det anbefales mellomlagring underveis. Lagreknapp nederst i skjemaet

Aktivitet 4	Gas Chromatography		
Uønsket hendelse 1	Electrical Hazards		
Eksisterende tiltak	Use of grounded equipment, circuit breakers, and insulated tools		
Sannsynlighet	Mindre sannsynlig		
Konsekvens	Menneske - En viss fare		Omdømme - Ingen/liten fare
	Øk./materiell - Ingen/liten fare		Ytre miljø - Ingen/liten fare
Begrunnelse	We have all the control measures to avoid this adverse event		
Kommentar / forslag til tiltak	Regularly inspect electrical systems		

☑ Legg til ny uønsket hendelse

Uønsket hendelse 2	Chemical Exposure		
Eksisterende tiltak	Suction point, PPE (gloves, goggles, lab coats), and proper ventilation.		
Sannsynlighet	Sannsynlig		
Konsekvens	Menneske - En viss fare		Omdømme - Ingen/liten fare
	Øk./materiell - En viss fare		Ytre miljø - En viss fare
Begrunnelse	We have all the control measures to avoid this adverse event		
Kommentar / forslag til tiltak			

☑ Legg til ny uønsket hendelse

Uønsket hendelse 3	High-Pressure Gas Cylinders mishaps		
Eksisterende tiltak	Use of pressure regulators, secure storage of cylinders, and proper training.		
Sannsynlighet	Mindre sannsynlig		
Konsekvens	Menneske - En viss fare		Omdømme - Ingen/liten fare
	Øk./materiell - Ingen/liten fare		Ytre miljø - En viss fare
Begrunnelse	We are working under low pressure		
Kommentar / forslag til tiltak			

☐ Legg til ny uønsket hendelse

Legg til ny aktivitet

Aktivitet 5	Data Analysis
Uønsket hendelse 1	Experimental results and theoretical results do not match
Eksisterende tiltak	N/A
Sannsynlighet	Mindre sannsynlig
Konsekvens	Menneske - Ingen/liten fare Omdømme - Ingen/liten fare Øk./materiell - Ingen/liten fare Ytre miljø - Ingen/liten fare
Begrunnelse	It is not necessarily a safety concern
Kommentar / forslag til tiltak	

Legg til ny uønsket hendelse

Legg til ny aktivitet

Aktivitet 6	Handling samples or operating the XPS instrument
Uønsket hendelse 1	Contamination of Samples or Instrument
Eksisterende tiltak	Use of cleanroom protocols and proper sample handling techniques.
Sannsynlighet	Mindre sannsynlig
Konsekvens	Menneske - Ikke aktuell Omdømme - Ingen/liten fare Øk./materiell - En viss fare Ytre miljø - Ikke aktuell
Begrunnelse	
Kommentar / forslag til tiltak	

Legg til ny uønsket hendelse

Uønsket hendelse 2	X-ray Radiation Exposure
Eksisterende tiltak	Shielding (lead or lead-equivalent materials), interlocks, and radiation warning signs.
Sannsynlighet	Mindre sannsynlig
Konsekvens	Menneske - Farlig Omdømme - En viss fare Øk./materiell - Ingen/liten fare Ytre miljø - Ingen/liten fare
Begrunnelse	
Kommentar / forslag til tiltak	

Legg til ny uønsket hendelse

Legg til ny aktivitet

Aktivitet 7	Using compressed gases (e.g., hydrogen, nitrogen, ammonia) in experiments
Uønsket hendelse 1	Gas Leaks
Eksisterende tiltak	Use of gas sensors, proper ventilation, fire extinguisher, central gas detector, and gas-tight fittings.

Sannsynlighet	Mindre sannsynlig	
Konsekvens	Menneske - Kritisk	Omdømme - Farlig
	Øk./materiell - En viss fare	Ytre miljø - Farlig
Begrunnelse	Control measures are strong enough	
Kommentar / forslag til tiltak		

☑ Legg til ny uønsket hendelse

Uønsket hendelse 2	Explosion	
Eksisterende tiltak	Suction point, Central Gas Detector	
Sannsynlighet	Mindre sannsynlig	
Konsekvens	Menneske - Kritisk	Omdømme - Kritisk
	Øk./materiell - Farlig	Ytre miljø - Farlig
Begrunnelse	Suction point, Central Gas Detector	
Kommentar / forslag til tiltak		

☑ Legg til ny uønsket hendelse

Uønsket hendelse 3	Running out of gases	
Eksisterende tiltak	Planning all the activities accordingly and pre-order necessasy gases in advance	
Sannsynlighet	Mindre sannsynlig	
Konsekvens	Menneske - Ikke aktuell	Omdømme - En viss fare
	Øk./materiell - Ikke aktuell	Ytre miljø - Ikke aktuell
Begrunnelse		
Kommentar / forslag til tiltak		

☑ Legg til ny uønsket hendelse

Uønsket hendelse 4	Asphyxiation	
Eksisterende tiltak	Use of gas sensors, proper ventilation, and warning signs.	
Sannsynlighet	Mindre sannsynlig	
Konsekvens	Menneske - Farlig	Omdømme - En viss fare
	Øk./materiell - Ikke aktuell	Ytre miljø - Ikke aktuell
Begrunnelse		
Kommentar / forslag til tiltak		

☐ Legg til ny uønsket hendelse

☑ Legg til ny aktivitet

Det anbefales mellomlagring underveis. Lagreknapp nederst i skjemaet

Aktivitet 8	Prolonged use of laboratory equipment or manual handling of samples
Uønsket hendelse 1	Ergonomic Hazards

Eksisterende tiltak

Sannsynlighet Mindre sannsynlig

Konsekvens Menneske - En viss fare

Omdømme - En viss fare

Øk./materiell - Ikke aktuell

Ytre miljø - Ikke aktuell

Begrunnelse

Kommentar / forslag til tiltak

☑ Legg til ny uønsket hendelse

Uønsket hendelse 2 Psychological Stress

Eksisterende tiltak Providing breaks, mental health resources, and workload management.

Sannsynlighet Sannsynlig

Konsekvens Menneske - En viss fare

Omdømme - Farlig

Øk./materiell - Ikke aktuell

Ytre miljø - Ikke aktuell

Begrunnelse

Kommentar / forslag til tiltak

☐ Legg til ny uønsket hendelse

☑ Legg til ny aktivitet

Aktivitet 9 Moving around the lab, especially when carrying equipment or samples.

Uønsket hendelse 1 Slips, Trips, and Falls

Eksisterende tiltak Clear walkways, proper signage, and non-slip flooring.

Sannsynlighet Mindre sannsynlig

Konsekvens Menneske - Farlig

Omdømme - En viss fare

Øk./materiell - Ingen/liten fare

Ytre miljø - Ikke aktuell

Begrunnelse Careful handling

Kommentar / forslag til tiltak

☐ Legg til ny uønsket hendelse

☑ Legg til ny aktivitet

Aktivitet 10 Cleaning Equipments

Uønsket hendelse 1 Exposing to corrosive and acidic elements

Eksisterende tiltak Using gloves, PPE

Sannsynlighet Sannsynlig

Konsekvens Menneske - Farlig

Omdømme - En viss fare

Øk./materiell - En viss fare

Ytre miljø - Ingen/liten fare

Begrunnelse Careful handling, gloves, ppe

Kommentar / forslag til tiltak

☑ Legg til ny uønsket hendelse

Uønsket hendelse 2	Glassware Breakage		
Eksisterende tiltak	Use of safety glassware, gloves, and proper handling techniques.		
Sannsynlighet	Sannsynlig		
Konsekvens	Menneske - En viss fare	Omdømme - En viss fare	
	Øk./materiell - En viss fare	Ytre miljø - Ikke aktuell	
Begrunnelse			
Kommentar / forslag til tiltak			

☐ Legg til ny uønsket hendelse

Oppsummering

	Ikke akseptabel risiko	**Antall rød:**	0
	Risiko må vurderes	**Antall gul:**	42
	Akseptabel risiko	**Antall grønn:**	35

Konklusjon

Gjør en totalvurdering av om arbeidet kan utføres, evt. om det må gjennomføres flere tiltak.

Begrunnelse

After the thorough risk analysis, we can conclude that the risks that we found for this project can be brought down to as low as ze measures. So, the project is feasible.

Gjennomføring av tiltak ☐ Trykk for beskrivelse

Godkjenning av risikovurdering ☐ Trykk for beskrivelse

☐ **Skjul beskrivelse**

Review rounds:

The following review rounds are linked to this risk element:

Start date	End date	Status
26.03.2025	05.04.2025	Active

Comment from Estelle Marie Madeleine Vanhoecke, 27.03.2025

god job Rashed! please do not forget to write down the leak test procedure that Willow will show you soon.